Reversal of Apoptosis-

A Potential Link to Carcinogenesis and Cancer Recurrence

TANG, Ho Lam

A Thesis Submitted in Partial Fulfillment

of the Requirements for the Doctor of Philosophy

in

Biology

The Chinese University of Hong Kong

December 2010

ProQuest LLC.
789 East Eisenhower Parkway
P.O. Box 1346
Ann Arbor, MI 48106 - 1346

Thesis committee:

Prof. FUNG, Ming Chiu (Supervisor)

Prof. CHEUNG, Chi Keung Peter (Chairman)

Prof. LAM, Hon Ming (Committee member)

Prof. MAK, Nai Ki (External examiner)

Preface

This thesis provides evidence on the reversal of apoptotic dying process in mammalian cells, and suggests its link to cancer recurrence and tumor formation. Chapter 1 introduces the general background of this research. Chapter 2 describes the materials and methods applied in this study. Chapter 3 and Chapter 4 dedicate to the works on the reversal of apoptosis in human cancer cells, and in mouse primary cells and non-cancer cell lines respectively. Chapter 5 is an independent work studying contribution of vimentin in mitochondrial morphology and organization. Each chapter from 3 to 5 provides its own specific introduction, results and discussion. Chapter 6 serves as the perspectives to provide insights of future works. References follow afterward.

Acknowledgements

I would like to express my sincerest appreciation to my thesis supervisor Prof. Ming Chiu FUNG for his support of this work and make this thesis possible; Ho Man TANG (Iowa State University) and Keng Hou MAK (Chinese University of Hong Kong, CUHK) for research design, optimization and critical support in experiments, especially in microscopy, inhibitor research, RT-PCR and quantification; Hiu Tung LAW (CUHK) for cartoon drawing; Ka Yan HO for abstract translation; Prof. Chi Keung CHEUNG, Prof. Hon Ming LAM (CUHK) and Prof. Nai Ki MAK (Hong Kong Baptist University) for their review of my thesis and invaluable comments in my study. I thank for the full support from my family.

Table of Contents

List of Abbreviations

α	Alpha
aa	Amino acids
AIF	Apoptosis inducing factor
APAF1	Apoptosis activating factors-1
β	Beta
BAK	Bcl-2 antagonist killer
BAX	Bcl-2 associated X protein
BCL-2	B-cell lymphoma-2
BSA	Bovine serum albumin
Caspase	Cysteine aspartase
cDNA	Complementary DNA
Cyto c	Cytochrome c
DIABLO	Direct IAP binding protein with low pI
DMSO	Dimethyl sulfoxide
DNA	Deoxyribonucleic acid
EndoG	Endonuclease G
EtOH	Ethanol
hr	Hour

HSP	Heat shock protein
IAP	Inhibitor of apoptosis protein
Jasp	Jasplakinolide
kDa	Kilodalton
mA	Mili-ampere
MEM	Minimum essential medium
min	Minute
mL	Mili-liter
mm	Mili-meter
mM	Mili-molar
μ	Micro (10^{-6})
μL	Micro-liter
μM	Micro-molar
PBS	Phosphate-buffered saline
SDS-PAGE	Sodium dodecyl sulfate polyacrylamide gel electrophoresis
SMAC	Second mitochondria-derived activator of caspases
STS	Staurosporine
XIAP	X-chromosome inhibitor of apoptosis protein

List of Figures

List of Table

Abstract

Despite of dramatic scientific gains and technological advancement, cancer remains an undaunted killer nowadays. According to the World Health Report 2008 by the World Health Organization (WHO), cancer will overtake heart disease to be the top killer in the world by 2010. Deficiency in cell death is a hallmark of cancer cells, and therefore, activation of apoptosis, a cell suicide process, in cancer cells is an important strategy for current anticancer treatment such as chemotherapy. However, cancer can relapse and new tumors form after cycles of chemotherapy, with mechanism unknown. The focus of the present study is to conduct basic research that in the long term makes cancer to be curable through studying new routes to attack cancer. The first part of this study reveals an unexpected escape tactic which cancer cells could use to survive chemotherapy through a novel phenomenon, ***the reversal of apoptotic dying process in cancer cells.*** Cancer cells undergoing apoptosis can survive and reverse the process of dying, despite passing through critical checkpoints in apoptosis that have been assumed as the points of no return, including mitochondrial fragmentation, caspase-3 activation and DNA destruction. These cells reverse apoptosis once chemicals to induce the apoptotic dying process were removed, but failed to recover when the nucleus had started to disintegrate – an event that has been known right at the end of the apoptotic cell death. Notably, these cells

display the increase in cell mobility and genetic alterations, which have been linked into metastasis and tumor progression in cancer recurrence. The second part of this study suggests ***reversal of apoptosis to promote oncogenesis in normal cells***, using mouse primary cells and non-cancerous cell lines as study models. While DNA destruction is an executing process that commits dying cells to demise in apoptosis, cells, that survive by reversing apoptosis harbor lasting DNA damage generated during apoptosis. Daughter cells derived from cells that reverse apoptosis display genetic alterations including variation of chromosomal numbers and formation of radical configurations, and also transformation phenotypes such as formation of foci and anchorage independent growth. These suggest that reversing apoptosis drives oncogenesis in normal cells in response to cytotoxin in anticancer treatments. Transcriptional regulation is critical to drive the reversal of dying process. Transient disturbance of transcription by a clinical drug, Actinomycin D (AMD), suppresses reversal of apoptosis, and promotes irreversible cell death. Time-course microarray analysis also suggests the potential contribution of pro-apoptotic factors, such as BCL-2, XIAP, MDM2 and Heat Shock Proteins (HSPs), in promoting reversal of apoptosis. These findings reveal the potential links between reversal of apoptosis, cancer recurrence and oncogenesis, and therefore, provide promising new therapeutic targets to the war of cancer.

摘要

儘管科學不斷進步，科技日新月異，人類至今仍無法抵抗癌症。根據世界衛生組織發表的世界衛生報告 2008，癌症會在 2010 年取替心臟病，成爲全球的頭號殺手。癌細胞的其中一個特徵是死亡機制有缺憾。因此，誘發細胞自我凋亡 (細胞的自殺過程)是目前抗癌治療的主要策略，如化療就是根據這個原理。不過，即使經過多次化療，癌症仍可能復發，形成新的腫瘤，而原因不明。

本研究重點探索對抗癌症的新方向，長遠目標希望可以治癒癌病。首部分的研究揭示出一個嶄新的現象—癌細胞能逆轉自我凋亡的死亡過程得以存活，顯示癌細胞可能利用一種迄今尚未認識的機制來逃避化療藥物的殺傷。研究發現即使藥物啓動了癌細胞的自我凋亡程式，並且在經過了一些公認爲非常關鍵而無法逆轉的凋亡檢測點後，仍能逆轉死亡過程，繼續存活。這些檢測點包括線粒體碎裂、3-半胱氨酸蛋白酶 (caspase-3) 活性化以及去氧核糖核酸損毀。只要將誘發細胞自我凋亡的化學物除去，這些正在步向死亡的細胞便能恢復過來。癌細胞只有在細胞核解體後才無法復原，細胞核解體亦代表細胞自殺過程已到了終段。從凋亡過程中復原的細胞，流動性明顯增加，而且出現基因變異，這些變化或與腫瘤擴散及進化的成因有關，引起癌症復發。

第二部分的研究證實，細胞凋亡的逆轉情況不單在癌細胞中發生，在老鼠的原代細胞以及正常細胞株中亦同樣出現，反映細胞凋亡的逆轉是個普遍的現象。去氧核糖核酸(DNA)的損毀一直被認爲是細胞自我凋亡的必經階段，然而本研究發現即使 DNA 受損，細胞仍能從自我凋亡過程中復原，並會帶著這些受損的 DNA 繼續進行細胞複製，分裂出來的細胞會出現基因變異，包括染色體數目的改變、以及輻射體構型的出現，細胞在表型上亦轉化了，例如形成集落及不依賴貼壁生長。

上述的結果反映了在抗癌治療中，藥物的毒性同樣作用於正常細胞，而細胞凋亡逆轉過程中造成的後果可引發腫瘤的形成。本研究亦指出轉錄調控對控制死亡逆轉過程起了重要作用。利用一種稱爲放綫菌素 (AMD) 的臨床藥物短暫干擾轉錄過程，發現細胞凋亡的逆轉受抑制，並促進細胞不可逆轉的死亡。實時逆轉錄 PCR 實驗亦揭示了細胞凋亡促進因子如 BCL-2、XIAP、MDM2 和 HSPs 在促進細胞凋亡逆轉上的潛能。這些發現將有助阻止腫瘤形成及癌症復發，並提供理想的新標靶療法以對抗癌症。

Chapter 1

Introduction

Chapter 1

Introduction

1.1 Overview in Apoptosis

Apoptosis, a cell suicide process, has been one of the most exciting and applicable biological discoveries in the century (Jacobson et al., 1997; Baehrecke et al., 2002; Lam 2004; Taylor et al., 2008). It plays essential role in regulating development and homeostasis in multicellular organisms by sculpting, deleting unwanted structure, controlling cell numbers, and eliminating abnormal, injured or dangerous cells (Jacobson et al., 1997; Baehrecke et al., 2002). The term of programmed cell death describes the occurrence of cell deaths in the predictable place and in the predictable time as planned and programmed during development (Lockshin & Williams 1964; Jacobson et al., 1997). The word of apoptosis is used in Greek to describe the "dropping off" or "falling off" of petals from flowers, or leaves from trees, and this word in English was proposed and is now used to describe this type of programmed cell death (Kerr et al., 1972).

Elucidating the regulatory mechanisms governing apoptotic cell death enhances our understanding on how cell death shape life during development. Dysfunction of

apoptosis results fatal consequence such as autoimmunity, cancer and neurodegeneration (Eguchi 2001; Friedlander 2003; Chan 2006; Stratton et al., 2009). For example, mutation in pro-apoptotic Bax and p53 promotes tumor formation (Mrózek et al., 2003; Vazquez et al., 2008). Mice with disturbance of gene encoding pro-apoptotic caspase-3 die in early development with excess of neuron in brain (Kuida et al., 1996). Therefore, controlling apoptosis is an important strategy for treating these intractable diseases.

While apoptosis is essential in multicellular organisms, it becomes clear that apoptosis also benefits unicellular organism to their survival of their progeny in adverse conditions (Gourlay et al., 2006; Carmona-Gutierrez et al., 2010). For example, during nutrient stress, "old' yeasts undergo apoptosis so that the "young" yeasts have better chance to survive. This contributes the survival of the population.

1.2 Conserved cell death machineries in evolution

Core apoptotic cell death machineries are highly conserved from human, fly to worm (Jacobson et al., 1997; Baehrecke 2002; Xu et al., 2009). For examples, the core gene family caspases, *Apaf-1*, *Bcl-2* and *Iap* in human are homologous to *Dcp-1* and *Drice*, *Ark/Dark*, *Debcl-1/Drob-1*, and *Diap-1* in fly, and also *Ced-3*, *Ced-4*, *Ced-9* and

Bir-1 in worm (Baehrecke 2002). Studies also revealed caspase-like proteases (CLPs) and Bax inhibitor-1 (BI-1) class of proteins in plant (Lam 2004), and also at least orthology of mammalian caspases, the metacaspase *Yac1p*, in yeast (Madeo et al., 2002; Gourlay et al., 2006; Carmona-Gutierrez et al., 2010). Interestingly, heterologous expression of human pro-survival Bcl-2 inhibits cell death in *Caenorhabditis elegans* (Vaux et al., 1992; Hengartner & Horvitz 1994). Expression of human pro-apoptotic Bax induces cell death in yeast, while expression of the human Bcl-2 can suppress the Bax-induced lethality (Eisenberg et al., 2007). These suggest the core mechanisms controlling apoptosis are conserved in evolution.

1.3 Control role of cell execution in apoptosis

In the past decade, researchers have identified mitochondria as the chief regulator in apoptosis (Wang 2001; Taylor et al., 2008). Mitochondria act as the center for apoptosis, which bridge the intrinsic and extrinsic cell death signals and the downstream processes of apoptosis. In response to apoptotic stimuli, the pro-apoptotic upstream factors such as BAX, BAD and BIM translocate to mitochondria to initiate mitochondrial outer membrane permeabilization (Wang 2001; Orrenius et al., 2003; Taylor et al., 2008; Chipuk et al., 2010). In the typical mitochondria-dependent apoptosis, proapoptotic upstream factors such as BAX

translocate to mitochondria, and trigger the release of mitochondrial-resided proteins including cytochrome c, SMAC (Second mitochondria-derived activator of caspases)/ DIABLO (direct inhibitor of apoptosis (IAP)-binding protein with low pI), AIF (apoptosis-inducing factor) and EndoG (endonuclease G). These are the downstream executing factors that commit cells to die by various mechanisms through caspase-dependent and -independent pathways.

Cytochrome c is one of the best characterized mitochondria downstream executing factors to initiate caspase-dependent apoptosis (Wang 2001; Taylor et al., 2008). After released from mitochondria, it engages APAF1 (apoptotic protease activating factor 1) to form apoptosome as a caspase activation platform, which recruits and activates initiator caspase-9, which then activates executioner caspase-3 and -7 (Li et al., 1997; Wang 2001; Riedl & Shi 2004).

Caspases are the cysteine proteases that cleave after an aspartate in their substrates (Alnemri et al., 1996; Riedl & Shi 2004). They serve as the central executioners in apoptosis by not only cleaving a wide range of substrates including cellular functional and structural components (Lüthi & Martin 2007), but also by further activating cell executioners such as apoptotic nucleases (Wang 2001; Taylor et al.,

2008). DNA fragmentation factor (DFF)40/ caspase-activated deoxyribonuclease (CAD) is one of the caspase-3 mediated apoptotic nuclease (Nagata et al., 2003; Widlak &, Garrard 2005). In the normal condition, its inhibitor DFF45/ICAD binds to DFF40/CAD; however, during apoptosis, caspase-3 cleaves DFF45/ICAD, and therefore, releases DFF40/CAD to fragment DNA (Liu et al., 1997; Liu et al., 1998; Enari et al., 1998; Sakahira et al., 1998). Activated caspase-3 also damages DNA repair systems for example, by cleaving the DNA repair enzyme Poly(ADP)-ribose polymerase-1 (PARP) (Lazebnik et al., 1994; D'Amours et al., 2001). It also activates additional caspases to strengthen caspase cascade for cellular demolition, resulting the morphological manifestations of apoptosis, including nuclear condensation, cell shrinkage, and membrane blebbing (Taylor et al., 2008).

Besides, the mitochondrial release of SMAC/ DIABLO suppresses IAP (inhibitor of apoptosis), which inhibits caspases, and therefore, strengthen the caspase cascade (Du et al., 2000; Verhagen et al., 2000; Chai et al., 2000; Chai et al., 2001; Riedl et al., 2001). While caspases can also be activated by mitochondria-independent pathway, however, the activated caspases can then activate the mitochondria upstream pro-apoptotic signal such as BID, in which its caspase-mediated truncated form, tBID, translocates to mitochondria to activate mitochondria dependent pathway

(Luo et al., 1998; Li et al., 1998).

Mitochondria also mediate caspase-independent apoptosis. AIF and EndoG are the apoptotic nucleases that trigger apoptosis independent to the activation of caspases. During apoptosis, AIF and EndoG are released from mitochondria, and then translocate to nucleus to fragment DNA (Susin et al., 1999; Miramar et al., 2001; Li et al., 2001; van Loo et al., 2001). Besides, damage of mitochondria during apoptosis results dysfunction in ATP generation (Waterhouse et al., 2001; Ricci et al., 2004). As ATP is the primary energy source, disturbance of ATP synthesis prevents survival of the cells.

1.4 Point of no return in apoptosis

Mitochondrial fragmentation and caspases activation are the morphological hallmarks of apoptosis (Wang 2001; Riedl & Shi 2004; Green & Kroemer 2004), and therefore, server as the important and commonly used markers to identify apoptotic cells from basic research to medical applications (Hotchkiss et al., 2009). Mitochondrial fragmentation and activation of caspases are generally assumed as the point of no return in apoptosis (Riedl & Shi 2004; Green & Kroemer 2004; Taylor et al., 2008; Chipuk et al., 2010). The fragmentation of mitochondria is the critical

apoptotic event that releases cell executioners to cytosol to initiate both caspase-dependent and –independent events, and either of these pathways can lead to cell death (Wang 2001; Green & Kroemer 2004; Kroemer & Martin 2005). Mitochondrion is also the bioenergetic and metabolic center so that its damage results cell death. Activation of caspases triggers caspase cascade for massive cellular destruction (Riedl & Shi 2004; Lüthi & Martin 2007; Taylor et al., 2008). After the release of the mitochondrial-resided executing factors, it is believed that caspases activation and apoptosis follow often within minutes (Chipuk et al., 2010).

1.5 Strategy of research

Dysfunction in apoptosis is an important cause of cancer (Chan 2006). Research on the mechanisms of apoptosis has received much attention because it has a big impact on the developing anti-cancer therapies. Based on the understanding of mechanisms of apoptosis, several potential agents such as soluble fibroblast-associated cell surface ligand (sFASL) and soluble tumor necrosis factor-related apoptosis-inducing ligand (sTRAIL) had been tested for their anti-cancer activities (Bremer et al., 2006; Clark & Robilotto 2007). Moreover, the inhibitor of apoptosis proteins (IAP) and Bcl-2 family proteins may be potential vaccine candidates for immune therapy of cancer (Andersen et al., 2005).

However, much about the basic biology of anti-cancer therapies remains to be understood. For example: anti-cancer therapies can promotes apoptosis in cancer cells efficiently, but how cancer relapses, with increase in metastasis and drug resistance, together with new tumor formation, remain to be defined. While current research focus on promoting cancer cells to die, it would be important to know how cancer cells survive the therapy, and what promote new tumor formation during cancer recurrence.

Therefore, we first induce cancer cells to undergo apoptosis, and study their response and consequences after removal of apoptotic stimuli (Figure 1). This leads to our discovery on the reversibility of cancer cells that reveals an unexpected mechanism that cancer cells could use to survive chemotherapy (Tang et al., 2009). Further research demonstrates reversal of apoptosis in primary cells and cells lines, and the cells acquire genetic alterations and transformation phenotypes. These suggest a link of reversal of apoptosis to cancer recurrence and cancer formation. We anticipate that our findings will increase in our understanding on the control of apoptosis and will support therapeutic advancement to anti-cancer therapy.

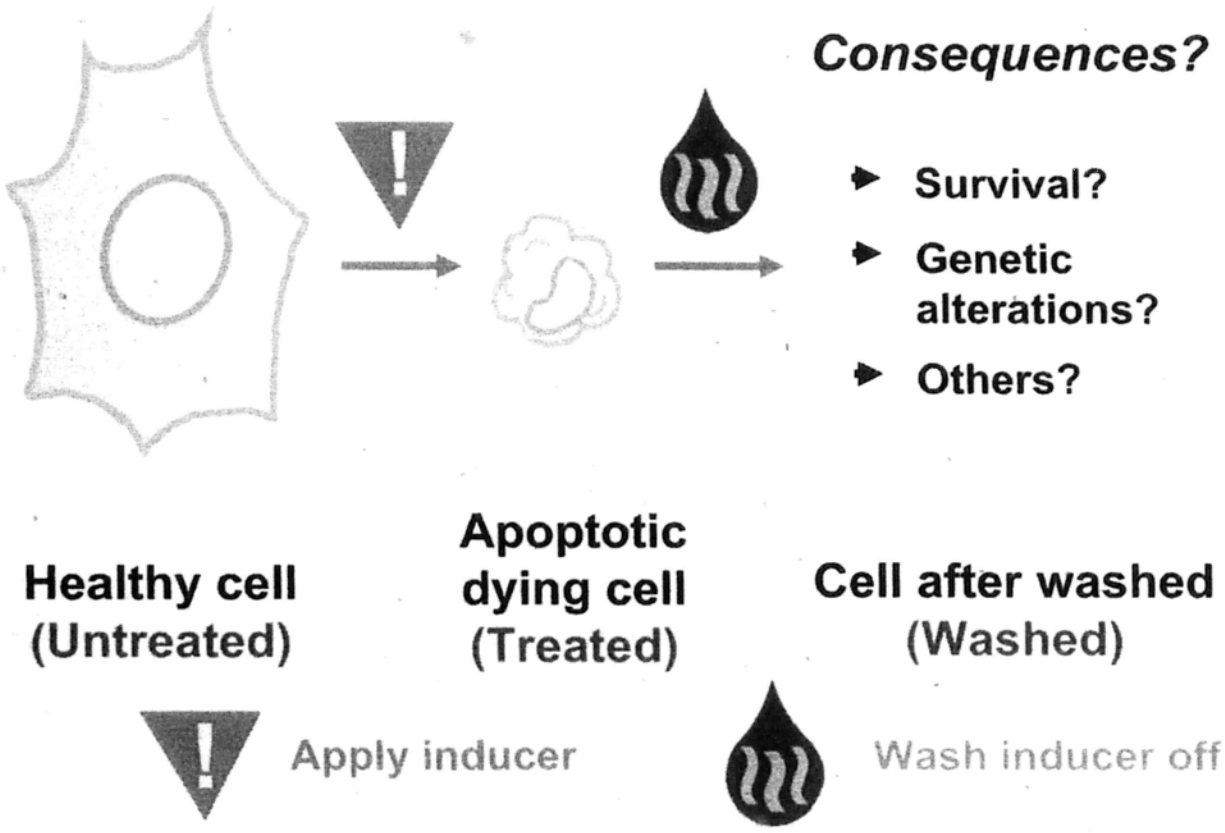

Figure 1 A schematic diagram summarizing the study approach of this research for studying reversibility of apoptosis and its potential consequences.

Chapter 2

Materials and Methods

Chapter 2

Materials and Methods

2.1 Materials

All cell lines are obtained from American Type Culture Collection (ATCC, Manassas, VA, USA. Primary culture cells are isolated from BALB/c mice. All other reagents and antibodies are obtained from Sigma (Sigma, St Louis, MO, USA) unless stated.

Material	**Source**	**CAT. No.**
Antibodies:		
Rabbit anti-AIF antibody, polyclonal	Santa Cruz Biotech	sc-5586
Rabbit anti-caspase-3 antibody, polyclonal	Cell signaling tech.	9662
Rabbit anti-EndoG antibody, polyclonal	Santa Cruz Biotech	sc-32935
Rabbit anti-m ICAD antibody, monoclonal	BDB PMG	550736
Rabbit anti-PARP antibody, monoclonal	Cell signaling tech	9532
Mouse anti-vimentin, monoclonal	Santa Cruz Biotech	sc-32322
Rabbit anti-calnexin, monoclonal	Sigma	C4731
Zenon Tricolor Rabbit IgG1 Labeling Kit	Invitrogen	Z-25370
Zenon Tricolor Mouse IgG1 Labeling Kit	Invitrogen	Z-25070
Anti-Rabbit Secondary Antibody	Amersham	NA934V
Anti-Mouse Secondary Antibody	Amersham	NA931V

Cell culture:		
DMEM F12	Gibco	10565042
Minimum Essential Medium (MEM)	Gibco	41500-034
RPMI Medium 1640, power	Gibco	23400062
Fetal bovine serum	Gibco	10091-148
Penicillin-Streptomycin, liquid	Gibco	15140-122
Trypsin	Gibco	25300120
CO_2-Independent Medium	Gibco	18045
Apoptosis induction:		
Ethanol	Scharlau	ET0021
DMSO	Sigma	D2650
Jasplakinolide	Invitrogen	J7473
Staurosporine	Sigma	S4400
Live cell stain:		
Hoechst 33342	Molecular probes	H1399
MitoTracker Red CMXRos	Molecular probes	M7512

Biochemical related		
Agar (cell culture grade)	Sigma	A1296
Glycerol	Sigma	G7893
Glycine	Sigma	G8898
Hepes	Gibco	11344-025
Sodium chloride	Sigma	S9625
Triton X-100	Sigma	X-100
Trizol reagent	Invitrogen	15596-026
Tween 20	Amersham	US20605
Trypan blue solution (0.4%)	Sigma	T8154
Paraformaldehyde	Sigma	P6148
Protein Assay	Bio-Rad	500-0006
ECL+ Western Blotting Detection Reagents	Amersham	RPN2132
Qiagen RNeasy Kit	Qiagen	74104
LightShift® Chemiluminescent EMSA Kit	Pierce	20148
Dynabeads Sheep anti-mouse IgG	Invitrogen	M280
Captivate magnetic separator	Invitrogen	c-24703
Qtracker 525 Cell Labeling Kit	Invitrogen	Q25041MP

2.2 Methods

2.2.1 Cell Culture

Human cervical cancer HeLa cells, skin cancer A375, liver cancer HepG2, breast cancer MCF7 cells, and the mouse embryonic fibroblast NIH3T3 cells were from American Type Culture Collection (ATCC). Primary liver cells were isolated from BALB/c mice by collagenase B according to the instruction from manufacturer (Worthington, New Jersey, NY, USA), and cultured as described (Zurlo & Arterburn 1996). The cells were cultured in DMEM/F-12 (Dulbecco's Modified Eagle medium: Nutrient Mixture F-12) supplemented with 10% FBS (Fetal bovine serum), 100U/mL penicillin and 100 μ g/mL streptomycin (Gibco, Carlsbad, CA, USA), at 37°C under an atmosphere of 5% CO_2/95% air. Human prostate cancer PC3 cells were cultured in same condition with RPMI-1640 medium. Human immortalized brown adipocyte PAZ-6 cells were obtained from the author and were cultured as described previously (Zilberfarb et al., 1997). Cells were seeded onto tissue culture plates for 2 days with 70% confluence before being subjected to each experiment. The medium was changed every 24 to 36 hours.

2.2.2 Apoptotic inductions

Apoptosis in human cancer cells was induced by 0.5 μ M jasplakinolide (Invitrogen,

Carlsbad, CA, USA) for 3 hours, 0.1 μ M staurosporine (Sigma) for 1 hour or 4.5% ethanol (Scharlau, Barcelona, Spain) in culture medium (v/v). Apoptosis in the primary liver cells and NIH3T3 cells was induced by 5-hour induction of 4.5% ethanol (Scharlau) and 20-hour induction of 10% DMSO (Sigma) in culture medium (v/v) respectively. For removal of apoptotic inducers, the apoptotic cells were washed for 3 times with culture medium and then cultured as the time indicated in individual experiments.

2.2.3 siRNA (small interfering RNA) transfection

Endogenous vimentin and β-tubulin expression was reduced by introducing Stealth™ RNAi (RNA interference) specific to vimentin and β-tubulin (Invitrogen) respectively into COS-7 cells by Lipofectamine™ RNAiMAX (Invitrogen). The RNAi negative control was from the Stealth™ RNAi negative control kit (Invitrogen). Cells were cultured for a further 3 days after transfection for each experiment.

2.2.4 Immunocytochemistry and fluorescence microscopy

Mitochondria and nuclei were stained in living cells with 50nM Mitotracker Red CMXRos and 250 ng/mL Hoechst 33342 (Invitrogen) respectively for 20 minutes in

culture medium. Cells with endocytosis were labeled by green fluorescence emitting Quantum Dot from Qtracker® 525 Cell Labeling Kit (Invitrogen) as described (Jaiswa et al., 2003). The cells were fixed with 3.7% (w/v) paraformaldehyde in PBS solution for 20 minutes in room temperature, and incubated with 0.1% triton x-100 (v/v) (Sigma) for 10 minutes before subjected to immunostaining. Endogenous AIF and EndoG were stained with anti-AIF and Anti-EndoG primary antibodies (Santa Cruz Biotech, Santa Cruz, CA, USA) and conjugated with green fluorescent Alexa Fluor®488 and red fluorescent Alexa®594 anti-rabbit IgG secondary antibodies with Zenon Tricolor Labeling kit (Invitrogen) respectively. Vimentin (Santa Cruz Biotech) and microtubules (Cell Signaling, Danvers, MA, USA) were stained with anti-vimentin and anti-(α-tubulin)/anti-(β-tubulin) primary antibodies and conjugated with green fluorescent Alexa Fluor® 488 anti-mouse IgG secondary antibodies (Molecular Probes). Cell images were captured with a monochromatic CoolSNAP FX camera (Roper Scientific, Pleasanton, CA, USA) on an inverted fluorescence microscope Cell Observer (Carl Zeiss, Jena, Germany) using a 63x numerical aperture (NA) 1.4 plan-Apochromat objective, and analyzed by using AxioVision 4.2 software (Carl Zeiss). Cell morphology was visualised by differential interference contrast (DIC) microscope device (Carl Zeiss).

2.2.5 Real-time living cell microscopy

Liver cells were cultured in CO_2-independent medium (Invitrogen) on a thermo-cell culture FCS2 chamber (Bioptechs, Butler, PA, USA), which was mounted onto the adapter in the stage of an inverted fluorescence microscope Cell Observer (Carl Zeiss). Apoptotic inductor in culture medium were introduced to the cell culture chamber through the perfusion tubes (Bioptechs) which was connected to the cell chamber. Fresh medium was also introduced to the chamber through the tube to remove the ethanol after apoptoic induction. Fluorescence signals of mitochondria and nuclei were visualized by fluorescence with excitation 561 and 405nm respectively. Time-lapse cell images were captured with a monochromatic CoolSNAP FX camera (Roper Scientific) using a × 63 numerical aperture (NA) 1.4 Plan-Apochromat objective (Carl Zeiss) as described in our fluorescence microscopy.

2.2.6 Confocal microscopy

Confocal cell images were captured with an inverted laser scanning microscope LSM 5 LIVE (Carl Zeiss), with 1 μm interval between each focal plane. The images were analysis by LSM image examiner software (Carl Zeiss).

2.2.7 Image quantification for cell viability

Images of the cell migration were analyzed with AxioVision 4.7 (Carl Zeiss). In each time-lapse imaging at least 3 cells in the each view were selected to trace their positions, defined as the midpoint of the nucleus, at different time points as indicated in the corresponding figure. By linking the temporal positions of each cell in chronological order, a migration footprint was drawn. The distances displaced at intervals were measured with the program and the velocities of individual cells were then calculated and averaged. The mean velocity of cells reversed from apoptosis was compared with that of control cells by two-tail *t*-test.

2.2.8 Biochemical and cell proliferation assays

One thousand cells were grown in a 96-well plate for 24 hours, and then treated with different conditions. At each designed time point, cells were subjected to the corresponding assays according to the manufacturer's instructions. The activity of effector caspases was measured by using the homogeneous caspase assay kit (Roche, Mannheim, Germany). The activity of mitochondria was measured by 3-(4,5-dimethylthiazol-2-yl)-2,5 -diphenyltetrazolium bromide (MTT) assay (Sigma). The cell survival was detected by the cell proliferation ELISA BrdU assay kit (Roche). Results of assays were measured by SpectraMax 250 microplate reader

(Molecular Devices Corp, Concord, ON, Canada).

2.2.9 Cell counting

The cellular morphology was observed by DIC, whereas mitochondria, nuclei and Quantum Dot were visualized by fluorescence microscopy. At least 100 cells were examined in at least three independent cell counting.

For cell proliferation, at each indicated time point, the cells were harvested by trypsinisation and thoroughly resuspended. The cells were stained with trypan-blue and counted in triplicate under a microscope with hemocytometer. Total cell number is calculated by multiplying the determined cell density with the total volume of suspension.

2.2.10 Protein Assay

Protein assay was performed to determined the concentrated of protein according to the manufacture's instructions (Bio-Rad, Hercules, CA, USA). Briefly, one part of protein assay mixed with 4 parts of double-distilled water before use. The BSA standards, in concentration 0.1 to 1 $\mu g/\mu L$, were used for preparing standard curve. Five micro-liter of protein sample was mixed with 150μL protein assay working solution, and then placed in 96-wells microtiter plate (Nunc, Roskilde, Denmark),

and then stranded at room temperature for 5 mins. The Results of assays were measured by SpectraMax 250 microplate reader (Molecular Devices Corp) with absorbance at 595nm. The concentration of protein sample was determined according to the standard curve.

2.2.11 Western Blot analysis

Approximately 3 μg protein from total cell lysate per lane was separated on a 12% SDS-PAGE gel and transferred onto a Hybond ECL® membrane (Amersham Biosciences, Chalfont St Giles, UK). After blocking, the membrane was incubated overnight at 4°C with primary antibody detecting targeting protein as stated at the text with dilution 1:1000, followed by another hour of incubation with the corresponding horseradish peroxidase-conjugated secondary antibody (Bio-Rad) at room temperature with 1:5000 dilution. Primary antibodies used were: anti-caspase-3 and anti-PARP (Cell Signaling Technology, Danvers, MA, USA) ; anti-ICAD and anti-Bak (Bcl-2 antagonist/killer) (BD PharMingen, BD Biosciences, Le Pont-de-Clax, France); anti-(α-tubulin), anti-(Cox IV) (cytochrome c oxidase complex IV) and anti-(golgin-97) (Invitrogen Molecular Probes, Carlsbad, CA, USA); anti-(β-tubulin), anti-(β-actin), anti-LDH (lactate dehydrogenase) and anti-calnexin (Sigma); anti-vimentin, anti-(cytochrome c) and anti-PCNA

(proliferating-cell nuclear antigen) (Santa Cruz Biotechnology, Santa Cruz, CA, USA). The signal from the secondary antibody was detected with the ECL Western blotting detection system (Amersham Biosciences). The signal was detected with the ECL Western blotting detection system (Amersham Biosciences, Chalfont St Giles, UK).

2.2.12 Single cell gel electrophoresis (comet) assay

Comet assay was performed by using the Trevigen Comet Assay™ kit (Trevigen, Gaithersburg, MD, USA) according to manufacturer's instruction. Alkaline electrophoresis of gelled slides was performed using Ready Sub-Cell GT Cells (Bio-Rad) on ice with 20 volt and 200 mA for 30 minutes. The current was adjusted by the volume of the buffer in the gel tank. The DNA was visualized by SYBR® Green stain (Trevigen) followed by fluorescence microscopy.

2.2.13 Cytokinesis-block micronucleus assay

Cells were grown on a glass coverslip (Marienfeld, Lauda-Künigahofen, Germany) with 70% confluence in 6-well cell culture plate (Nunc), and were induced to apoptosis as described in our above section of Apoptotic Inductions. To study genome damage in apoptotic cells that reversed apoptosis and proliferated, the

apoptosis-induced cells were washed and cultured for 16 hours in fresh medium containing cytokinesis-blocking cytochalasin B (3 µg/mL; Sigma). Cells without apoptotic induction served as control. The cells were then fixed by incubating in methanol/acetic acid (5:1, v/v) twice for 15 minutes followed by overnight fixation at 4°C. After washed three times with phosphate-buffer saline (PBS), the fixed cells were stained for nucleus by incubation of 250 ng/mL Hoechst 33342 in PBS for 20 minutes at room temperature. Slides were then prepared as described for fluorescence microscopy and observed under a 63x objective to image micronucleus. The micronuclei in the cytokinesis-blocked cells were scored as described (Fenech 2007). Only binucleated cells were scored, so as to include only cells that have divided once after addition of cytochalasin B. The two main nuclei should have clear boundaries from each other and micronuclei were counted only when clear boundary from the main nuclei was observed. The diameter of a micronucleus should lie between 1/16 and 1/3 that of the main nuclear diameter. Also, triplicates were performed with more than 100 cells for each condition per set.

2.2.14 Karyotyping

Metaphase chromosome spreads were prepared accordingly (MacLeod et al., 2007) with modifications. Briefly, cells were arrested at metaphase by adding colchicine

(Sigma) at a final concentration of 1ug/mL into growing culture for 6 hours. The arrested cells were then collected with trypsinization with immediate neutralization with cell culture medium and then followed by 5 minutes centrifugation at 400g. After discarding the supernatant, the cell pellet was loosened by gentle flicking in residual medium. To swell the mitotic cells, the cell suspension was incubated in hypotonic buffer, potassium chloride (5.59g/L diluted in double distillated water) and sodium citrate (9.0g/L diluted in double distillated water) in 1:1 (v/v), for 8 and 15 minutes, for NIH3T3 and primary liver cells respectively, at 37℃. The cells were then pelleted at 400G for 5 minutes to remove the hypotonic buffer. The cells were then fixed by gently adding freshly prepared ice-cold fixative (methanol and acetic acid, 3:1 v/v) to the pellet while agitating the centrifuge tube for the whole time, so as to prevent cell clumps and encourage mixing. The fixative was changed once and then the cells were fixed overnight at 4℃. Next, the cells were concentrated in fixative of a volume that the suspension became slightly cloudy for optimal cell concentration. To spread the metaphase of the fixed cells onto slides, cell suspension was dropped from height onto a chilly pre-cleaned SuperFrost® Plus microscopic slide (Gerhard. Menzel, Braunschweig, Germany) slightly-sloped on a freezer block. Then the slides were breathed on to enhance spreading and were mounted with DAPI/Antifade kit (MetaSystems, Altlussheim, Germany) after dried. The metaphase

chromosomes of metaphase-arrested cells were identified and captured by automated cytogenetic scanner workstation (MetaSystems) for analysis. Only metaphases of distinctly separated chromosomes and of chromosome spreading pattern from one nucleus were counted in order to avoid overlapped metaphases. Three replicates of more than 100 metaphases each were counted for the present of radial configurations in each corresponding metaphase spread for chromosomal abnormality.

2.2.15 Transformation assays

For focus formation assay: Cells were seeded in $10cm^2$ culture dish (Nunc) to reach 70% confluence. They were induced to apoptosis and subsequently washed to remove the inducer as in above section of Apoptotic Inductions. Then the culture medium was changed every 3 days. After 3 weeks of culture, morphologically transformed foci whose diameter exceeded 0.5 mm were counted. The assay was performed three times. From each replicate, at least five transformed foci were isolated by picking with sterile pipette tip and were then cultured for soft agar assay to validate their transformation potential. For soft agar assay: Anchorage-independent colony formation of NIH-3T3 cells reviving from reversal of apoptosis was determined as described previously (Cifone & Fidler 1980) with some modifications. Briefly, the cells were harvested by trypsinization. A total of $3x10^3$

cells were resuspended in 1.5mL completed cell culture medium containing 0.3% agarose. The suspensions were cultured in single wells of 6-well cell culture plate (Nunc) above a layer of solidified 0.5% agarose in the medium. After incubation at 37°C under an atmosphere of 5% CO_2/95% air for 5 weeks, plates were stained with 0.5 mL of 0.005% crystal violet solution (Sigma) for 1 hour before subjected to microscopy.

2.2.16 New RNA Detection

For newly synthesized RNA detection, the cells were incubated in the presence of 50 μM 4-thiouridine (Sigma) for 1 hour, and the total RNAs were extracted by Trizol (Invitrogen). The RNAs were then subjected to biotinylation as described (Zeiner et al., 1996). The biotin-labeled RNAs were agarose electrophoresed, transferred to nylon membrane (Bio-Rad, Hercules, CA, USA) with Trans-Blot® SD DNA/RNA Blotting Kit (Bio-Rad), and then detected by chemiluminescence using LightShift® Chemiluminescent EMSA Kit (Pierce, Rockford, IL, USA).

2.2.17 Microarray and gene expression data analysis

Mouse primary liver cells were treated with 4.5% ethanol for 5 hours (R0), and then washed and cultured in fresh medium for 3 hours (R3), 6 hours (R6), 24hours (R24)

and 48 hours (R48). The untreated cells serve as control (Ctrl). Total RNA from the cells in these conditions was isolated and purified by RNeasy Mini Kit (Qiagen, Cologne, Germany). As a first level of quality control, to detect possible batch effect or sample outliers, principal component analysis (PCA) was performed with Partek Genomics Suit 6.5 (Partek Inc., St. Louis, MO) on all samples' log2 normalized signal values and biologic replicate samples were observed to cluster together. Further, an analysis of variation (ANOVA) was run on all data including variables for cell sample, batch and error, which analysis also showed an excellent signal (biologic variation) to noise (batch and error) ratio. The RNA was subjected to reverse transcription using SABiosciences C-03 RT² First Strand Kit (SABiosciences - QIAGEN, Frederick, MD). These cDNA samples were analysized on the Illumina MouseWG-6 v2.0 Expression BeadChip (Illumina, Inc., San Diego, CA).

Processed Illumina signal value data were imported into the Partek and Spotfire DecisionSite 9.1 (TIBCO, Palo Alto, CA) platforms for evaluation for expression fold change at the gene level between time points, and for fold change across time when compared to a common starting point. First, all signal values were converted into log2 space and quality control tests run to ensure data integrity. Signals for the three biological replicates at each time point were taken together for comparison to

other time points; the Student's t-test used to determine statistical significance as p-values and fold change was based on averaged values. For our time course analysis all time points were compared to time point R-0, the time at which ethanol treatment ended. Functional Gene Ontology (The Gene Ontology Consortium, www.geneontology.org) and pathway analyses were run with Spotfire's Gene Ontology Browser and Ingenuity Pathway Analysis (IPA) (Ingenuity Systems, www.ingenuity.com) software, respectively.

Statistical and functional analyses of microarray expression data were performed at the JHMI Deep Sequencing & Microarray Core, The Johns Hopkins University, Baltimore, MD, USA.

2.2.18 Quantitative real-time reverse transcription polymerase chain reaction

Total RNA was isolated and purified by RNeasy Mini Kit (Qiagen, Cologne, Germany), and 1.5 μg of the total RNA was reverse transcribed into cDNA via the M-MLV reverse transcriptase (Invitrogen, Carlsbad, CA, USA) with oligo dT as primer. RT-PCR was performed on an IQ^{TM}5 machine (Bio-Rad) using SYBR® GreenER^{TM} qPCR SuperMix (Invitrogen) in 25 μL reaction with the following PCR cycle parameters as follows: 10 minutes at 95°C (pre-denaturation and hot start),

40 cycles of 35 seconds at 95°C /35 seconds at 58°C/ 30 seconds at 72°C (denaturation/annealing/amplification). The following primers were used for detection of their corresponding mRNA. Bcl-2 forward primer sequence: 5'-CCT GTG GAT GAC TGA GTA CC-3'; Reverse primer sequence: 5'-GAG ACA GCC AGG AGA AAT CA-3' (Sigma). X-IAP forward primer sequence: 5'-CTG AAA AAA CAC CAC CGC TAA C-3'; Reverse primer sequence: 5'-CTA AAT CCC ATT CGT ATA GCT TCT TG-3'; Mdm2 forward primer sequence: 5'- CGG CCT AAA AAT GGC TGC AT -3'; Reverse primer sequence: 5'-TTT GCA CAC GTG AAA CAT GAC A-3'; glyceraldehyde 3-phosphate dehydrogenase (GAPDH) forward primer sequence: 5'-TGC CTC CTG CAC CAC CAA CT-3'; Reverse primer sequence: 5'- CGC CTG CTT CAC CAC CTT C-3'.All RT-PCR assays were completed in triplicate and the threshold cycle of each reaction was converted to DNA equivalent by reading against its corresponding standard curve generated by amplifying dilutions of cDNA containing the relevant target sequences. The relative mRNA expression levels of the target genes were normalized to the mean of GAPDH (Glyceraldehyde 3-phosphate dehydrogenase), which served as the internal control.

2.2.19 Subcellular fractionation

Subcellular fractionation was performed as previously described (Spector et al.,

1997). Briefly, cells were harvested and homogenized in MS buffer [210 mM mannitol, 70 mM sucrose, 5 mM Tris/HCl (pH 7.5), 1 mM EDTA and 1% CompleteTM protease inhibitor cocktail (Roche)] by passing the cell mixture through a 22-gauge needle at 4 °C. The homogenate was centrifuged at 1300 g for 10 min at 4 °C to pellet the nuclei and the unlysed cells. The soluble cytosolic fraction and membrane fractions of the ER (endoplasmic reticulum) and mitochondria were purified from the supernatant by stepwise sucrose-density-gradient centrifugation (Figure 2). The supernatant was suspended in 1 mL of ice-cold MS buffer and laid on the top of a 1.0, 1.2 and 1.5 M sucrose buffer gradient before being centrifuged at 10000 rev./min for 30 min at 4 °C (SW60Ti rotor, Beckman). The soluble cytosolic fraction was collected from the top MS buffer fraction. The gradient-purified ER-containing and mitochondria-enriched fractions were collected at the MS buffer/1.0 M and 1.2/1.5 M sucrose buffer interphases respectively, were washed with MS buffer and dissolved in 0.5% SDS lysis buffer on ice for 30 minutes.

2.2.20 Immunoprecipitation of mitochondria by magnetic beads

Sheep anti-mouse IgG Dynabeads (M-280; Invitrogen) were bound to mouse anti-human mitochondria monoclonal antibody recognizing the surface of the intact mitochondria (Chemicon, Temecula, CA). Briefly, 10 μL of Dynabeads were

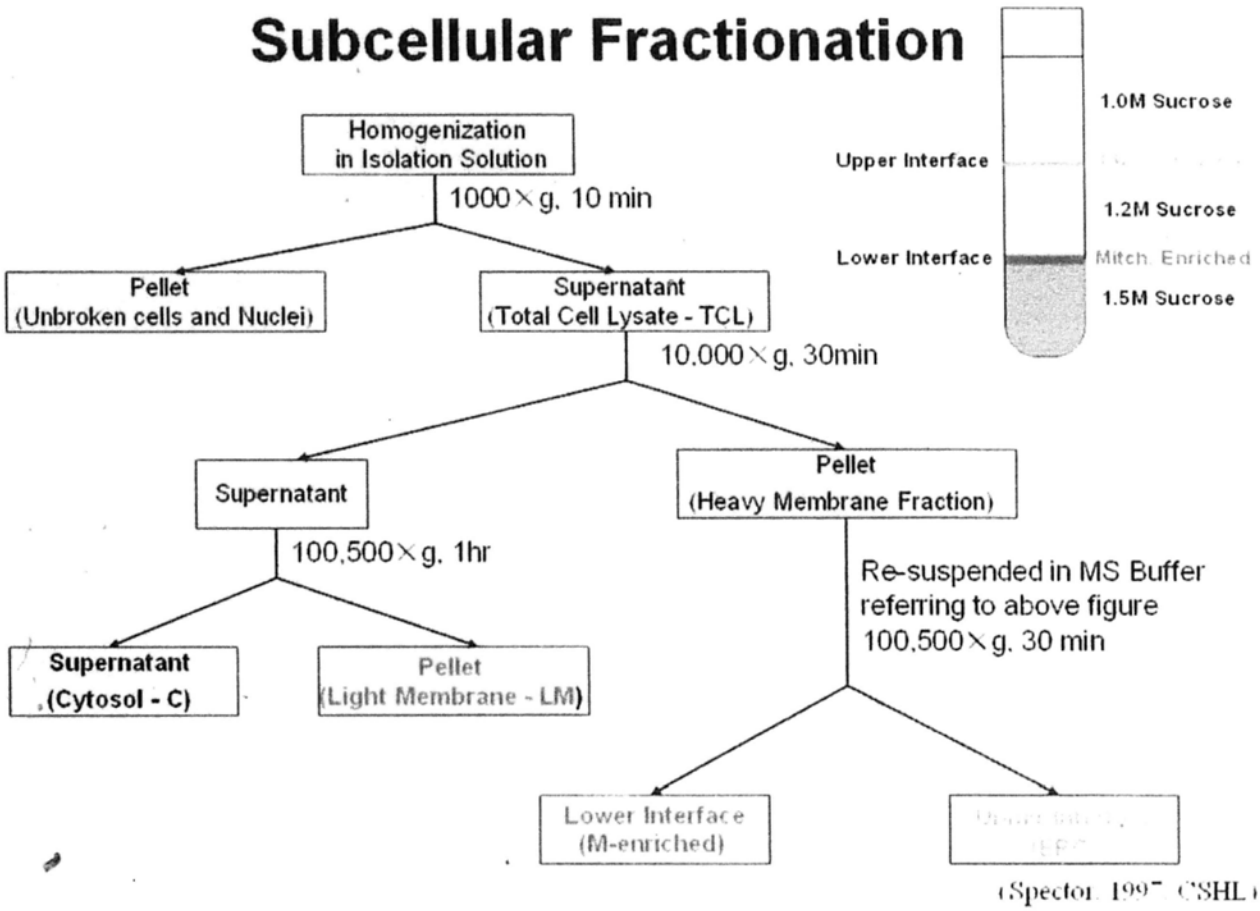

Figure 2 A Subcellular fractionation by sucrose-density-gradient centrifugation

washed with 200 μL of MS buffer, and incubated with 1 μL of antibody in 200 μL of MS buffer with 1% BSA for 3 hours at 4 °C on a rotating wheel. The beads were washed with MS buffer (at 4 °C) to remove unbound antibody, and incubated in 200 μL of MS buffer with 10 mg of COS-7 total cell lysate and protease inhibitor cocktail for 3 hours at 4 °C on a rotating wheel, and then washed with MS buffer. Mitochondrial membrane bound to the beads was subjected to Western blot analysis.

Chapter 3

Reversibility of apoptosis in cancer cells

Chapter 3

Reversibility of apoptosis in cancer cells

3.1 Introduction

The ultimate goal of cancer research is to learn how to cure cancer completely. Despite technological advancement and significant improvements in the treatments of cancer, nowadays, cancer remains one of the top killers of human beings. For the current standard of care for cancer treatments, surgical resection is usually the first step in therapy to remove the major tumor, followed by adjuvant radiation (Stupp et al., 2006). When a complete resection is impossible, chemotherapy is applied as one of the major treatments to destroy the spread cancer cells by exposing body to agents that kill cancer cells more efficiently than the cells in normal tissues (Chabner and Roberts 2005). Cancers initially retreated in response to the repeated course of chemotherapy (Stephens et al., 1977; Norton and Simon 1977; Davis and Tannock 2000; Wu and Tannock 2003; Kim and Tannock 2005). However, cancer recurrence commonly occurs, and results patient death. The common features of cancer cells during cancer recurrence include the increase in mobility (metastasis), growth rate and drug resistance (Kamura 1996; Hentschel and Lang 2003; Kim and Tannock 2005). Accumulating studies reported that over 90% patients die in 5 years with

cancer recurrence after chemotherapy (Villavicencio et al., 2009; Ríos et al., 2007). Until now, there is no effective therapy to suppress cancer recurrence.

To date, a complete picture of how cancer cells escape chemotherapy has not yet emerged. It is generally believed that repopulation of surviving cancer cells during the intervals between treatments is an important cause of the treatment failure (Kim and Tannock 2005). The survival of cancer cells during treatments has been mainly attributed into the deficiency of apoptotic pathways in cancer cells (Letai 2008), anticancer drug resistance of tumorigenic stem cells (Dean et al., 2005), and inefficiency of drug penetration into solid tumors for achieving a therapeutic effect (Minchinton and Tannock 2006). Although studies improving chemotherapy has been carrying on in this direction for past decades, problems of cancer recurrence remains. Therefore, other undiscovered mechanism to contribute into cancer cell survival after chemotherapy might be involved.

3.2 Specific aims

In the present study, we investigated whether cancer cells could survive even after initiation of apoptosis, and test this in various cancer cell lines and in different apoptotic stimuli. Our findings reveal another possibility that may contribute into the

cancer cell survival during therapy: reversibility of apoptosis in cancer cells.

3.3 Results and Discussion

3.3.1 Survival of HeLa cells from jasplakinolide-induced apoptosis

Our aim was to induce cancer cells undergoing apoptosis, and investigate whether the apoptotic dying cancer cells could survive after the removal of apoptotic reagents. We initially exposed human cervical carcinoma HeLa cells to an apoptotic inducer jasplakinolide (Odaka et al., 2000), and observed the change in the cellular morphology by real-time living cell microscopy. Figures 3.1 and 3.2 show that, in untreated healthy cells, mitochondrial network was extensively interconnected and appeared filamentous extended throughout cytoplasm, and nucleus is in round shape, as previous studies described (Kerr et al., 1972; Jacobson et al., 1997; Taylor et al., 2008). In 3hour-induction, as expected, the cells displayed morphological landmarks of apoptosis-associated mitochondrial fragmentation, perinuclear redistribution of mitochondria, nuclear condensation and cytoplasmic shrinkage (Figures 3.1 and 3.2). The initiation of apoptosis was further confirmed by the biochemical landmarks of apoptosis (Wang 2001), the activation of apoptotic protease caspases detected by colorimetric caspases assay (Figure 3.3), and also the dysfunction of mitochondria by MTT assay (Figure 3.4). Then, the apoptotic dying cells were washed and further

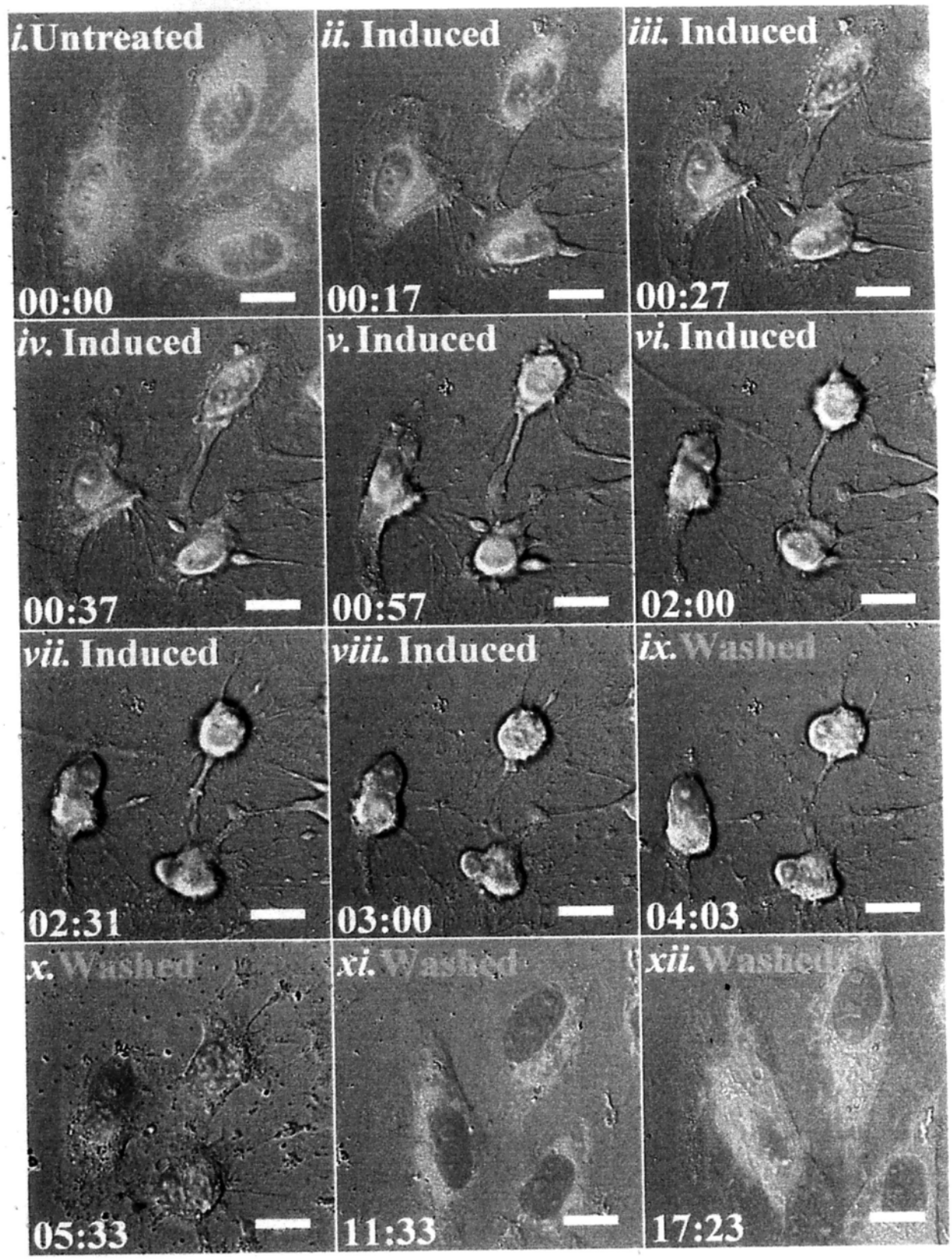
i. Untreated
00:00
ii. Induced
00:17
iii. Induced
00:27
iv. Induced
00:37
v. Induced
00:57
vi. Induced
02:00
vii. Induced
02:31
viii. Induced
03:00
ix. Washed
04:03
x. Washed
05:33
xi. Washed
11:33
xii. Washed
17:23

Figure 3.1 Time-lapse living cell microscopy of HeLa cells under and after jasplakinolide induction. Real time imaging of the same cells before 0.5 μM jasplakinolide induction (Untreated, *i*), induced for 3hours (Induced, *ii* to *viii*), and then washed and further incubated with fresh culture medium for another 14.5hours (Washed, *ix* to *xii*). Merged images: mitochondria (red) and nucleuses (blue) were visualized by fluorescence, and cell morphology was by DIC. Time presented as hour:minute. Scale bar, 10 μm.

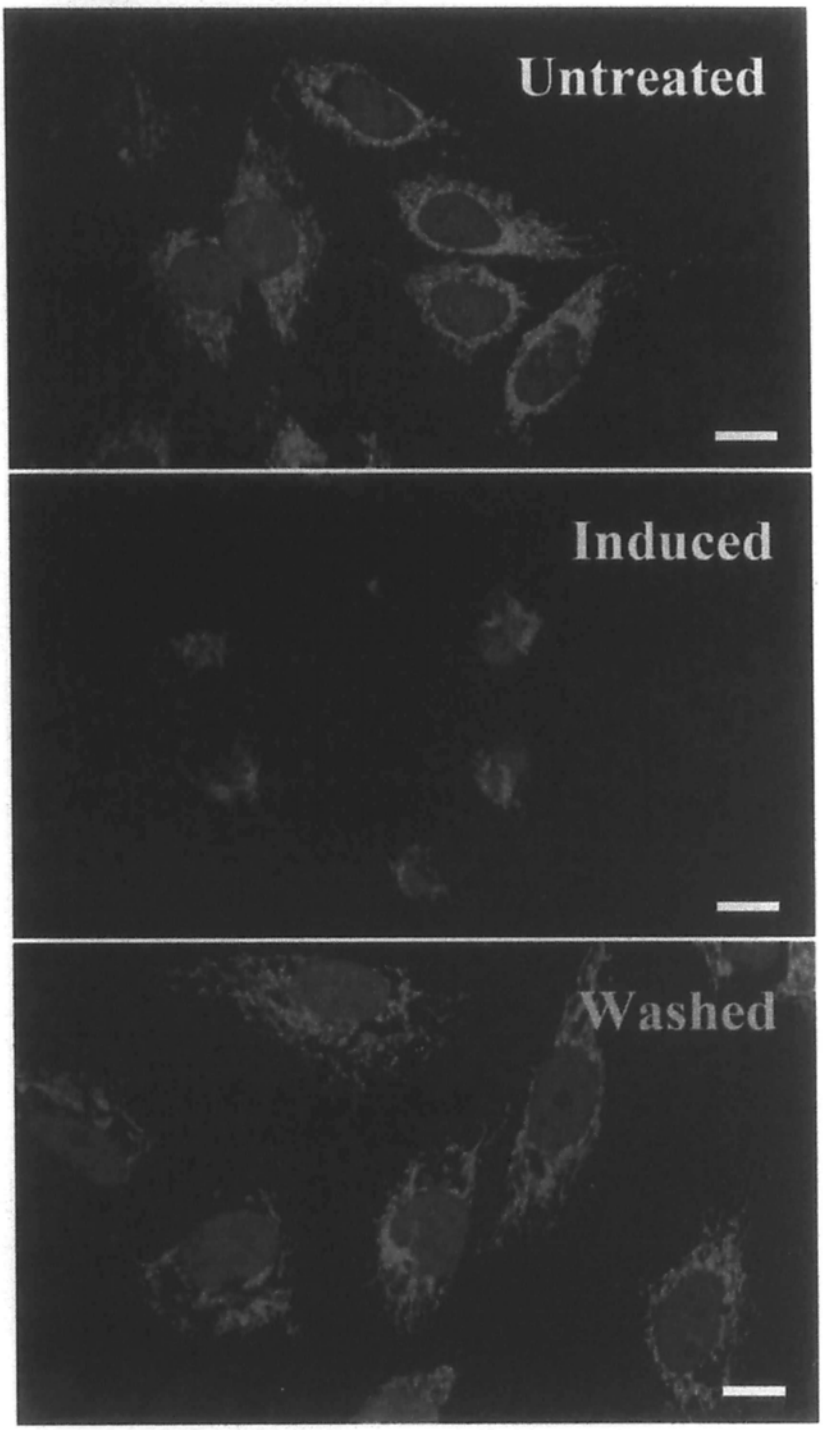
Untreated
Induced
Washed

Figure 3.2 Confocal microscopy for verification on the morphological alterations of HeLa cells during reversal of apoptosis. Confocal imaging of the HeLa cells before 0.5 μM jasplakinolide induction (Untreated), induced for 3hours (Induced), and the induced cells washed and further incubated with fresh culture medium for another 24hours (Washed). Merged images: mitochondria (red) and nuclei (blue) were visualized by fluorescence. Scale bar, 10 μm.

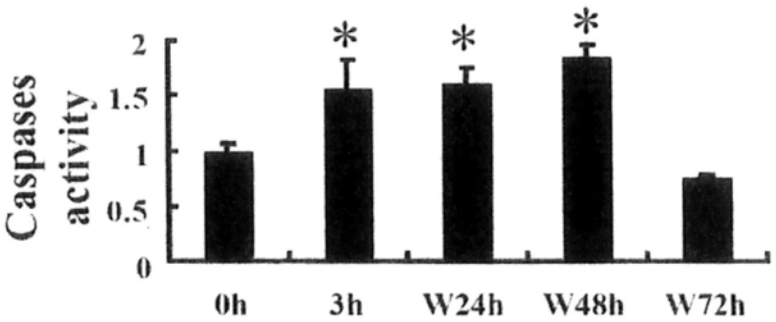

Figure 3.3 Caspases activity of the HeLa cells during apoptotic induction and reversal of apoptosis. Caspases activity of the cells before the 0.5 μM jasplakinolide induction (0h), induced for 3hours (3h), and then washed and cultured for 24hours (W24h), 48hours (W48h) and 72hours (W72h). A thousand of corresponding cells were subjected to caspases assay. The degree of corresponding caspases activities were normalized with the control. Mean $\pm$ s.d, n=3, $^*P<0.02$.

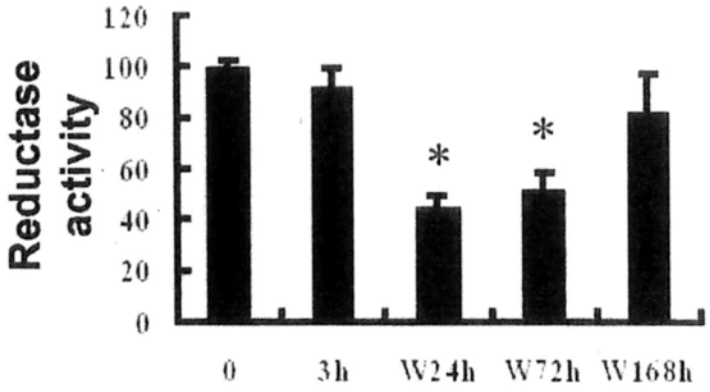

Figure 3.4 Reductase activity of the HeLa cells during apoptotic induction and reversal of apoptosis. Reductase activity of the untreated HeLa cells before the 0.5 μM jasplakinolide induction (0h), induced for 3hours (3h), and then washed and cultured for 24hours (W24h), 72hours (W48h) and 168hours (W168h). Mean $\pm$ s.d. n=3, *P<0.02.

cultured in fresh cell medium (the wash). It has been generally assumed that cell displaying all these apoptotic landmarks are determined to die (Kerr et al., 1972; Jacobson et al., 1997; Green and Kroemer 2004; Taylor et al., 2008). Mitochondrial destruction and activation of caspases have been known to indicate irreversible cell death (Green and Kroemer 2004; Riedl and Shi 2004). Here, we reasoned that, if the apoptotic dying cells could survive even after the activation of caspases, the cells should be able to restore themselves and proliferate after the wash.

Interestingly, our results indicate that HeLa cells could actually survive after the apoptotic induction. Our living cell microscopic analysis showed that the shrunk cells regained their normal cellular morphology in 14.5 hours after the wash (Figure 3.1). Our confocal microscopic analysis was performed to verify the morphological recovery of the cells at 24 hours after removal of the inducer (Figure 3.2). The cell counting results showed that 96% cell displayed all the morphological landmarks of apoptosis in 3 hour-induction, while 92% of the cells regained their normal morphology after the wash in 24 hours (Figures 3..2 and 3.5). Besides, the caspases and mitochondria activity also returned back to the level of the control cells in 72 hours and 168 hours after the wash, respectively (Figures 3.3 and 3.4). Furthermore, survival of the cells after the wash was proven by cell proliferation. The result of cell

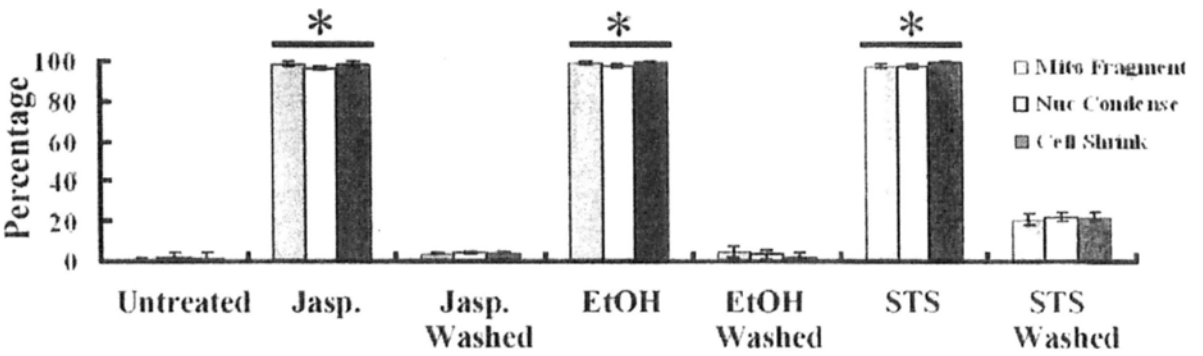

Figure 3.5 Reversibility of apoptosis in HeLa cells in different apoptotic inductions. Percentage of cells showing mitochondrial fragmentation (Mito. Fragment), nuclear condensation (Nuc. Condense), and cell shrinkage (Cell Shrink) of the control HeLa cells (Untreated), the cell treated with 0.5 μ M jasplakinolide for 3hours (Jasp.), 6% (v/v) ethanol for 30 min (EtOH) or staurosporine for 1hour (STS), and the corresponding cells washed and cultured with fresh medium for 24hours (Washed). Mean $\pm$ s.d., n=3, *P<0.02.

count showed the increase in the cell number after the removal of the inducer (Figure 3.6).

3.3.2 Nuclear fragmentation as point of no return in apoptosis

The cell survival after reversal of apoptosis was further assessed by the uptake of a DNA synthesis marker bromodexyuridine (BrdU) (Figure 3.7a). The percentage of proliferation of the cells did not significantly differ between the control and the 3 hour-induced cells after the wash (Figure 3.7a). Our data shows that the morphological and biochemical landmarks of apoptosis vanished in 24 hours after the removal of the apoptotic jasplakinolide induction, and the induced cells survived afterward. Noticeably, our time-course study in cell count showed that the percentage of cell displaying nuclear fragmentation increased along the continuous apoptotic induction, and that was inversely proportional to the cell proliferation ability after removal of the apoptotic reagent at that time point (Figure 3.7a and b). Perhaps nuclear fragmentation is the apoptotic landmark event indicating the irreversible stage of apoptosis.

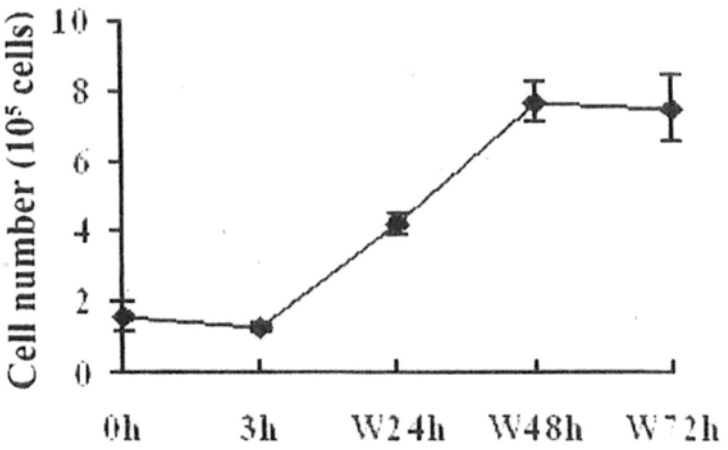

Figure 3.6 Proliferation of the jasplakinolide-induced cells after removal of inducer. HeLa cells were induced with 0.5 μM jasplakinolide for 3hours (3h), then washed and further incubated in fresh medium for 24hours (W24h), 48hours (W48h) and 72hours (W72h). Mean $\pm$ s.d., n=3.

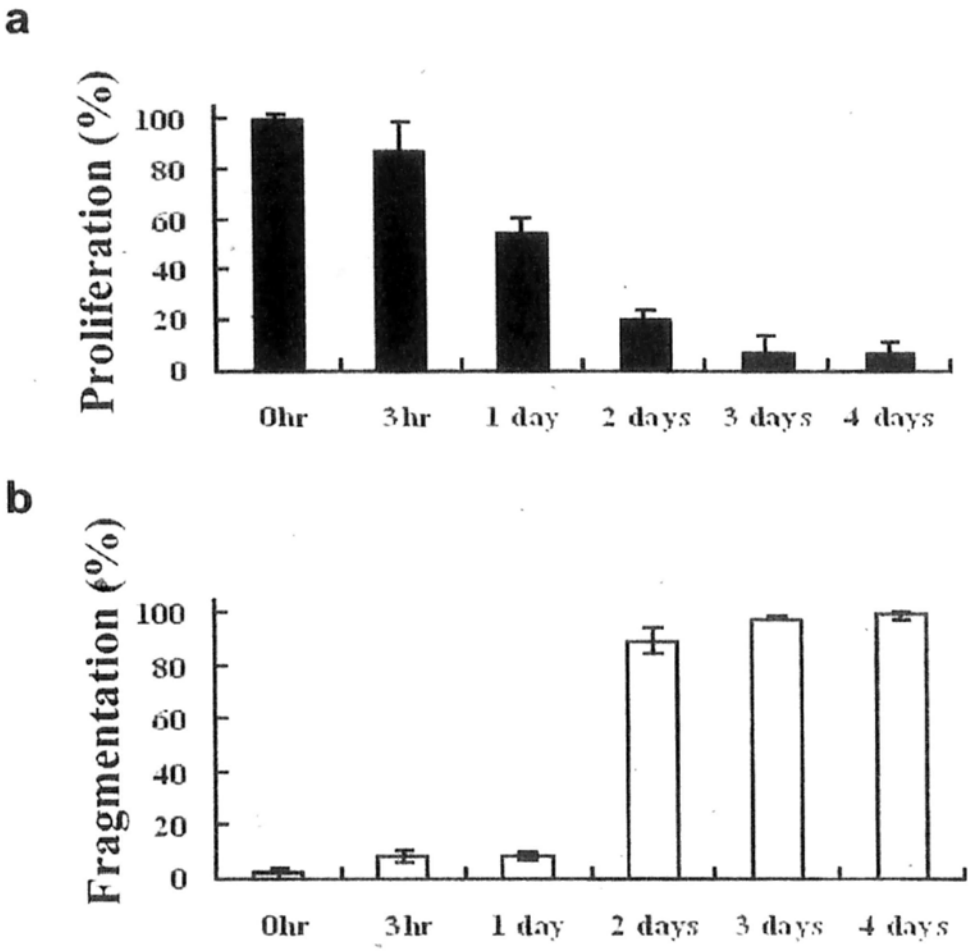

Figure 3.7 Reversibility of apoptosis after different duration of jasplakinolide-induction. HeLa cells were treated with 0.5 μM of jasplakinolide for 0 hour (0hr), 3 hours (3hr), 1 day, 2 days, 3 days and 4 days.

a) Percentage of HeLa cell proliferation (detected by BrdU assay) after removal of the inducer at the indicated time and cultured for another 5 days in fresh medium.

b) Percentage of corresponding cells showing nuclear fragmentation (detected by fluorescence microscopy followed by cell counting) at the inducted time before the removal of the inducer.

Mean $\pm$ s.d, n=3.

3.3.3 Reversibility of apoptosis in different inducers and in various cancer cell lines

Our discovery on reversibility of jasplakinolide-induced apoptosis in HeLa cells evoked a novel phenomenon that cancer cells could survive after initiation of apoptosis, and therefore promoted us to investigate whether this is a general phenomenon in different apoptotic inductions and in various cancer cell lines. Our results on other apoptotic stimuli to HeLa cells showed that, in response to the induction of apoptotic inducers ethanol and staurosporine (Young et al., 2003; Bertrand et al., 1994), HeLa cells underwent apoptosis characterized by excessive mitochondrial fragmentation, nuclear condensation and cell shrinkage (Figure 3.5). After removal of the inducers, the indicated cells regained their normal morphology in 24 hours in the culture of fresh medium. In further experiments, jasplakinolide was applied to various cancer cell lines which are widely used in cancer research including human skin cancer A375, liver cancer HepG2, breast cancer MCF7 and prostate cancer PC3 cells, and all of them displayed the morphological features of apoptosis (Figure 3.8). Consistently, after removal of jasplakinolide, the morphological recovery was observed in 24 hours in all the cell lines (Figure 3.8). These results suggest that the reversibility of apoptosis is a general phenomenon in cancer cells.

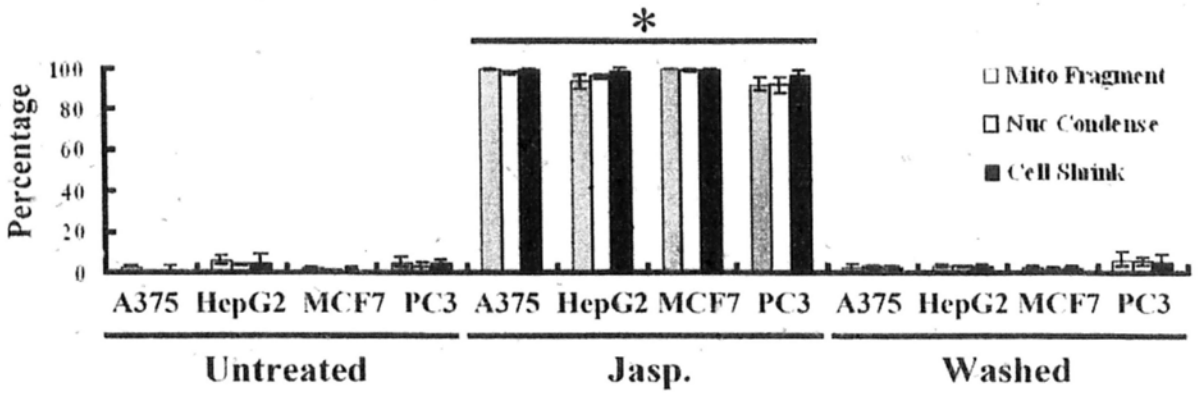

Figure 3.8 Reversibility of jasplakinolide-induced apoptosis in various cancer cell lines. Percentage of cells showing mitochondrial fragmentation (Mito. Fragment), nuclear condensation (Nuc. Condense), and cell shrinkage (Cell Shrink) of the control A375, HepG2, MCF7 and PC-3 cells (Untreated), the corresponding cells treated with 0.5 μM jasplakinolide for 3hours (Jasp.), and washed and cultured with fresh medium for 24hours (Washed). Mean $\pm$ s.d., n=3, *P<0.02.

3.3.4 Increase in cell mobility after reversal of apoptosis in HeLa cells

This study focuses the potential correlation between reversal of apoptosis in cancer cells and metastasis during recurrence. We study whether the mobility of cancer cells increases after reversal of apoptosis, as metastasis, which involves invasion characterized by the increase in mobility of cancer cells (Steeq 2006), is a common feature during cancer recurrence (Arimura et al., 2005; Orlando et al., 2009; Nguyen et al., 2009). We therefore studied the mobility of the cells before and after reversal of apoptosis

Our living cell microscopic analysis showed that the untreated HeLa cells remained in their original location during our 40-hour experimental period, and even the cells underwent cell division or spontaneous apoptosis (Figure 3.9a). We then studied the mobility of HeLa cells after reversal of jasplakinolide-induced apoptosis. In response to an apoptotic inducer jasplakinolide, HeLa cells displayed morphological hallmarks of apoptosis including fragmentation of mitochondria, condensation of nucleus and shrinkage of cytoplasm, and also biochemical hallmark of apoptosis the activation of caspases (Figures 3.1 and 3.9b *i* to *ii*). After removal of the inducer, the apoptotic dying cells survived and the hallmarks retracted (Figures

a

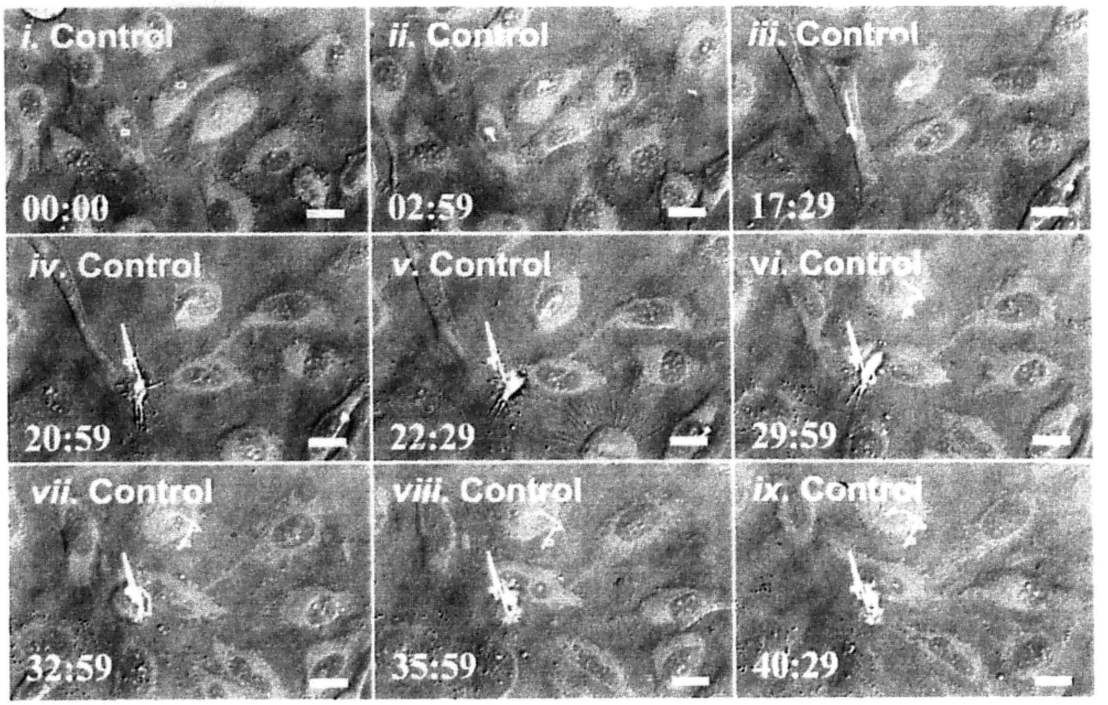
i. Control
00:00
ii. Control
02:59
iii. Control
17:29
iv. Control
20:59
v. Control
22:29
vi. Control
29:59
vii. Control
32:59
viii. Control
35:59
ix. Control
40:29

b

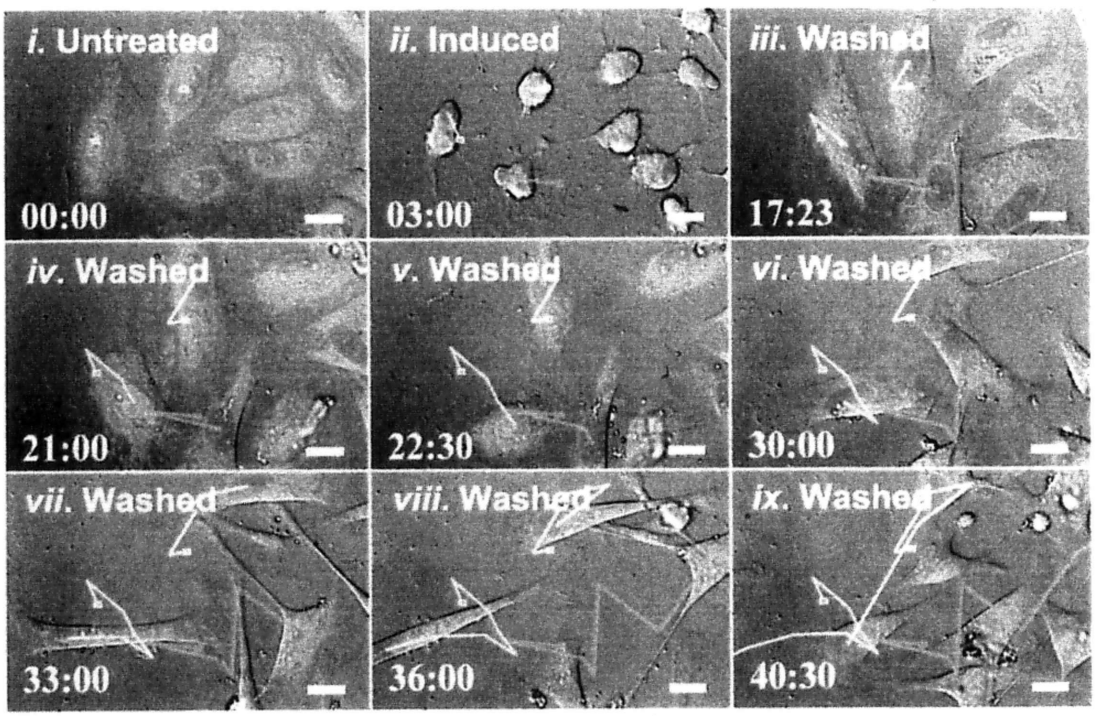
i. Untreated
00:00
ii. Induced
03:00
iii. Washed
17:23
iv. Washed
21:00
v. Washed
22:30
vi. Washed
30:00
vii. Washed
33:00
viii. Washed
36:00
ix. Washed
40:30

Figure 3.9 Increase in mobility of HeLa cells after reversal of Jasplakinolide - induced apoptosis.

a) Time-lapse living cell microscopy of the cell without jasplakinolide induction (Control). The green path follows the cells that underwent cell division; the yellow path follows the cell without division; the white path follows the cell that underwent spontaneous apoptosis.

b) Time-lapse living cell microscopy of the same cell before 0.5 μM jasplakinolide induction (Untreated, *i*), induced for 3 hours (Induced, *ii*), and then washed and further incubated with fresh culture medium for another 37 hours (Washed, *iii* to *ix*).

Green, white and yellow lines indicate the footprints of the corresponding same cells throughout the experiment with time. In figure 3B ix, only the cell with white footprint is present in the original view while the other 2 cells have migrated out of the monitored view. Merged images: mitochondria (red) and nuclei (blue) were visualized by fluorescence, and cell morphology was by DIC. Time presented as hr:min.

Scale bar, 10 μm.

3.1 and 3.9b *iii*). We further analyzed the imaging at later time points data, and found that the cells displayed a significant increase in cell mobility (Figure 3.9b *iii* to *ix*). After quantification, our data shows that the mobility of the HeLa cells after reversal of apoptosis was 3 times higher than the untreated HeLa cells (Figure 3.10).

Furthermore, the increase in mobility was also observed in the reversal of ethanol-induced apoptosis in HeLa cells. Our microscopic study showed that, in response to ethanol induction, HeLa cells displayed morphological hallmarks of apoptosis (Figure 3.11 *ii* to *iv*). Consistently, after removal of the inducer, the cell regained their normal morphology (Figure 3.11*v* to *vii*), followed by cell migration (Figure 3.11a *viii* to *xx*), in which the cells velocity was 5 times higher than the untreated cells (Figure 3.12). This finding agrees with the time-course analysis on the reversal of jasplakinolide-induced apoptosis in HeLa cells (Figure 3.9).

3.4 Conclusion

In the present study, we have shown that cancer cells could survive after initiation of apoptosis induced by different stimuli, and the reversibility of apoptosis was observed in various cancer cell lines. We provided evidence that cancer cells could escape from demise even after the cells undergoing critical apoptotic events such as

a

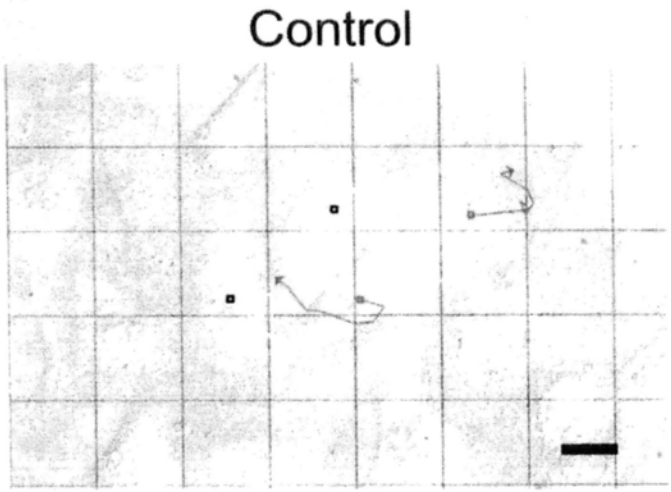

b

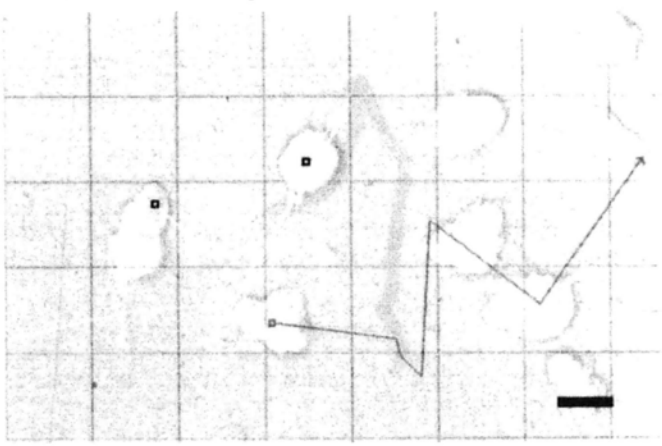

c

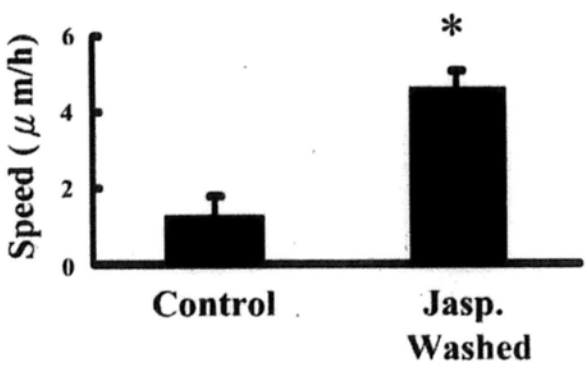

Figure 3.10 Quantification of speed of the corresponding cells indicated in the figures 3.9a (Control) and 3.9b (Jasp. Washed).

a) Foot print of the untreated HeLa cells (Control) corresponding to the figure 3.9a.

b) Foot print of the HeLa cells reversed the jasplakinolide-induced apoptosis (Jasp. Washed) corresponding to the figure 3.9b. Scale bar, 10 μm.

c) Speed of cell movement of the Control and Jasp. Washed cells was measured as described in Materials and Methods. Mean ±s.d., n=3, *P<0.001.


i. Untreated
00:00
ii. Induced
00:10
iii. Induced
00:30
iv. Induced
00:51
v. Washed
00:56
vi. Washed
01:11
vii. Washed
02:00
viii. Washed
03:30
ix. Washed
04:30
x. Washed
05:30
xi. Washed
06:00
xii. Washed
06:30
xiii. Washed
07:30
xiv. Washed
08:00
xv. Washed
08:30
xvi. Washed
09:30
xvii. Washed
10:00
xviii. Washed
10:30
xix. Washed
11:00
xx. Washed
13:30

Figure 3.11 Increase in mobility of HeLa cells after reversal of ethanol-induced apoptosis.

Time-lapse living cell microscopy of the same cell before 5% ethanol induction (Untreated, *i*), induced for 55mins (Induced, *ii* to *iv*), and then washed and further incubated with fresh culture medium for another 13 hours (Washed, *v* to *xx*). Green, white and yellow lines indicate the footprints of the corresponding same cells throughout the experiment with time. Merged images: mitochondria (red) and nuclei (blue) were visualized by fluorescence, and cell morphology was by DIC. Time presented as hr:min. Scale bar, 10 μm.

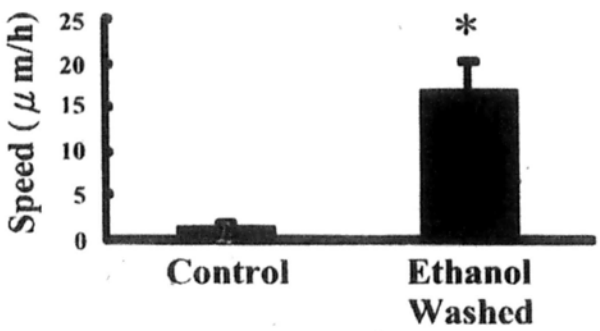

Figure 3.12 Quantification of speed of the corresponding cells indicated in the figures 3.9a (Control) and 3.11 (Ethanol Washed). Speed of cell movement was measured as described in Materials and Methods. Mean ±s.d., n=3, *P<0.001.

mitochondrial fragmentation and dysfunction, nuclear condensation, cell shrinkage and activation of caspases. Importantly, the reversibility of apoptosis was abolished when the cells reached the apoptotic event of nuclear fragmentation, suggesting that this is an important cellular event indicating the point-of-no-return in apoptosis.

We also found the increase in mobility of cancer cells after reversal of apoptosis. This suggests a potential important correlation between reversal of apoptosis in cancer cells and metastasis during cancer recurrence. To date, resection is an important treatment to remove localized tumor. To promote complete resection, multiple doses of chemotherapy are applied as a presurgical anti-cancer treatment in order to reduce the size to tumor before surgical treatment. Original tumor can be completely removed, however, cancer recurrence is often observed, and new tumors are commonly found at great distance from the site of the major tumor. As mobility of cancer cells increases after reversal of apoptosis, it could be possible that reversal of apoptosis occurs during intervals between cycles of chemotherapy, and the reversed cancer cells migrate to distance site away from the tumor. Therefore, the migrated cells form new tumors while the original tumor was removed. In case that is true, interference on reversal of apoptosis in cancer cells should suppress cancer recurrence and metastasis after therapies.

Our discovery on the reversibility of apoptosis in cancer cells lead to several unanswered key questions: what are the components of the machinery driving the reversibility of apoptosis, and how are they linked to the regulation of apoptosis in cancer cells as a whole? To what extent does the reversibility of apoptosis contribute to the survival, the repopulation and the metastasis of cancer cells during the cycles of anti-cancer treatment? Intriguingly, can inhibition on the reversibility of apoptosis in cancer cells suppress cancer relapse? Providing answers to these questions will be critical in understanding the mechanism for regulation on the reversibility of apoptosis, and provide us new potential targets for therapeutic advancement to our war of cancer. A more in-depth analysis will be required to clarify these points.

Chapter 4

Cells that survive by reversing apoptosis harbor lasting DNA damage

Chapter 4

Cells that survive by reversing apoptosis harbor lasting DNA damage

4.1 Introduction

Genomic destruction is a hallmark apoptosis (Kerr et al., 1972; Jacobson et al., 1997; Taylor et al., 2008). During this cell suicide process, mitochondria fragment (Figures 4.1 and 4.2) (Taylor et al., 2008; Green and Kroemer 2004), releasing apoptosis-inducing factor (AIF) and endonuclease G (EndoG), which then translocate to the nucleus and fragment DNA (Figure 4.3) (Liu et al., 1997; Susin et al., 1999). Independently, intrinsic and extrinsic pro-apoptotic signals activate apoptotic protease caspase-3, which then unlocks DNA fragmentation factor (DFF40) by cleaving its inhibitor DFF45 (Figure 4.4) (Liu et al., 1997). Activated caspase-3 also damages DNA repair systems for example, by cleaving the DNA repair enzyme Poly(ADP)-ribose polymerase-1 (PARP) (Lazebnik et al., 1994) (Figure 4.4). Activated caspase-3 also activates additional caspases to strengthen caspase cascade for cellular demolition (Taylor et al., 2008), resulting the morphological manifestations of apoptosis (Kerr et al., 1972; Jacobson et al., 1997; Taylor et al., 2008) including nuclear condensation, cell shrinkage, and membrane blebbing

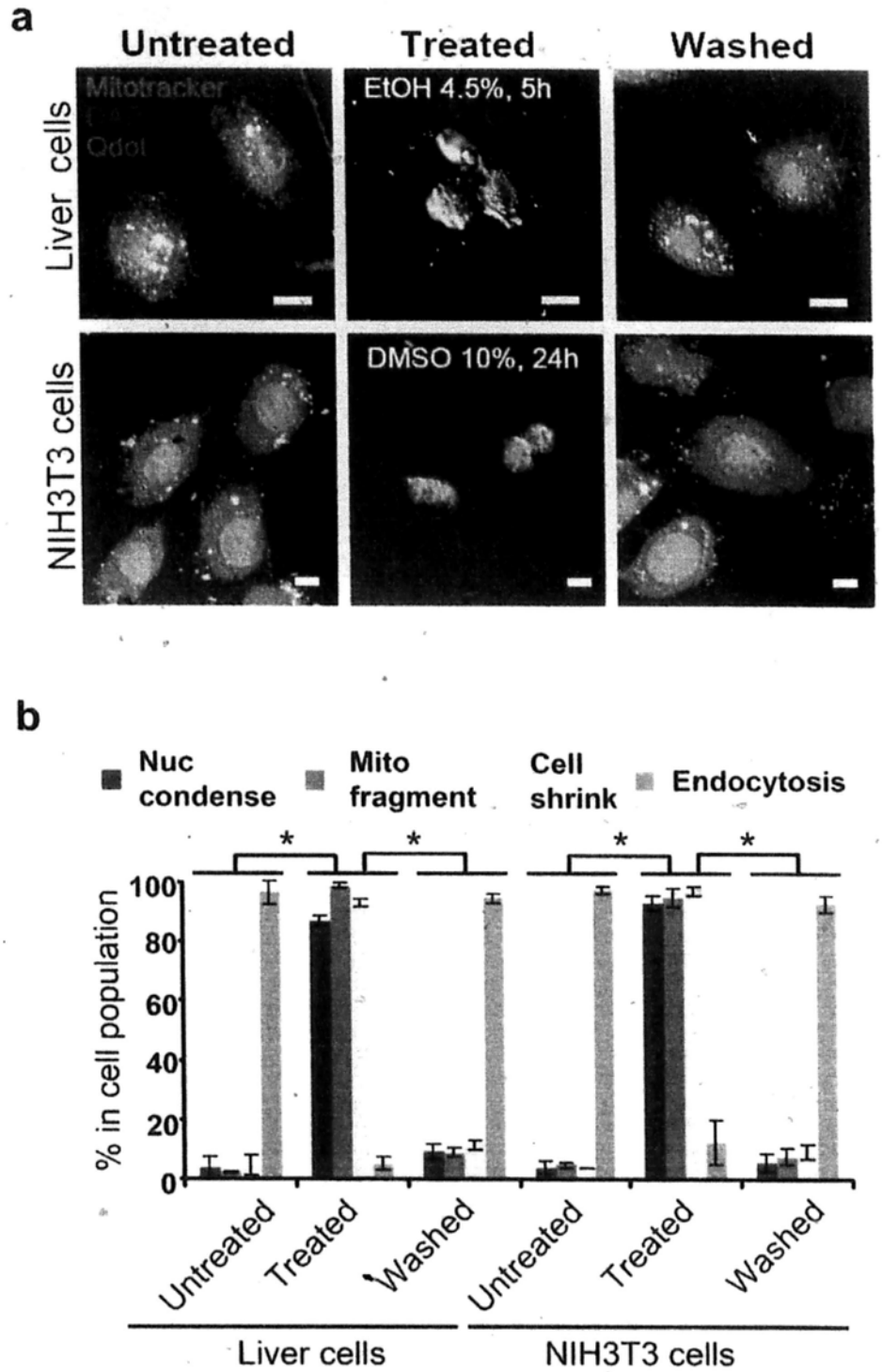
a
Untreated
Treated
Washed
Liver cells
NIH3T3 cells
Mitotracker
Qdot
EtOH 4.5%, 5h
DMSO 10%, 24h
b
Nuc condense
Mito fragment
Cell shrink
Endocytosis
% in cell population
100
80
60
40
20
0
*
*
*
*
Untreated
Treated
Washed
Untreated
Treated
Washed
Liver cells
NIH3T3 cells

Figure 4.1 Reversibility of apoptosis in mouse primary liver cells and mouse embryonic fibroblast NIH3T3 cells.

a) Fluorescence and DIC microscopy of healthy (untreated) liver and NIH3T3 cells, the cells were exposed to apoptotic inducers (Liver cells: 4.5% ethanol for 5 hours; NIH3T3 cells: 10% DMSO for 20 hours) (treated), and the induced cells were washed to remove apoptotic inducers and further cultured for 24 hours (Washed). Merged images: Mitotracker stains for mitochondria (red), Hoechst (DAPI) for nucleus (blue), Quantum dots (Qdot) taken up by endocytosis (green). Scale bar, 10 μ m.

b) Percentage of the untreated, the treated and the washed liver cells and NIH3T3 cells that displayed mitochondrial fragmentation (Mito fragment), nuclear condensation (Nuc condense), cell shrinkage (Cell shrink) and uptake of Quantum dots by endocytosis (Endocytosis).

Mean$\pm$ s.d., n=3, *P<0.01.

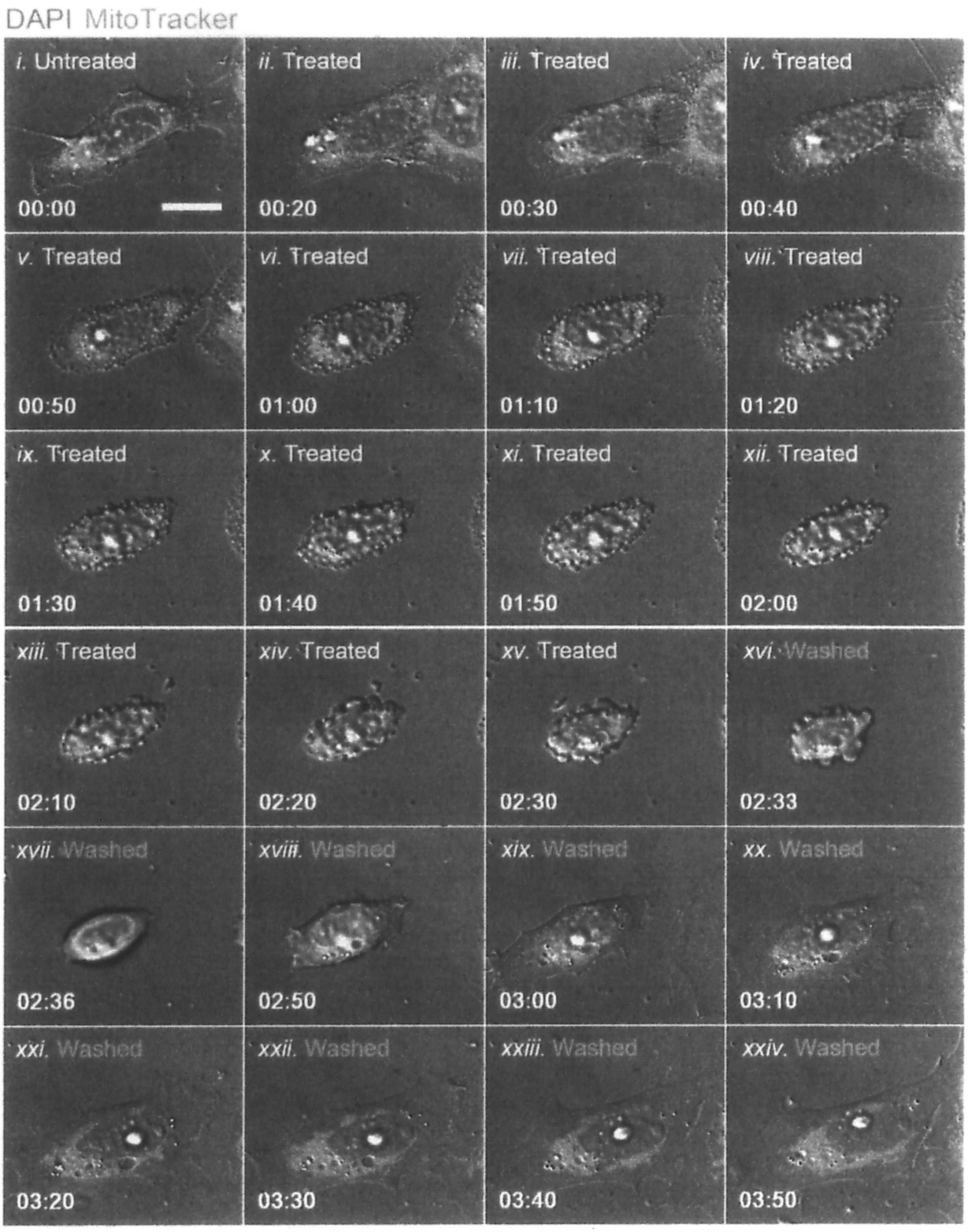
DAPI MitoTracker
i. Untreated
00:00
ii. Treated
00:20
iii. Treated
00:30
iv. Treated
00:40
v. Treated
00:50
vi. Treated
01:00
vii. Treated
01:10
viii. Treated
01:20
ix. Treated
01:30
x. Treated
01:40
xi. Treated
01:50
xii. Treated
02:00
xiii. Treated
02:10
xiv. Treated
02:20
xv. Treated
02:30
xvi. Washed
02:33
xvii. Washed
02:36
xviii. Washed
02:50
xix. Washed
03:00
xx. Washed
03:10
xxi. Washed
03:20
xxii. Washed
03:30
xxiii. Washed
03:40
xxiv. Washed
03:50

Figure 4.2 Real-time living cell microscopy of a primary liver cell before, during and after exposure to ethanol.

Time-lapse living cell image of the same liver cell before ethanol induction (Untreated, *i*), induced by 4.5% of ethanol in culture medium for 2.5 hours (treated, *ii* to *xv*), and then washed and further cultured with fresh medium (Washed, *xvi* to *xxiv*). Merged images: mitochondria (red) and nuclei (blue) were visualized by fluorescence, and cell morphology by DIC microscopy. Time is shown in hour:minute. Scale bar, 10 μm.

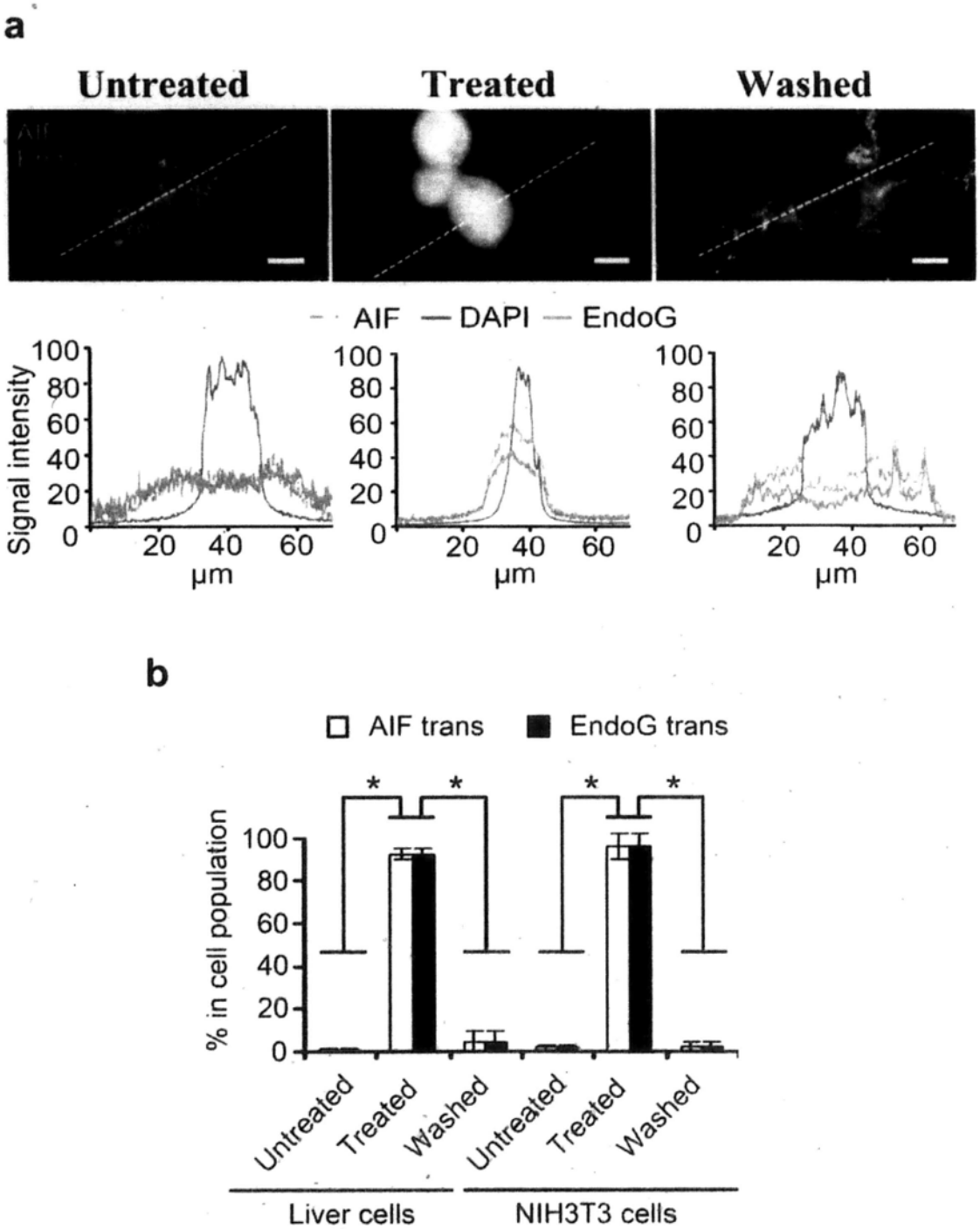
a
Untreated
Treated
Washed
AIF
DAPI
EndoG
Signal intensity
100
80
60
40
20
0
20
40
60
μm
b
AIF trans
EndoG trans
% in cell population
*
Untreated
Treated
Washed
Liver cells
NIH3T3 cells

Figure 4.3 Fluorescence microscopy for the subcellular localization of AIF (green), EndoG (red) and nucleus (blue) in the untreated, the treated and the washed primary liver cells.

a) Quantification of the corresponding fluorescence signals of AIF, EndoG and nucleus along the dotted line as indicated at their respective images. Scale bar, 10 μ m.

b) Percentage of the untreated, the treated and the washed liver cells and NIH3T3 cells that displayed nuclear translocation of AIF (AIF trans) and EndoG (EndoG trans).

Mean $\pm$ s.d., n=3, *P<0.01.

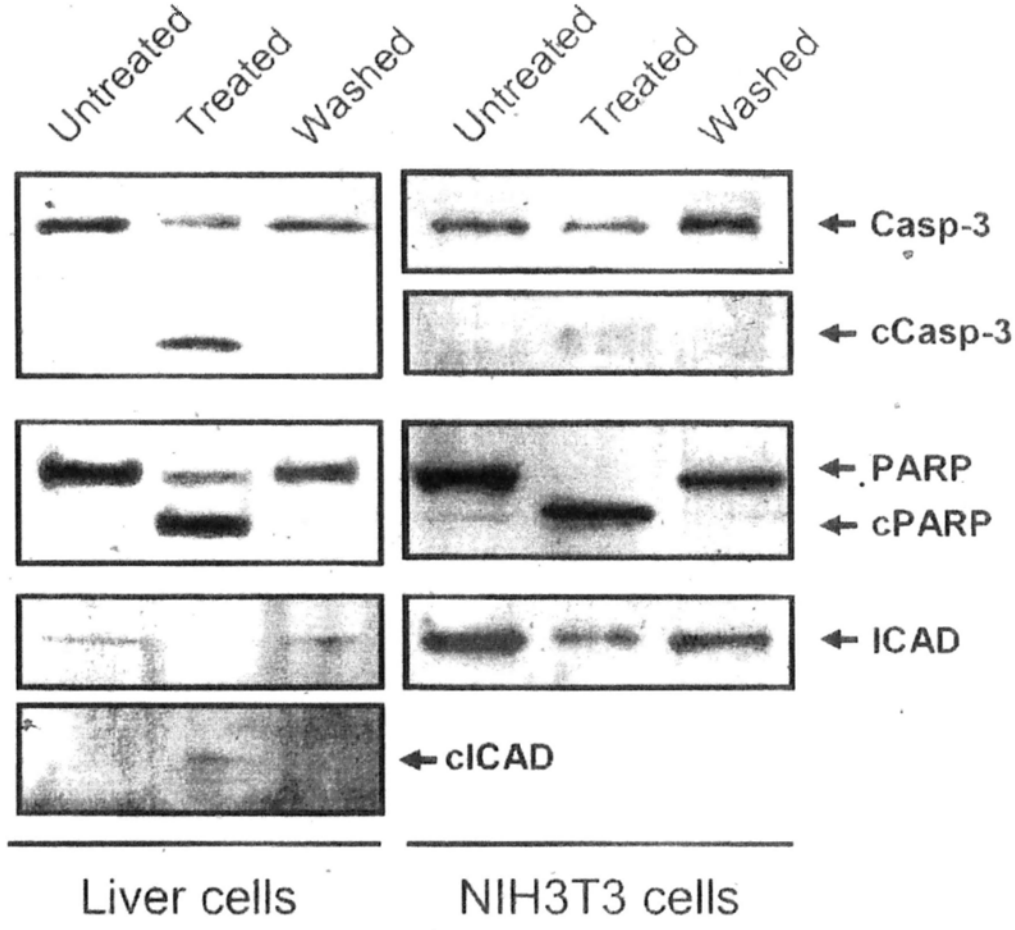

Figure 4.4 Western blot analysis on the total cell lysate of the untreated, the treated, and the washed liver cells and NIH3T3 cells for the protein level of caspase-3 (Casp), PARP and ICAD. c, cleaved form. Note that the cleaved form of ICAD in NIH3T3 cells was not recognized by the ICAD primary antibody.

(Figure 4.1).

4.2 Specific aims

While genomic destruction has been generally assumed to be the critical death checkpoint, recent studies reveal that apoptotic cancer cells can reverse apoptosis even after they have experienced mitochondrial fragmentation and caspase-3 activation (Tang et al., 2009; Albeck et al., 2008) which suggested that surviving cells might harbor DNA damage caused during the apoptotic process (Sheridan and Martin 2008). Therefore we decided to investigate the underlying mechanisms and consequences of the reversal of apoptosis (Figure 1).

4.3 Results and discussion

4.3.1 Reversibility of apoptosis in primary cell and cell line

We first tested the reversibility of apoptosis in primary mouse liver cells and the embryonic fibroblast NIH3T3 cell line, as they are important models for studies of general cellular mechanisms of apoptotic cell death and oncogenesis (McKillop and Schrum 2005; Rubin 2008). Ethanol and dimethyl sulfoxide (DMSO) serve as apoptotic inducers owing to their cytotoxicity and low mutagenicity (Phillips and Jenkinson 2001; Santos et al., 2003). Exposing liver cells to ethanol or NIH3T3

cells to DMSO resulted in the expected morphological (Figures 4.1 and 4.2), molecular (Figure 4.3) and biochemical (Figure 4.4) hallmarks of apoptosis. We defined reversal of apoptosis as the loss of these hallmarks following removal of the apoptotic inducers. Interestingly, after washing and then culturing the apoptotic cells in fresh medium for 24 hours, all these signs of apoptosis vanished (Figure 4.1 to Figure 4.4). Using real-time living cell fluorescence microscopy, we verified that the morphologically characterized apoptotic liver cell could regain its normal morphology after removal of the apoptotic inducer (Figure 4.2). The survival of the cells that had experienced reversal of apoptosis was further assessed by their ability to take up Quantum dots (Jaiswal et al., 2003) through endocytosis (Figure 4.1). In contrast, dying cells exposed to continuous apoptotic induction exhibited full permeability of the plasma membrane and shrank in size (Figure 4.5) (Silva et al., 2008). From these experiments, we conclude that reversal of apoptosis does occur in these two models.

4.3.2 Activation of apoptotic nucleases and damage of DNA in the dying cells before reversal of apoptosis

Destruction of the genome by apoptotic nucleases such as mitochondrial mediated nuclear translocation of AIF and EndoG (Figure 4.3) (Susin et al., 1999; Li et al.,

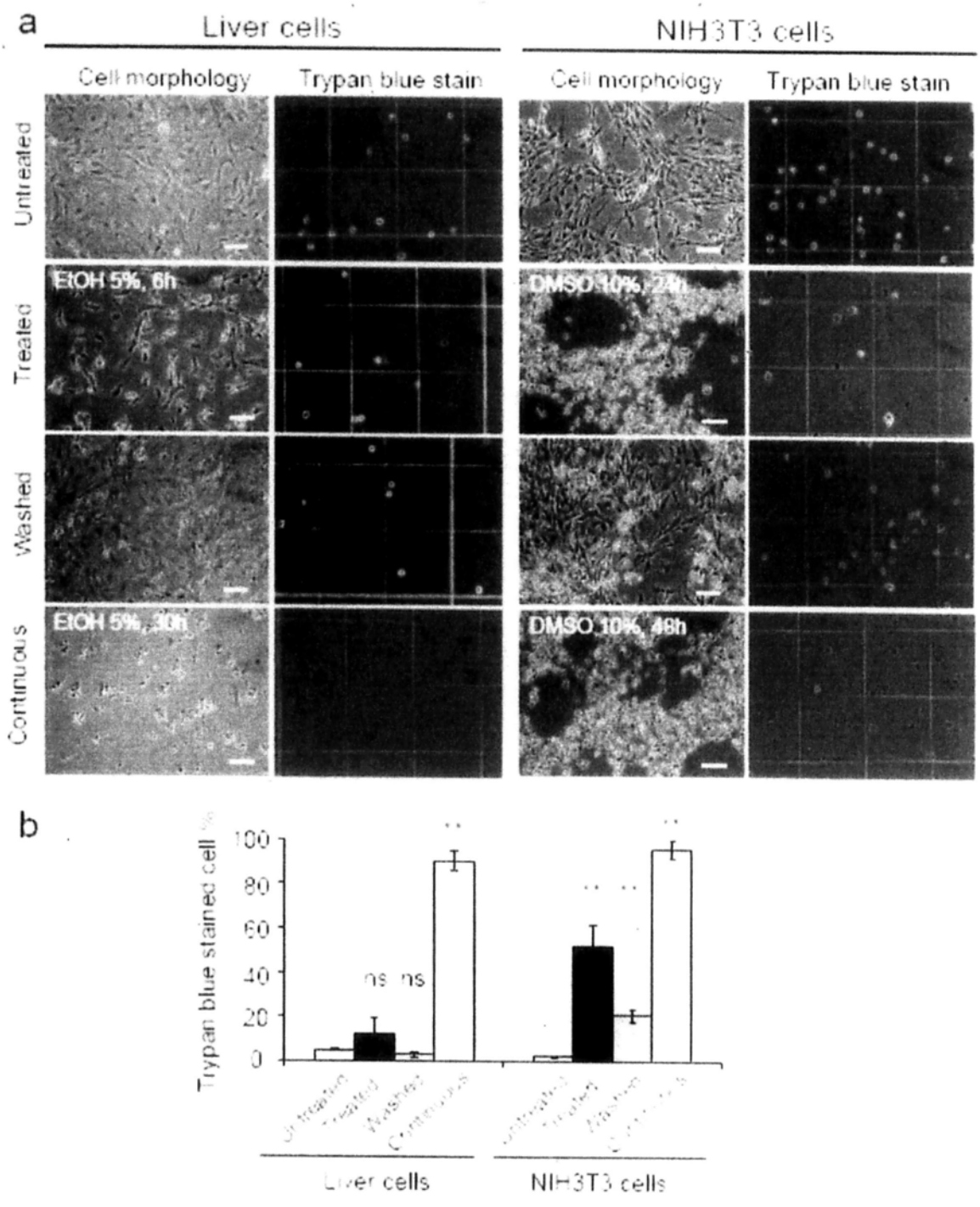
a
Liver cells
NIH3T3 cells
Cell morphology
Trypan blue stain
Cell morphology
Trypan blue stain
Untreated
Treated
Washed
Continuous
EtOH 5%, 6h
DMSO 10%, 24h
EtOH 5%, 30h
DMSO 10%, 48h
b
Trypan blue stained cell %
100
80
60
40
20
0
ns
ns
**
**
**
**
Liver cells
NIH3T3 cells

Figure 4.5 Plasma membrane integrity of the primary liver cells and NIH3T3 cells in apoptotic inductions and after reversal of apoptosis.

a) Phase contrast images of the untreated (Untreated), the apoptosis-induced (treated), the washed (Washed), and the continuously induced (Continuous) liver cells and NIH3T3 cells on culture plate and in trypan blue stain after trypsinization. Apoptotic induction of liver: 4.5% ethanol in culture medium for 5 hours; NIH3T3: 10% DMSO in culture medium for 20 hours. Scale bar, 100 μ m.

b) Percentage of the untreated, the treated, the washed, and the continuously induced liver cells and NIH3T3 cells that displayed trypan blue stain.

Mean $\pm$ s.d., n=3, ns: $P>0.05$; $^{**}P<0.01$.

2001) as well as caspase-3-mediated DFF40 (Figure 4.4) (Liu et al., 1997). DNA destruction is a universal feature of apoptosis (Kerr et al., 1972; Jacobson et al., 1997; Taylor et al., 2008). The activation of these nucleases suggested that DNA damage occurred before cells reversed apoptosis. By immunofluorescence microscopy and quantitative analysis, we found that AIF and EndoG, which normally reside in mitochondria, translocated to the nucleus in dying liver and NIH3T3 cells before the removal of apoptotic stimuli (Figure 4.3). Our Western blot analysis also showed cleavage of the inhibitor of caspase-activated deoxyribonuclease (ICAD) in the apoptotic dying cells (Figure 4.4), and that indicates the unlocking of CAD, the DFF40 in mouse form (Sakahira et al., 1998; Enari et al., 1998), for DNA destruction in the dying cells before they reversed apoptosis.

We then evaluated the actual genome damage in the dying cells before reversing apoptosis by single cell gel electrophoresis (comet) assay, which detected DNA damage (Figure 4.6), including DNA single- and double-strand breaks in the individual cells (Olive, P. L. & Banath 2006). After removal of apoptotic inducers, the DNA damage significantly reduced (Figure 4.6). This indicates that cells with DNA damage can survive and reverse the process.

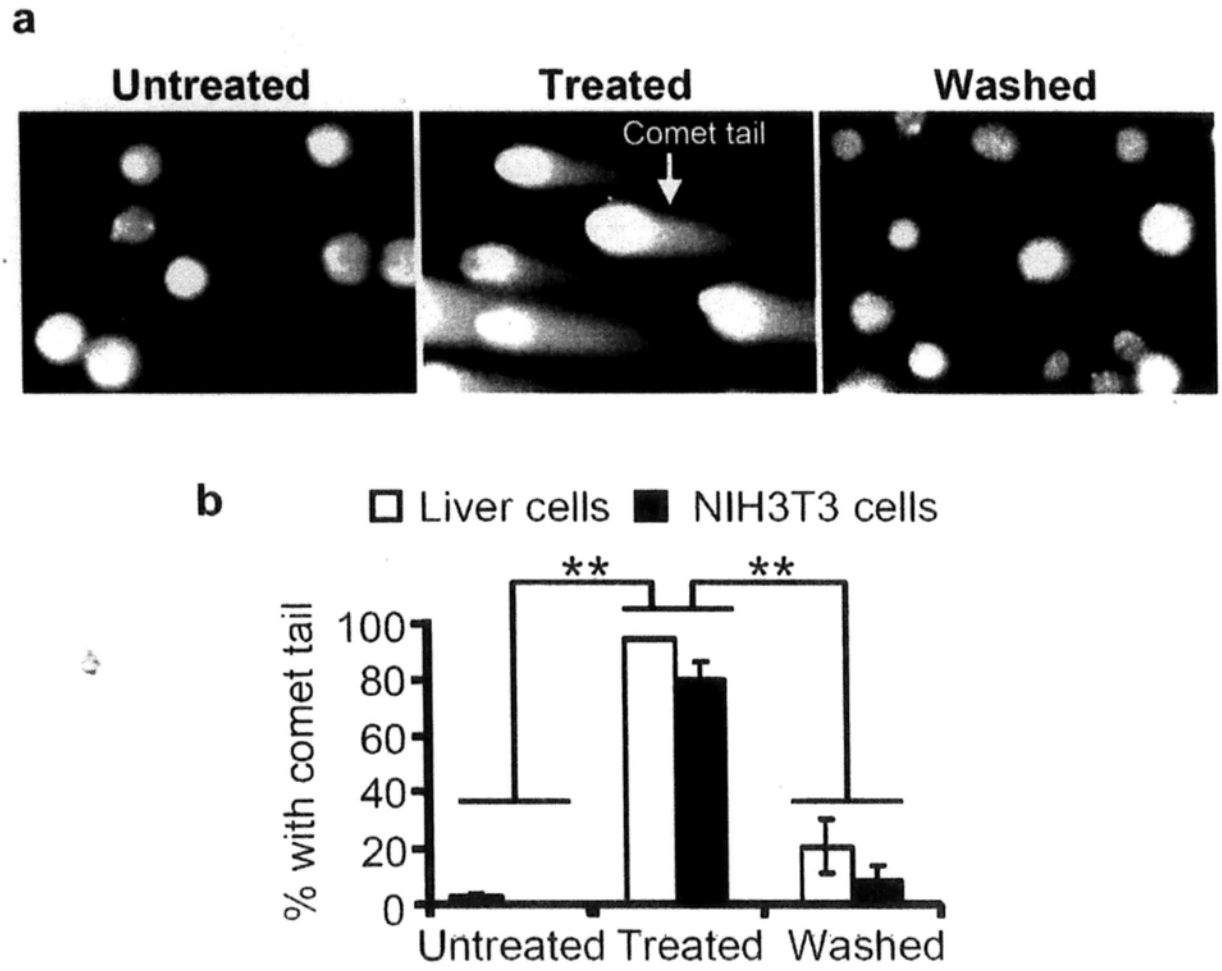

Figure 4.6 Damage of DNA in the dying cells before reversal of apoptosis

a) Fluorescence microscopy for the DNA stain of the untreated, the treated and the washed liver cells subjected to comet assay. Damaged DNA ran out from nuclear envelop after electrophoresis, and displayed comic tail as indicated in one of the treated cells by arrow. Intact DNA unmigrated, remained in nuclear envelop as in the untreated cells.

b) Percentage of the untreated, the treated and the washed liver cells and NIH3T3 cells that displayed comet tail.

Mean $\pm$ s.d., n=3, $^{**}P<0.01$.

4.3.3 Genetic alterations of the cells after reversal of apoptosis

To address how completely the DNA damage could be repaired, we performed cytokinesis-block micronucleus assays. Following reversal of apoptosis we observed an increase in the number of binucleated cells to display micronuclei (Figure 4.7), which are biomarkers of DNA damage, chromosome breakage and/or whole chromosome loss in the dividing cells (Fenech 2007). The formation of micronuclei evidences unrepaired DNA damage (Figure 4.8), possibly due to damage of DNA repair mechanisms. This is supported by the caspase-3 mediated cleavage of DNA-repairing enzyme PARP (Figure 4.4) as interference of PARP results in genome instability and deficiency in DNA repair (Rouleau 2010). The cleaved form of PARP also inhibits the repairing function of remaining uncleaved PARP (D'Amours et al., 2001) in the cells.

The emergence of unrepaired DNA damage in the cells after reversal of apoptosis raises the question of whether their daughter cells acquire genetic alterations. Therefore, we performed karyotyping on colchicine-treated, metaphase-arrested cells three days after they reversed apoptosis. We found a significant increase in chromosomal aberrations including variations in chromosomal number (Figure 4.9) and radial configurations, the latter resulted from misjoining of broken chromatids

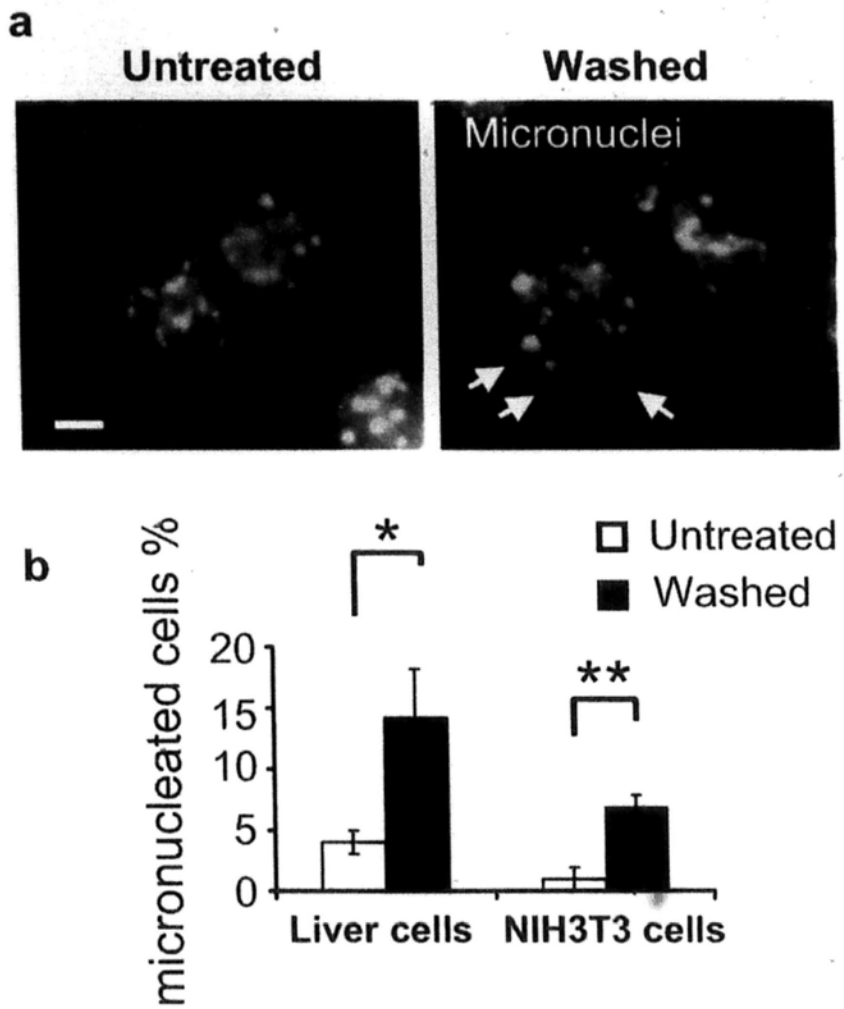

Figure 4.7 Formation of micronuclei after reversal of apoptosis

a) Fluorescence microscopy on nuclear morphology of the untreated and the washed binucleated primary liver cells 16 hours after reversal of apoptosis. Arrows indicate micronuclei in the washed cells.**b)** Percentage of the untreated, the treated and the washed liver cells and NIH3T3 cells that displayed comet tail. Scale bar, 10 μ m.

b) Percentage of the untreated and the washed binucleated liver cells and NIH3T3 cells that displayed micronuclei.

Mean $\pm$ s.d., n=3, *P<0.05, **P<0.01.

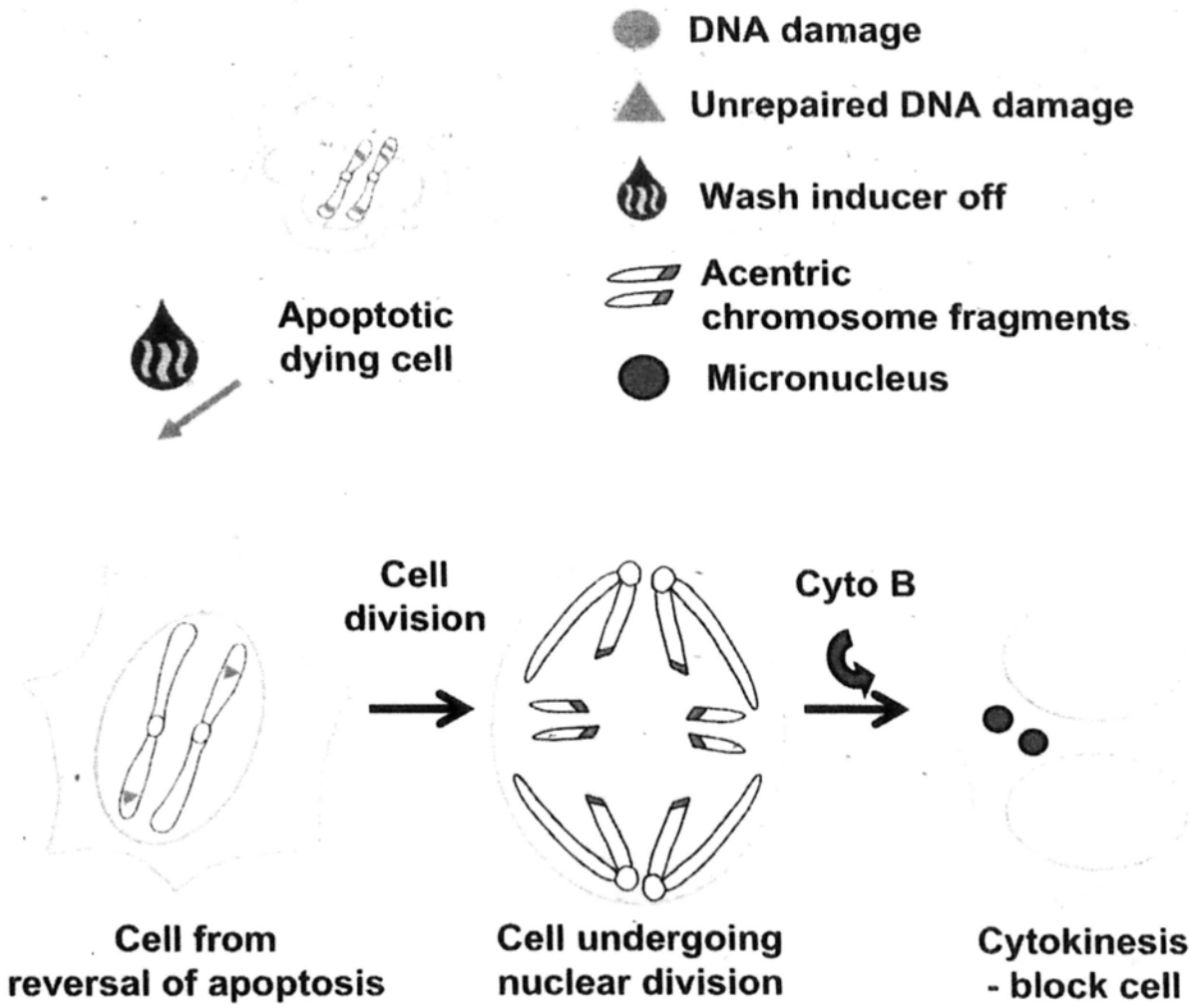

Figure 4.8 Proposed model for the formation of micronuclei in the once-divided cells after reversal of apoptosis as the result of unrepaired DNA damage.

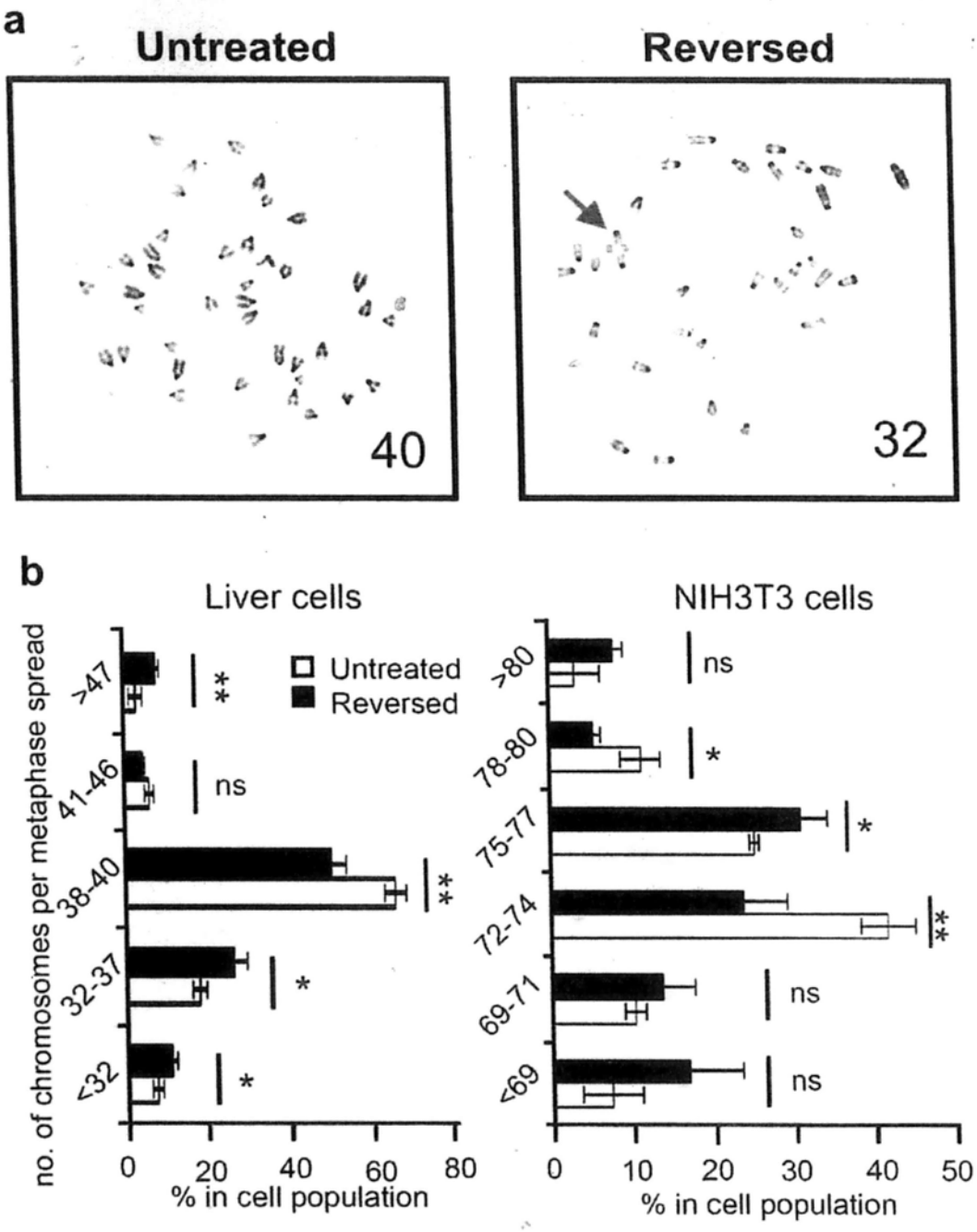

Figure 4.9 Genetic alterations after reversal of apoptosis

a) Inverted DAPI-banding image of metaphase spread of the untreated and the washed liver cells 3 days after reversal of apoptosis (Reversed). Number of metaphase chromosomes was labeled at the corresponding images. Abnormal chromosomal configuration is indicated by an arrow.

b) Percentage of the untreated and the reversed liver and NIH3T3 cells displaying indicated number of chromosomes in metaphase spread.

Error bars denote s.d., n=3, ns: $P>0.05$, *$P<0.05$, **$P<0.01$.

(German et al., 1964) (Figure 4.10), comparing with the untreated cells. This indicates the inheritance of alterations in genome of the cells after reversal of apoptosis.

4.3.4 Transformation of the cells after reversal of apoptosis

Acquisition of heritable genetic alterations in individual cells promotes phenotypic diversity (Stratton et al., 2009; Bloom et al., 1972), and can lead to transformation (Bloom 1972; Rubin 2008) Therefore we tested whether NIH3T3 cells undergone reversal of apoptosis had higher transformation potential than control cells. These cells displayed classic transformed phenotypes, including focus formation, an indication of loss of contact inhibition of growth (Figure 4.11), and proliferation in soft agar, indicating anchorage independent growth (Figure 4.12). These phenotypes are also hallmarks of cancer cells (Bloom et al., 1972; Rubin 2008; Mori 2008), suggesting that reversal of apoptosis may represent a novel mechanism of carcinogenesis.

4.3.5 Critical role of transcription in reversal of apoptosis

To gain insight into the mechanism by which cells reverse apoptosis and survive, we first tested whether new transcription contributes to the reversal of apoptosis. We

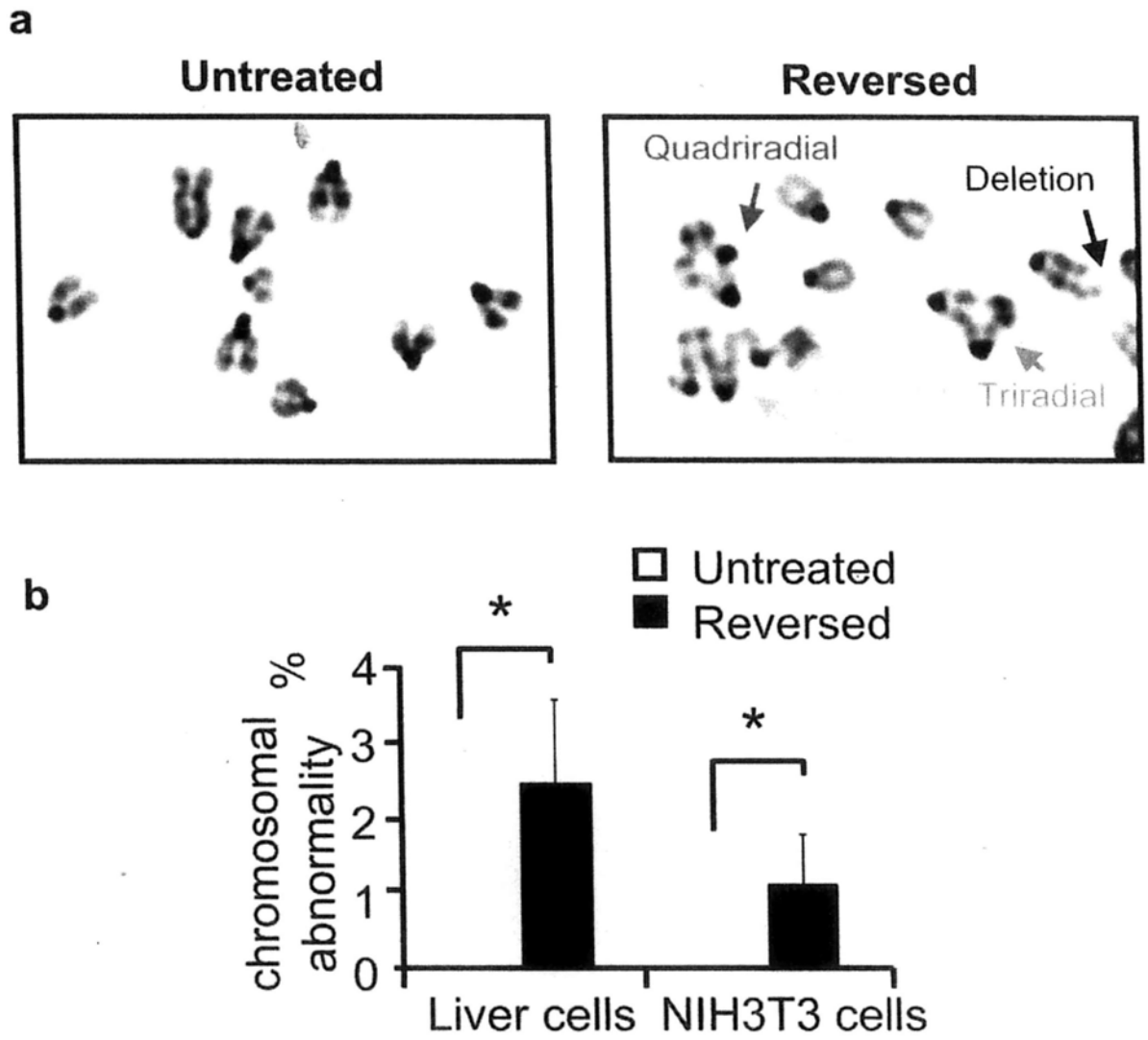

Figure 4.10 Chromosomal abnormality after reversal of apoptosis

a) Representing inverted DAPI-banding images of the configuration of metaphase chromosomes of the untreated and the reversed liver cells. Configuration indicated by arrows: triradial (red); quadriradial (blue); complex figures (green). Deletion (black).

b) Percentage of the untreated and the reversed liver and NIH3T3 cells displaying indicated number of chromosomes in metaphase spread.

Mean $\pm$ s.d., n=3, *P<0.05.

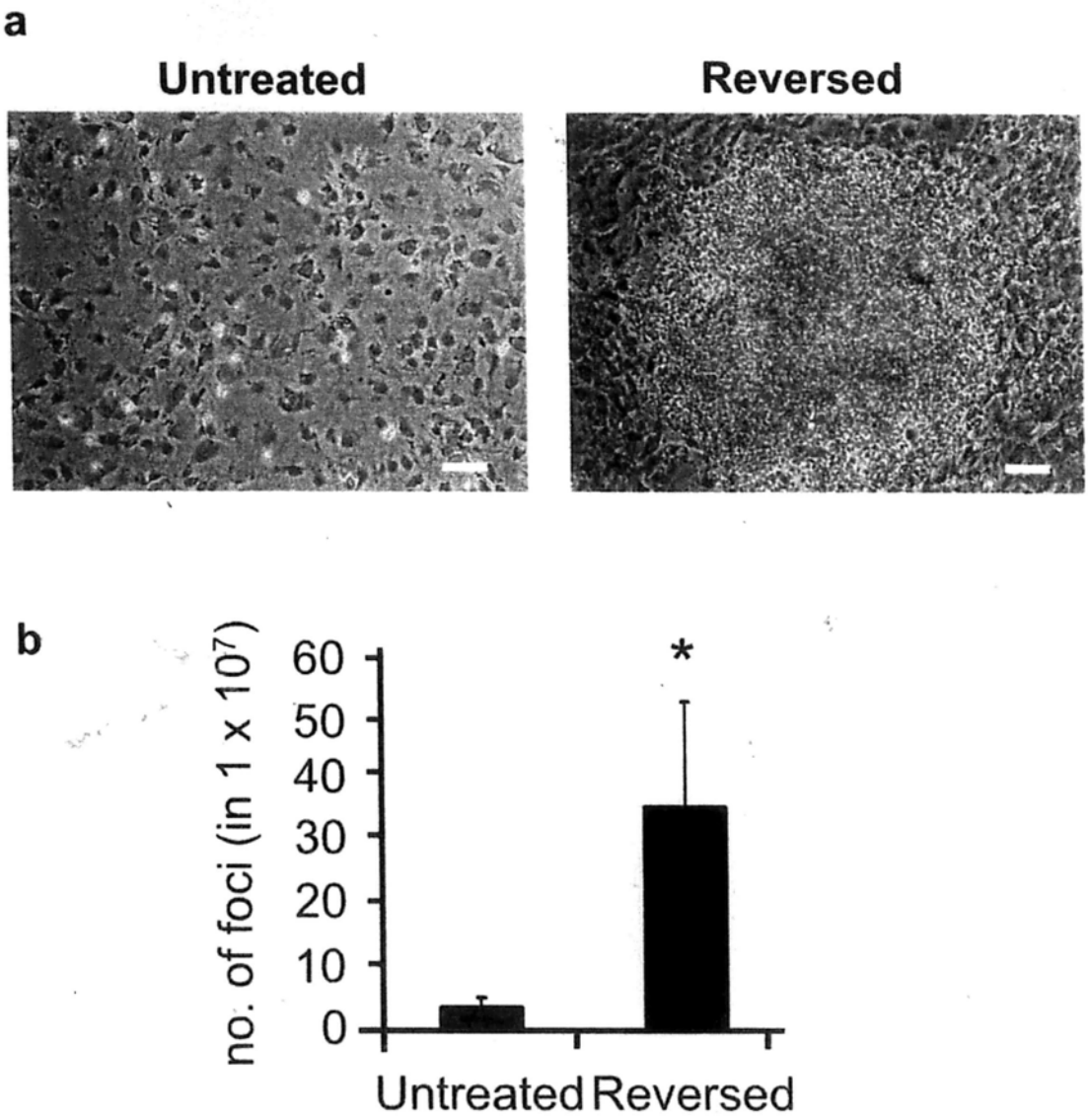

Figure 4.11 Foci formation of NIH3T3 cell after reversal of apoptosis

a) Image of the untreated NIH3T3 cells and the focus from the cells after reversal of apoptosis (Reversed) after 3 weeks of culture. Scale bars: 50 μ m.

b) Number of foci of the untreated and the reversed NIH3T3 cell cultures at 3 weeks of culture.

Mean $\pm$ s.d., n=3, *P<0.05.

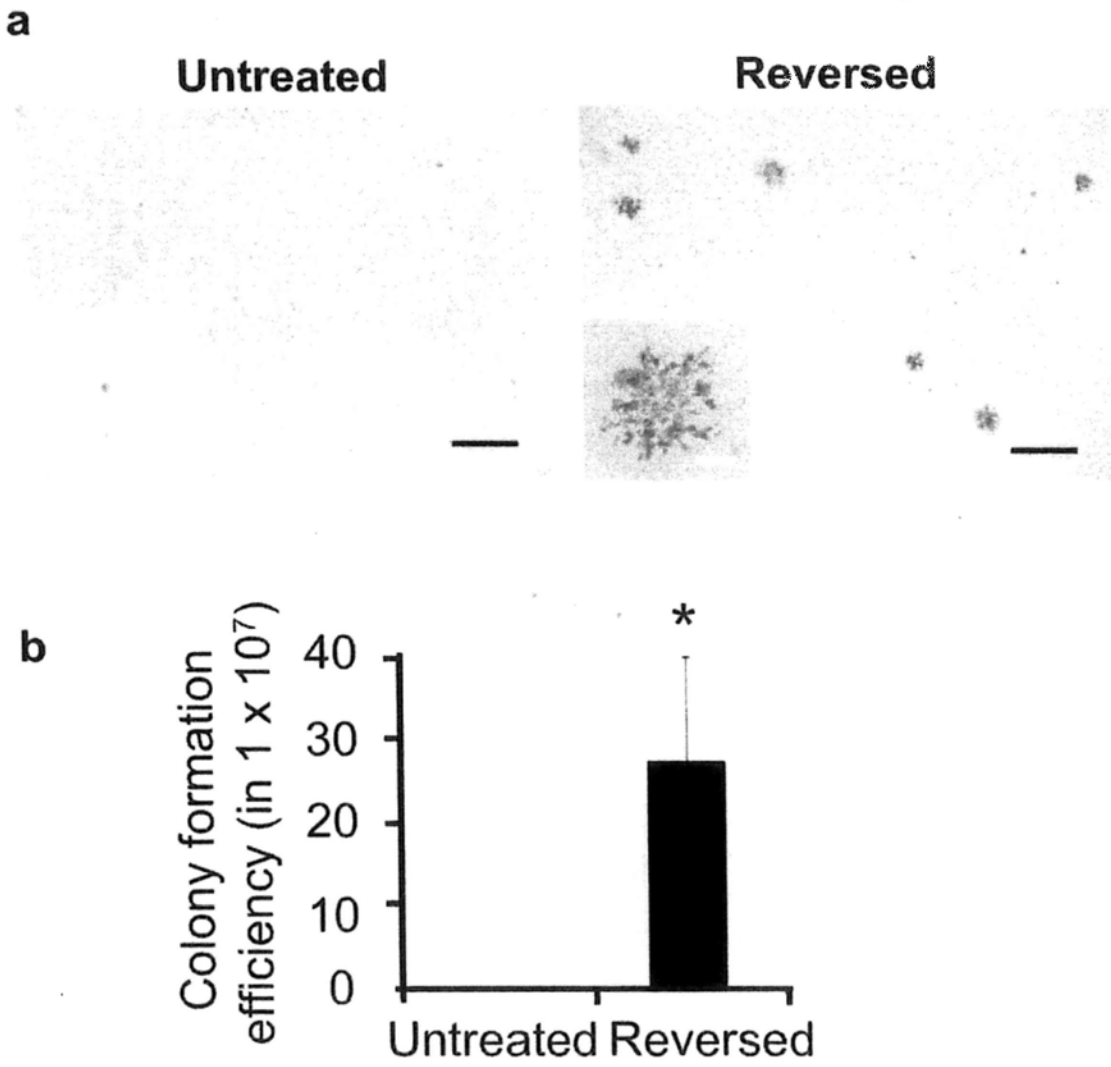

Figure 4.12 Anchorage independent growth of NIH3T3 cell after reversal of apoptosis

a) Image of crystal violet stained colonies in soft agar of the untreated and the reversed NIH3T3 cells from the foci at the third week of culture. Insert: enlarged image of a colony. Scale bars: 400 μ m (white); 2 mm (black).

b) Number of colonies formed in soft agar of the untreated and the reversed NIH3T3 cells after 5 weeks of culture.

Mean $\pm$ s.d., n=3, *P<0.05.

detected new RNA synthesis after removal of the apoptotic inducers (Figure 4.13), suggesting that new transcription might be required. To test this hypothesis, we exposed cells transiently to the reversible transcription inhibitor actinomycin D (AMD) (Sawicki Godman 1972) (Figure 4.14). This promoted persistence of cleaved caspase-3 (Figure 4.14), an increase in the full plasma membrane permeability (Figure 4.15), and thus irreversible cell death. In contrast, AMD did not cause significant apoptosis in control cells that had not been treated with apoptotic inducers (Figures 4.14 and 4.15). These results indicate that new transcription is required for the reversal of apoptosis, and suggest a therapeutic approach to eliminating damaged cells by transient suppression of transcription during reversal of apoptosis.

4.3.6 Increased in transcription of pro-survival factors during reversal of apoptosis

We used RNA microarray analysis and real-time reverse transcription polymerase chain reaction (real-time RT-PCR), to determine the transcriptional profiles of cells undergoing reversal of apoptosis. We observed enhanced expression of multiple pro-survival signals, including Bcl-2, X-IAP and Mdm2, a pro-survival factor, following reversal of apoptosis (Figure 4.16). Previous studies indicate that Mdm2 inhibits apoptosis by facilitating p53 degradation (Sander et al., 1974), therefore,

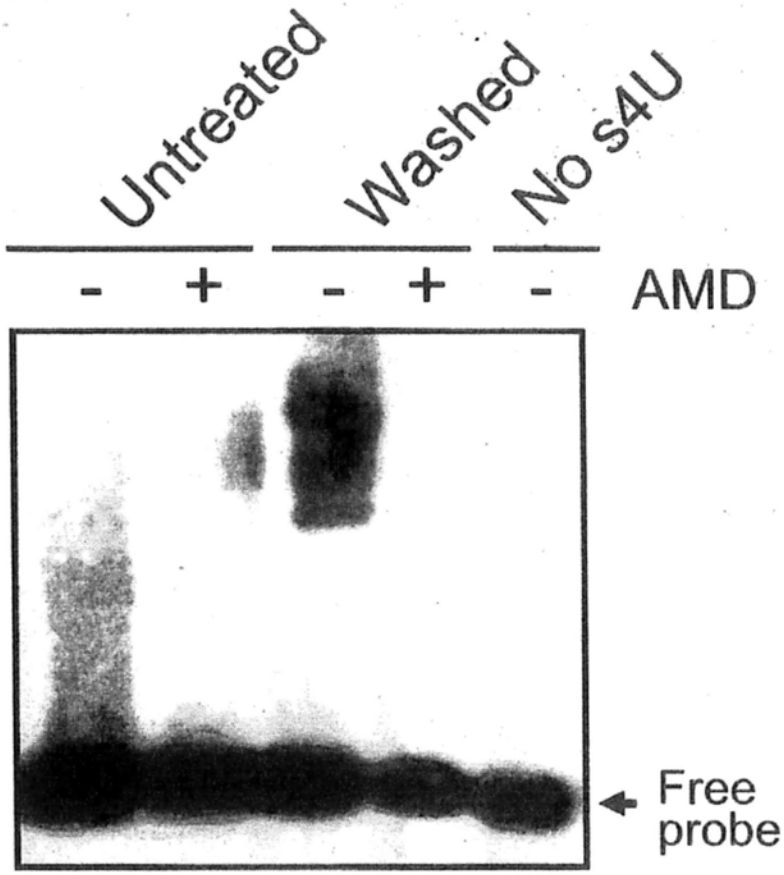

Figure 4.13 RNA blot for detecting new RNA synthesis on the untreated and the one-hour-after-washed liver cells with and without transient exposure (1 hour, 1 μg/ml) of actinomycin D (AMD). No s4U served as negative control for the probe binding to RNA. Detailed procedure is described in supplementary methods.

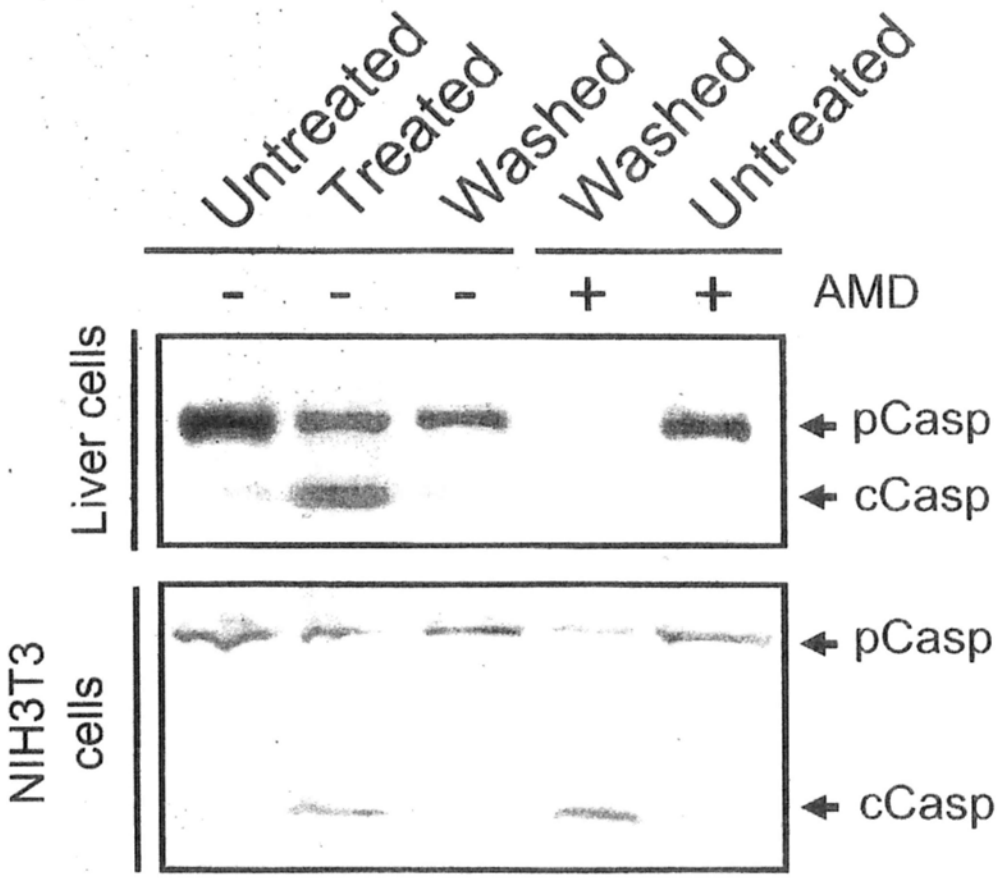

Figure 4.14 Western Blot analysis of the cleavage of caspase-3 (Casp) on the total lysate of the untreated, the treated and the washed liver cells and NIH3T3 cells with and without the exposure of AMD immediately after removal of apoptotic stimuli. The lysate was collected 23 hours after the exposure of AMD. c, cleaved form.

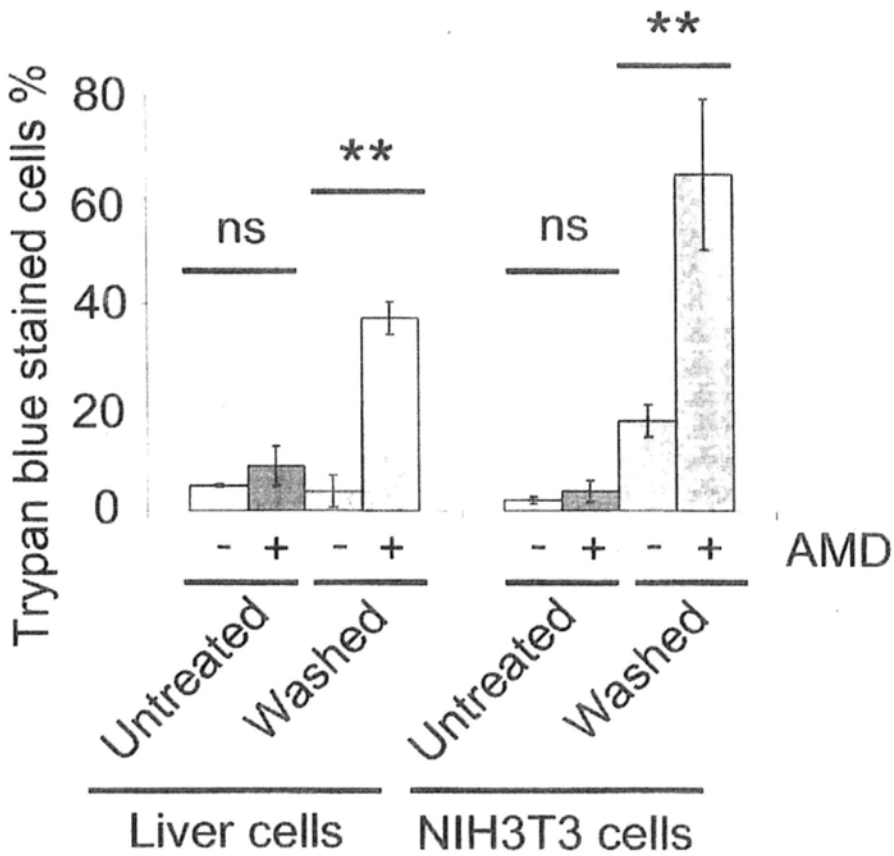

Figure 4.15 Percentage of the untreated and the washed liver cells and NIH3T3 cells with and without the AMD exposure that displayed full plasma membrane permeability in trypan blue exclusion assay.

Mean ± s.d., n=3, ns: $P>0.05$, $^{**}P<0.01$.

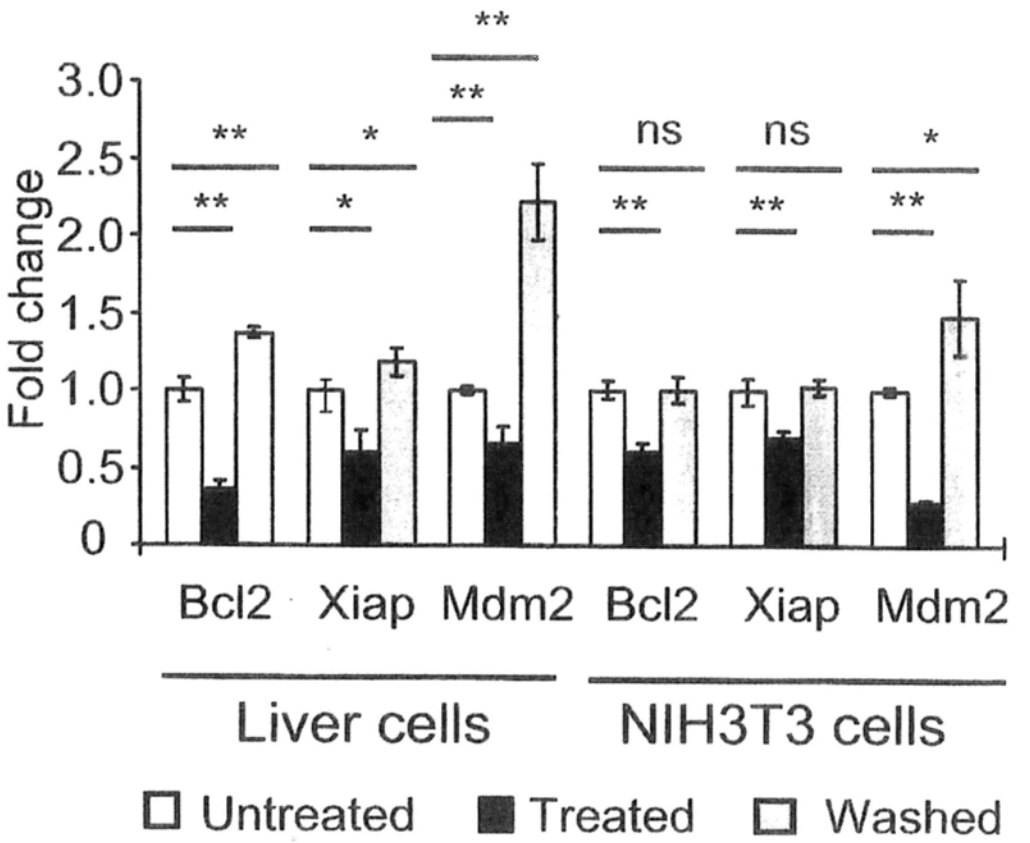

Figure 4.16 Real-time RT-PCR analysis of Bcl2, Xiap and Mdm2 of the untreated, the treated and the washed liver cells and NIH3T3 cells.

Mean ± s.d., n=3, ns: $P>0.05$, *$P<0.05$, **$P<0.01$.

suggesting it as a potential mediator in reversal of apoptosis.

4.4 Conclusion

Our research reveals how failure of cells to complete apoptosis once the process begins results in persistent genetic alterations and cellular transformation, and a practical approach to suppress it (Figure 4.17). These findings suggest that reversal of apoptosis might cause diseases such as cancer, and a new direction for potential subsequence treatment by promoting the dying cells to irreversible cell death. In fact, repeating exposure of apoptotic chemicals such as ethanol and DMSO has been linked to carcinogenesis (Boffetta and Hashibe 2006; Sander et al., 1974; Davaris et al., 1992). Noticeably, transformation of the cell after reversal of apoptosis might also explain the recent observations that prevention of actual demise in apoptotically stimulated cells potently promotes overgrowth, which associates to formation of cancer (Fan and Bergmann 2008; Martin et al., 2009). Cancer cells that experienced reversal of apoptosis might also accumulate mutation from cycles of chemotherapy (Stratton et al., 2009), in which apoptosis is a major strategy to destroy them, and therefore, leads to chemotherapy-resistance recurrence. Future research into reversal of apoptosis such as its specific regulators, modifiers and inhibitors will provide valuable insights into the biology of cancer.

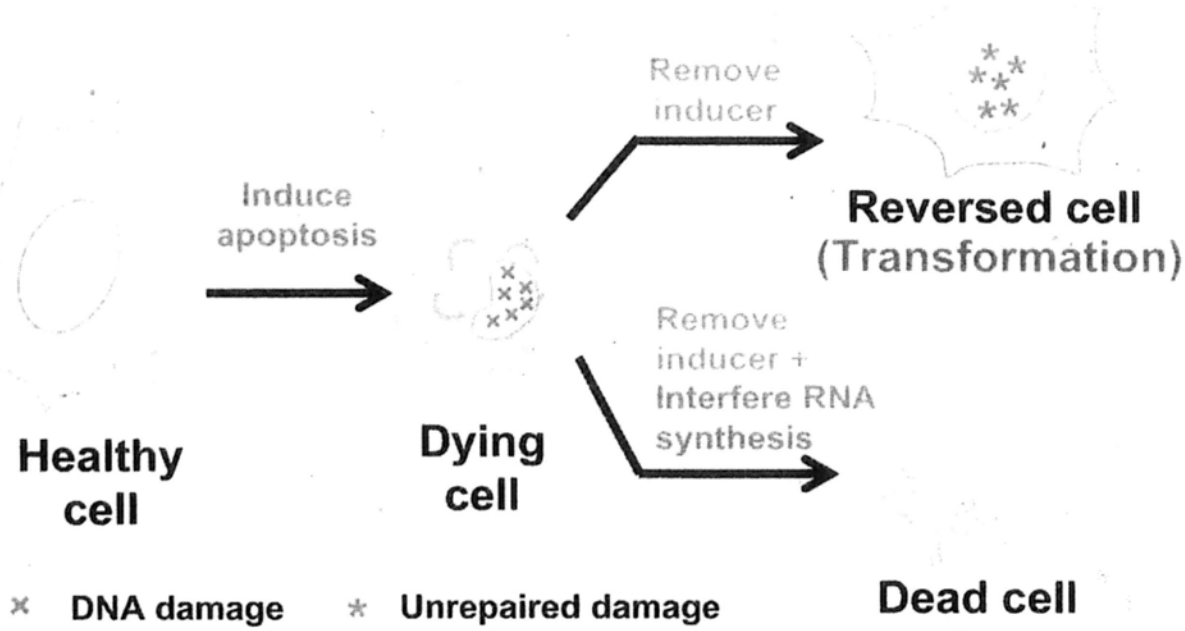

Figure 4.17 A schematic diagram summarizing the study on reversal of apoptosis. Dying cell reverses apoptosis once after removal of inducer, acquires genetic alterations from apoptosis, and displays transformation phenotype. Interference of RNA synthesis suppresses reversal of apoptosis, and lead to irreversible cell death, and therefore, serves as an promising strategy to inhibit the reversal of dying process.

Chapter 5

Vimentin supports mitochondrial morphology and organization

Chapter 5

Vimentin supports mitochondrial morphology and organization

5.1 Introduction

Mitochondria are important organelles that mediate energy metabolism, cell signaling and homoeostasis in eukaryotic cells (Chan 2006). These organelles form a complex tubular branching network in a healthy cell (Yaffe 1999). Accumulating evidence indicates that specific changes in mitochondrial morphologies are required during animal development (Chen et al., 2003; Jagasia et al., 2005), while disturbance in the mitochondrial dynamics and organization result in the dysfunction of mitochondria which leads to fatal consequences including disorders in respiration, neurodegeneration and tumorigenesis (Chen et al., 2003; Jagasia et al., 2005; Stowers et al., 2002; Li et al., 2004; Chen et al., 2005; Alirol et al., 2006). As mitochondrial morphology and organization determine the functions of mitochondria, characterizing their regulation is important in understanding the diversity of its biological roles.

As mitochondria are composed of outer limiting membranes and complex

networks of internal membranes, the highly curved morphology of these organelles is maintained and stabilized by specific mechanisms, such as the attachment to a rigid cellular structure, for example, the cytoskeleton (Voeltz et al., 2007). The cytoskeleton is mainly composed of the interconnected networks of actin, microtubules and intermediate filaments, which extend throughout the cytoplasm of the entire cell (Hirokawa 1982; Svitkina et al., 1996). Apart from structural support, the cytoskeleton functions in cell motility, intracellular trafficking and organelle positioning in a cell (Gross et al., 2007). Traditionally, microtubules are recognized as the key elements that associate with mitochondria on the basis of their cellular co-localization reported in previous microscopy studies (Yaffe 1999; Voeltz et al., 2007; Hirokawa 1982; Heggeness et al., 1978; Caviston and Holzbaur 2006). Disturbance in the integrity of microtubules by microtubule-disturbing drugs triggers mitochondrial fragmentation, suggesting that microtubules are important in mitochondrial support (Heggeness et al., 1978; Kedzior et al., 2004).

5.2 Specific aims

Growing evidence also indicates the contribution of intermediate filaments in the support of mitochondria (Anesti et al., 2006). For example, a fluorescence microscopic study has shown that the signal of vimentin intermediate filaments

overlaps with mitochondria and microtubules (Summerhayes et al., 1983). Desmin intermediate filaments have also been suggested to contribute to the distribution and function of mitochondria, as the knockdown of desmin in mouse cardiac muscle cells results in the disturbance of the mitochondrial organization and the respiration rate (Milner et al., 2000). In the present study, we investigated the interaction of mitochondria with vimentin intermediate filaments, and studied its potential roles in supporting the morphology, organization and function of mitochondria. Our findings reveal that vimentin interacts and co-localizes with mitochondria to a greater extent than other cytoskeleton components such as microtubules and actin filaments, suggesting that vimentin is critical to support mitochondria (Tang et al., 2008).

5.3 Results and discussion

5.3.1 Protein analysis of vimentin in the mitochondrial fraction of mammalian cells

In order to investigate the mechanism regulating mitochondrial morphology and organization, we initially studied the mitochondrial association of microtubules by subcellular fractionation. Sucrose-density-gradient centrifugation was performed to purify mitochondria from the immortalized brown adipocyte PAZ-6 cells for Western blot analysis of microtubules. Microtubules are composed of a heterodimer of α- and

β-tubulin, and the heterodimers form the filamentous tube-shaped protein polymers in an eukaryotic cell (Dutcher 2001). Surprisingly, both of the core microtubule components α-tubulin and β-tubulin were mainly found in the cytosol and only trace amounts of α- and β-tubulin were observed in the purified mitochondrial fraction in PAZ-6 cells (Figure 5.1). The presence of the mitochondrial outer- membrane protein BAK and inner-membrane protein Cox IV in the mitochondrial fraction indicates that the purified mitochondria were intact. It is possible that the isolation of mitochondria could disturb the integrity of microtubule filaments, and that might disrupt their association with microtubules.

By screening various cytoskeletal members, we found that the actin cytoskeleton was not specifically localized in the mitochondrial fraction, as the actin marker β-actin was mainly localized in the cytosolic fraction (Figure 5.1). Interestingly, our results showed that the intermediate filament vimentin was distinctively localized in the mitochondrial fraction, whereas a moderate amount of vimentin was observed in the cytosolic fraction and a barely detectable amount of vimentin protein was found in the ER-containing fraction in PAZ-6 cells (Figure 5.1). This specific mitochondrial association of vimentin was also observed in various cells lines including the human cervical carcinoma HeLa cells, HEK (human embryonic kidney)-293T cells, COS-7

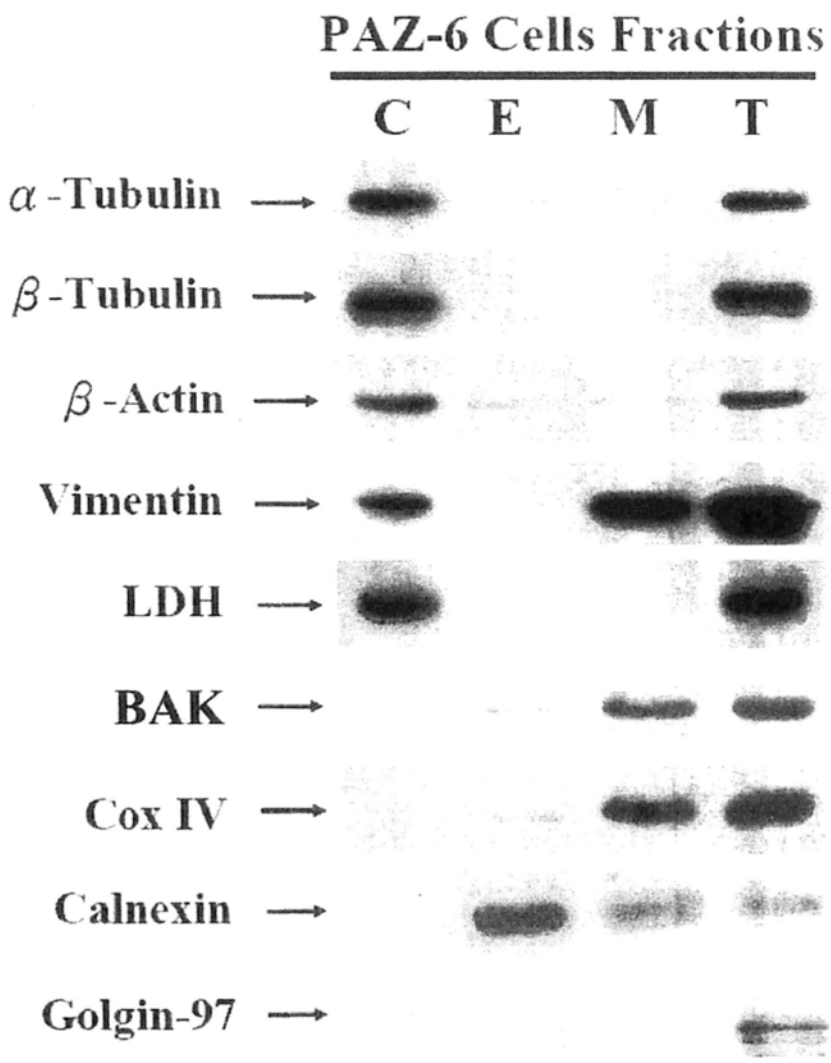

Figure 5.1 Mitochondrial localization of vimentin in PAZ-6 cells.

Western blot analysis of microtubules (α- and β-tubulin), actin (β-actin) and vimentin in the cytosolic (C), ER-containing (E) and mitochondrial-enriched (M) fractions from sucrose-density-gradient centrifugation, and total cell lysate (T) of PAZ-6 cells. The mitochondrial markers BAK and Cox IV indicate that the majority of mitochondria were present in the mitochondrial fraction. LDH, calnexin and golgin-97 served as the cytosolic, ER and Golgi apparatus markers respectively.

cells, the mouse myoblast C2C12 cells, NRK (normal rat kidney) cells and the Mustela putoris furo (ferret) normal astrocytes CRL 1656 cells (results not shown), suggesting that this is a general phenomenon in the mammalian system.

5.3.2 Interaction of vimentin with mitochondria

Vimentin has been reported to interact with several organelles such as the nucleus, Golgi apparatus, endosomes and lysosomes (Hartig et al., 1998; Gao and Sztul 2001; Styers et al., 2004), but its interaction with mitochondria remains to be determined (Toivola et al., 2005). A previous microscopic study demonstrated that mitochondria overlayed with microtubules and vimentin filaments, but they did not provide direct evidence on the mitochondrial interaction with microtubules and vimentin (Summerhayes et al., 1983). To identify this novel direct interaction between vimentin and mitochondria, we performed immunoprecipitation studies to purify intact mitochondria from the total cell lysate of COS-7 cells. By Western blot analysis, we detected the presence of a significant amount of vimentin in the immunoprecipitated mitochondrial protein complex, including the mitochondrial markers, BAK and Cox IV (Figure 5.2). The above findings indicate that vimentin interacts with mitochondria, and this is also in agreement with the results of subcellular fractionation on the co-localization of vimentin and mitochondria in

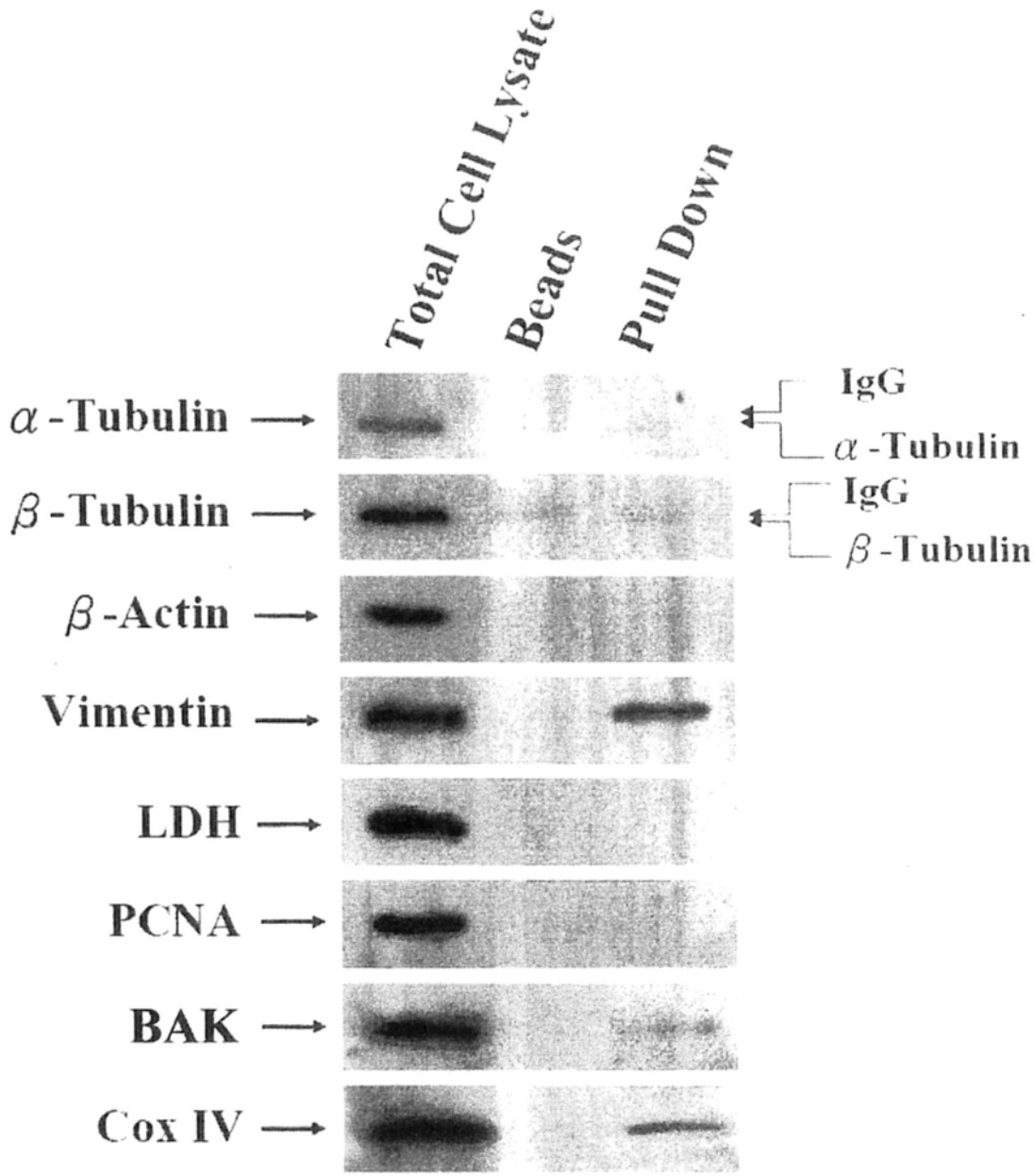

Figure 5.2 Mitochondrial association of vimentin in COS-7 cells.

Western blot analysis of coimmunoprecipitated microtubules (α- and β-tubulin), actin (β-actin) and vimentin with intact mitochondria isolated using Dynabeads bound with monoclonal antibody targeting the surface of intact mitochondria from the cell lysate (Pull Down). The total cell lysate and the Dynabeads conjugated with the antibody alone (Beads) served as the positive and negative controls respectively. LDH, PCNA, BAK and Cox IV served as the cytosolic, nuclear and mitochondrial outer and inner membrane markers respectively.

PAZ-6 cells (Figure 5.1). Figure 5.2 shows that both of the microtubule markers, α- and β-tubulin, were detectable in the mitochondrial pulldown complex, but their signals were weak and their sizes were close to the signal contributed by the antibody IgG chain at 52 kDa (Figure 5.2). The weak interaction between microtubules and mitochondria might be due the isolation of mitochondria; as discussed in the previous section, the isolation process could disturb the integrity of the microtubule filaments.

5.3.3 Co-localization of vimentin and mitochondria

Immunofluorescence microscopy was performed to verify the mitochondrial association of vimentin, as this is a less invasive approach to study the localization of cellular components as compared with subcellular fractionation and immunoprecipitation. We observed that the tubular mitochondria aligned and co-localized with a significant portion of the vimentin filaments in PAZ-6 cells (Figure 5.3A). The fluorescence signals were quantified (Figure 5.3B), and the results indicated that the vimentin filaments specifically co-localized with mitochondria.

To corroborate the significance of the mitochondrial association of vimentin, we

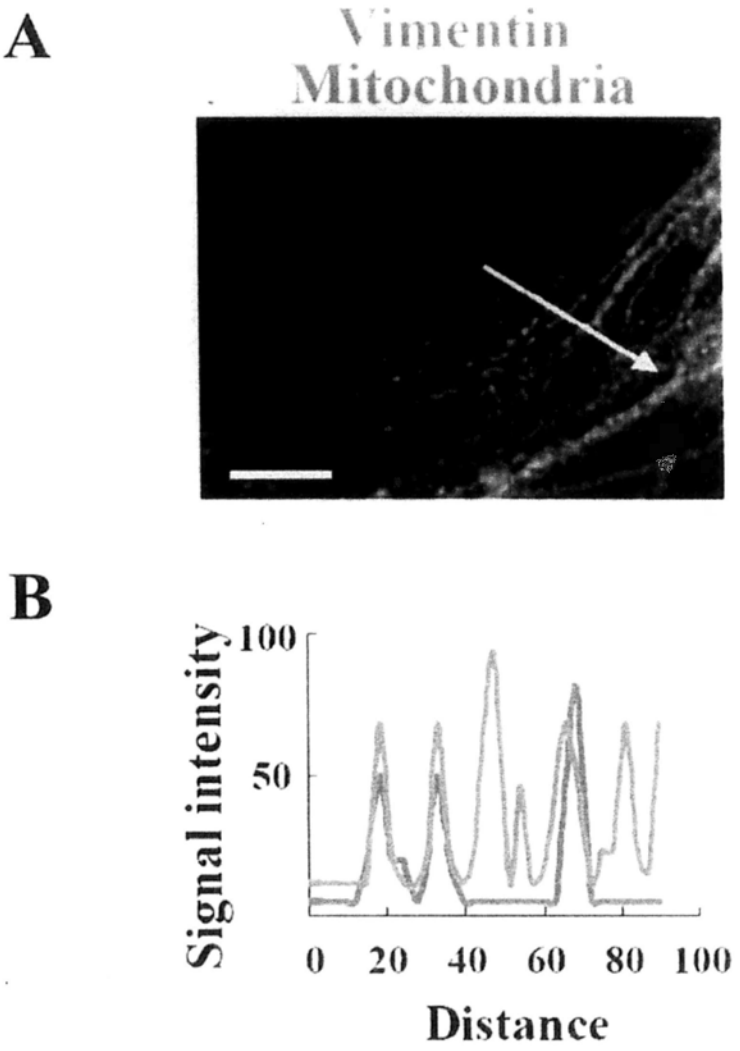

Figure 5.3 Fluorescence microscopy of vimentin and mitochondria of a PAZ-6 cell.

(A) A merged image of vimentin (green) and mitochondria (red). Scalc Bar, 5 μ m.

(B) Fluorescent signal intensity of vimentin (green) and mitochondria (red) were quantified along the solid-arrow in **(A)**.

compared the relative localization of mitochondria, vimentin, microtubules and F-actin by fluorescence microscopy analysis. The mitochondria, vimentin, microtubules and F-actin were co-stained in the mouse embryonic fibroblast NIH 3T3 cells. In agreement with our earlier observation in the PAZ-6 cells, almost all mitochondria aligned with the vimentin filaments in these cells (Figure 5.4A). On the other hand, we observed that the intensive refined microtubule filaments radiated from the perinuclear region through the cytoplasm to the edges of the cells, and certain portions of these filaments overlapped with the tubular mitochondria (Figure 5.4B). We observed that F-actin ran longitudinally across the cells (Figure 5.4C). However, these filaments did not specifically overlap with the tubular mitochondria (Figures 5.4A(*iv*) and (*v*), 5.4B(*iv*) and (*v*), and 5.4C(*iv*) and (*v*)), and the signal quantification results showed that the correlation of mitochondria with vimentin is significantly higher than that with microtubules or F-actin (Figure 5.4D).

5.3.4 Mitochondrial morphology and organization depend on the integrity of the vimentin network

As vimentin associates with mitochondria, we investigated the contribution of vimentin to the mitochondrial morphology by disturbing the integrity of the vimentin network through knockdown of vimentin. For the control COS-7 cells transfected

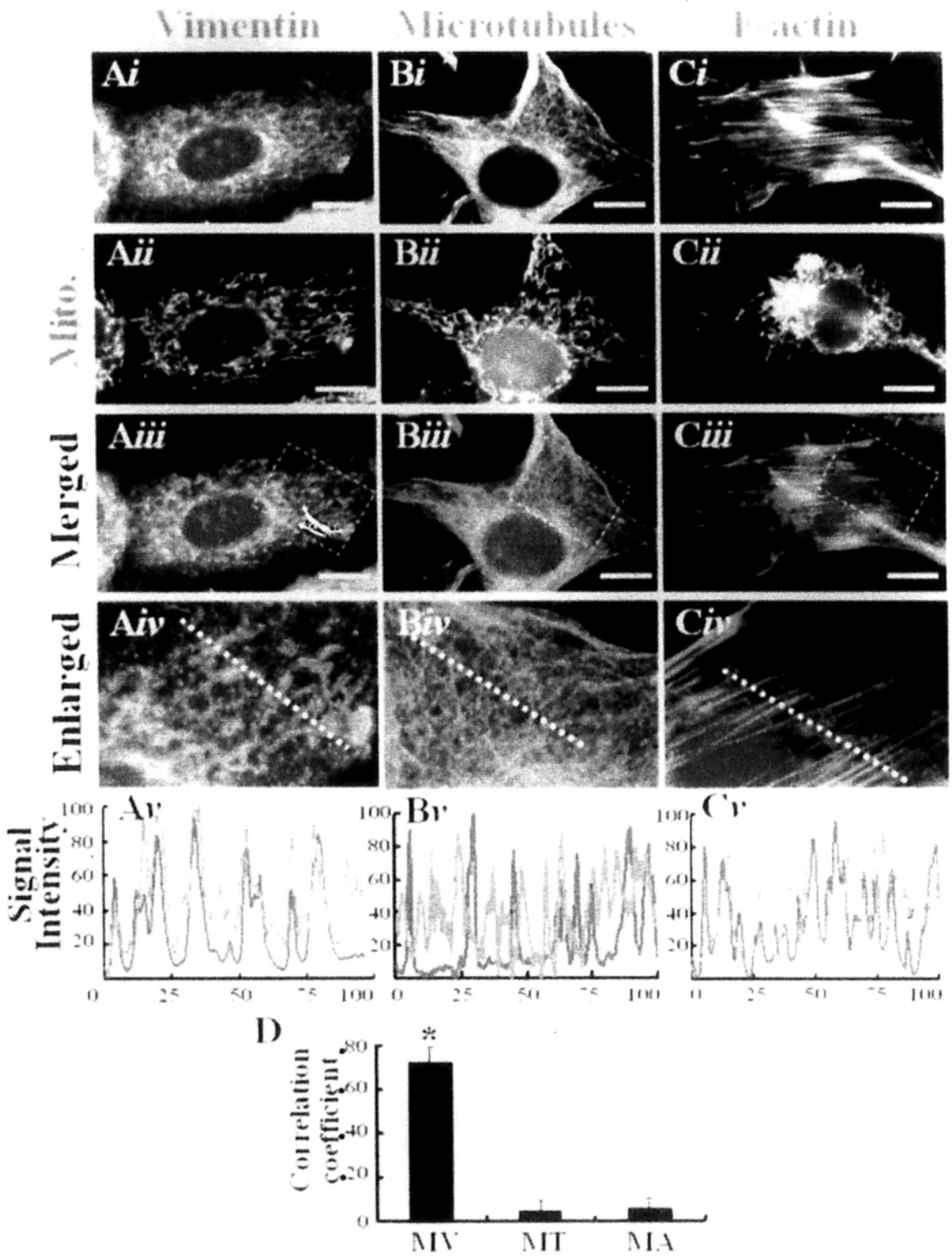
Vimentin
Microtubules
F-actin
Mito.
Merged
Enlarged
Ai
Bi
Ci
Aii
Bii
Cii
Aiii
Biii
Ciii
Aiv
Biv
Civ
Signal Intensity
Av
Bv
Cv
100
80
60
40
20
0
25
50
75
100
D
Correlation coefficient
*
MV
MT
MA

Figure 5.4 Mitochondrial co-localization of vimentin in NIH 3T3 cells.

Fluorescence microscopy of **(A)** vimentin, **(B)** microtubules (α-tubulin) and **(C)** F-actin cytoskeleton in NIH 3T3 cells. (*i*) Monochromatic images of the cytoskeleton. (*ii*) Monochromatic images of mitochondria (Mito.) from the same corresponding cells as in (*i*). (*iii*) Merged images of (*i*) (green) and (*ii*) (red) and the corresponding nucleus (blue). (*iv*) Enlarged images of the dotted boxes in (*iii*). Images presented in **(A–C)** are representative of three independent experiments with similar results. (*v*) The fluorescence signal intensity was quantified along the dotted lines in (*iv*). **(D)** Mean±S.D. correlation coefficients of the fluorescence signals of mitochondria and vimentin (MV), mitochondria and microtubules (MT), and mitochondria and F-actin (MA) respectively in three independent signal-quantification measurements in (*iv*). Each correlation coefficient was calculated as described previously (Berenson and Levine 1999). *P<0.0003; n=3; Student's *t* test. Scale bar, 10 μm.

with the non-specific siRNA, the extended tubular mitochondria still aligned along the vimentin filaments (Figure 5.5A). For the vimentin knockdown of COS-7 cells, the mitochondrial network was broken down and underwent mitochondrial fragmentation, swelling and disorganization as indicated by the perinuclear redistribution of mitochondria (Figure 5.5B). Furthermore, our Western blot analysis suggested that the cytochrome c level in the vimentin-knockdown cells was reduced compared with the control cells (Figure 5.6). As cytochrome c serves as a mitochondrial electron carrier which contributes to the mitochondrial polarization and this is essential for ATP synthesis (Reed 1997), reduction of cytochrome c levels might disturb the mitochondrial polarization and ATP generation, implying that the morphology and function of the mitochondria are dependent on the integrity of the vimentin network.

Traditionally, microtubules have been recognized to support mitochondrial morphology; this is supported by the observation that disturbance in the mitochondrial integrity by microtubule-disturbing drugs such as colcemid, nocodazole and taxol results in mitochondrial fission (Heggeness et al., 1978; Kedzior et al., 2004). However, these anti-tubulin agents in fact are the anti-cancer drugs which induce apoptosis (Sherwood et al., 1994; Kook et al., 2000; Jordan et al.,

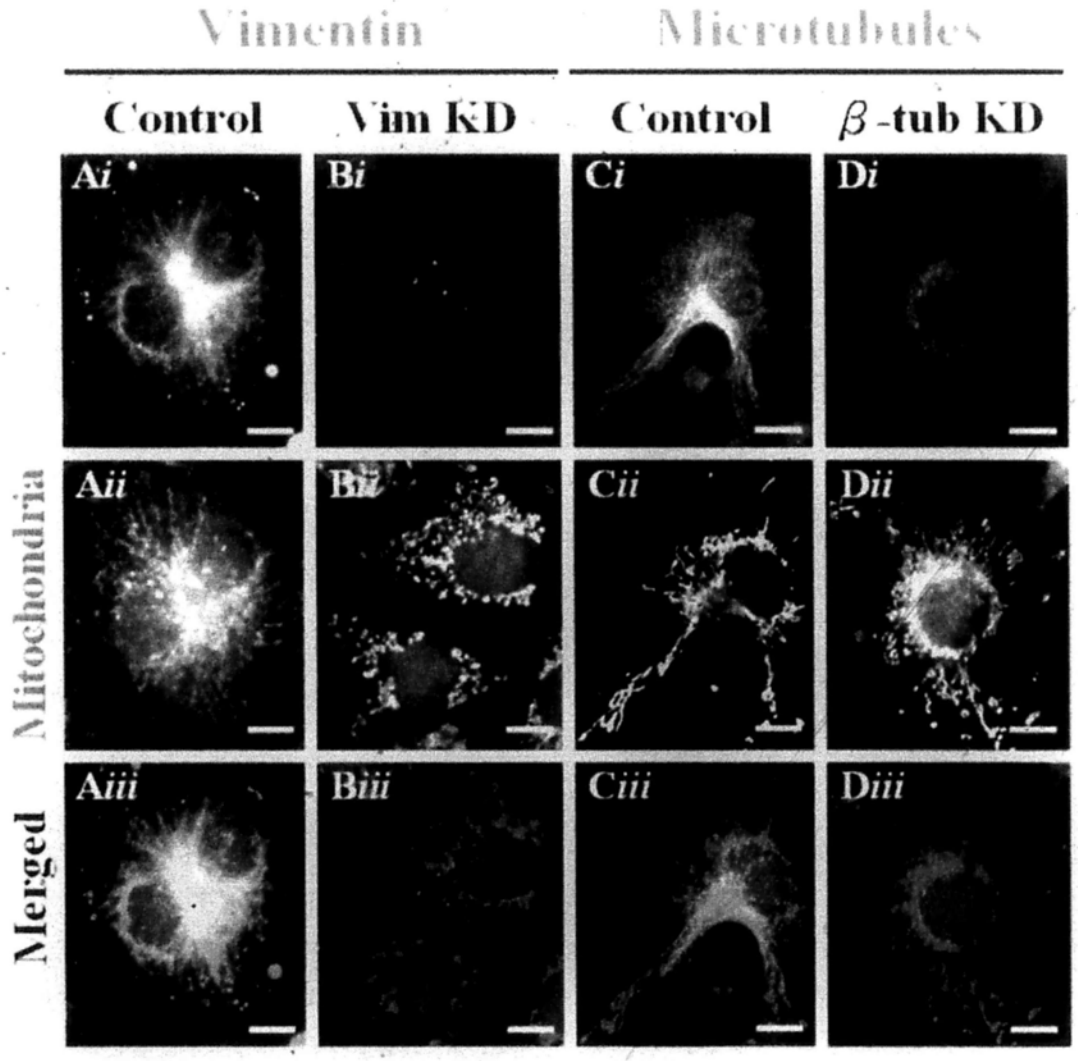

Figure 5.5 Mitochondrial morphology of vimentin-knockdown COS-7 cells

Fluorescence microscopy of vimentin stain in COS-7 cells transfected with **(A)** non-specific siRNA (Control) and **(B)** siRNA specific to vimentin (vimentin knockdown, Vim KD), and the microtubules (β-tubulin) stained in the COS-7 cells transfected with **(C)** non-specific siRNA (control) and **(D)** siRNA specific to β-tubulin (β-tubulin knockdown, β-tub KD). (*i*) Monochromatic images of the corresponding cytoskeleton as indicated. (*ii*) Monochromatic images of mitochondria from the same cells as in (*i*). (*iii*) Merged images of (*i*) (green) and (*ii*) (red) and the corresponding nucleus (blue). Scale bar, 10 μm.

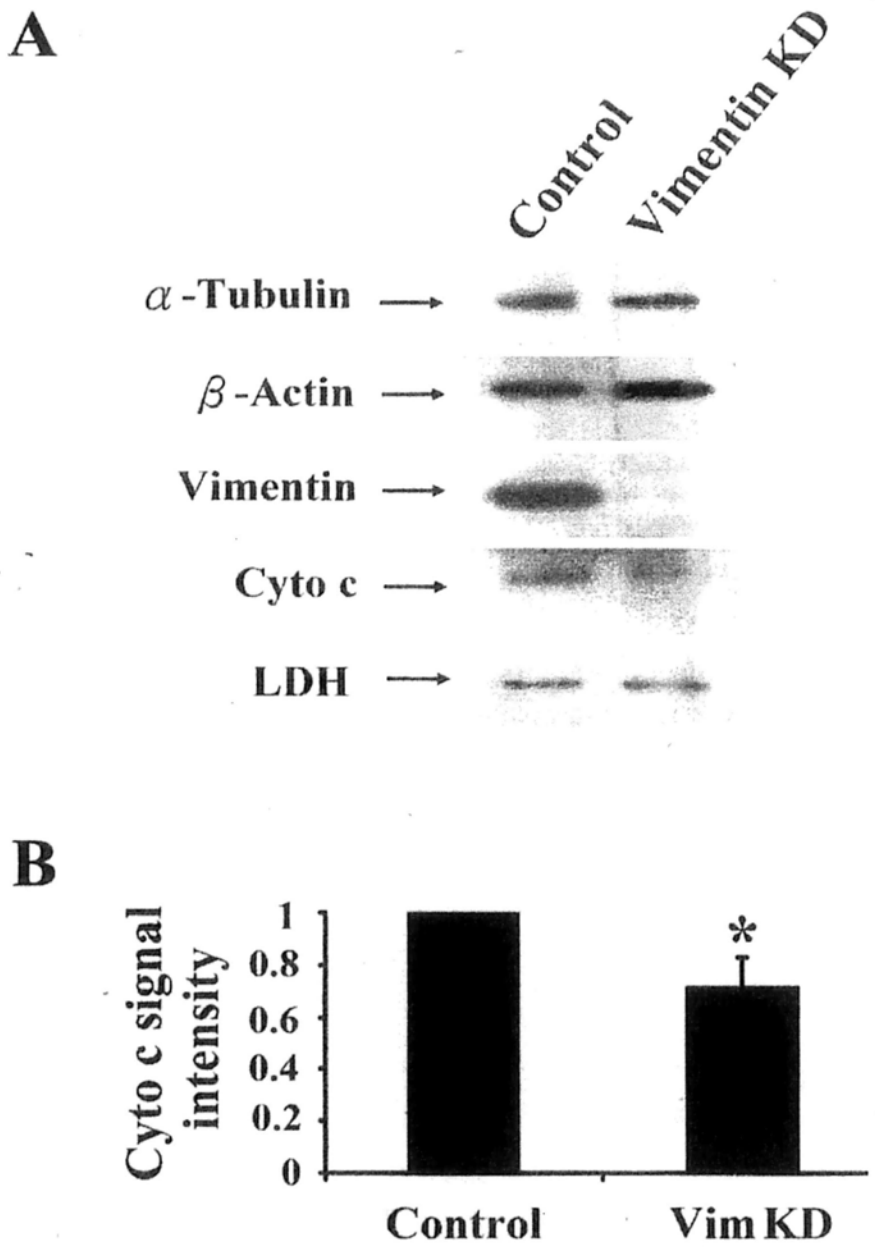

Figure 5.6 Cytochrome c level in vimentin knock-down cells

(A) Western blot analysis of vimentin and cytochrome c (Cyto c) in the total cell lysate of the control and vimentin knock-down COS-7 cells. Alpha (α)-tubulin, beta (β)-actin, and lactate dehydrogenase LDH served as a loading control. (B) Mean $\pm$S.D. relative signal intensity of the cytochrome c level of the control and the vimentin knock-down (Vim KD) cells in the panel (A). Mean $\pm$ s.d., n=3, *P<0.011.

1996). As mitochondrial fission is a universal phenomenon in apoptosis (Youle and Karbowski 2005), there is a concern as to whether the mitochondrial fission induced by these drugs is the cause or the consequence of apoptosis. Therefore we examined the functional role of microtubules in the mitochondrial support by knockdown of the coremicrotubule element, β-tubulin, so as to disturb the microtubule integrity. Figure 5.5 shows that the knockdown of β-tubulin could result in certain mitochondrial disorganizations such as mitochondrial swelling; however, extensive mitochondrial fragmentation was not observed (Figure 5.5C and D). Taken together with the vimentin knockdown results, we demonstrated that the morphology of mitochondria depends more primarily on the integrity of vimentin than the microtubule network. In addition, we found that the knockdown of vimentin resulted in a significant reduction of α-tubulin levels in the mitochondrial fraction of COS-7 cells, and the remaining mitochondrial α-tubulin level was almost undetectable after the vimentin knockdown (Figure 5.7). This suggests that vimentin might contribute to the mitochondrial association of microtubules. It has been reported that microtubules could mediate the mitochondrial morphology and distribution through the microtubule-based cytoskeletal motors such as kinesin and dynein (Caviston and Holzbaur 2006). As microtubules regulate the dynamics of vimentin (Liao and Gundersen 1998; Yoon et al., 1998; Helfand et al., 2002; Charke and Allan 2002), it might be possible that

A

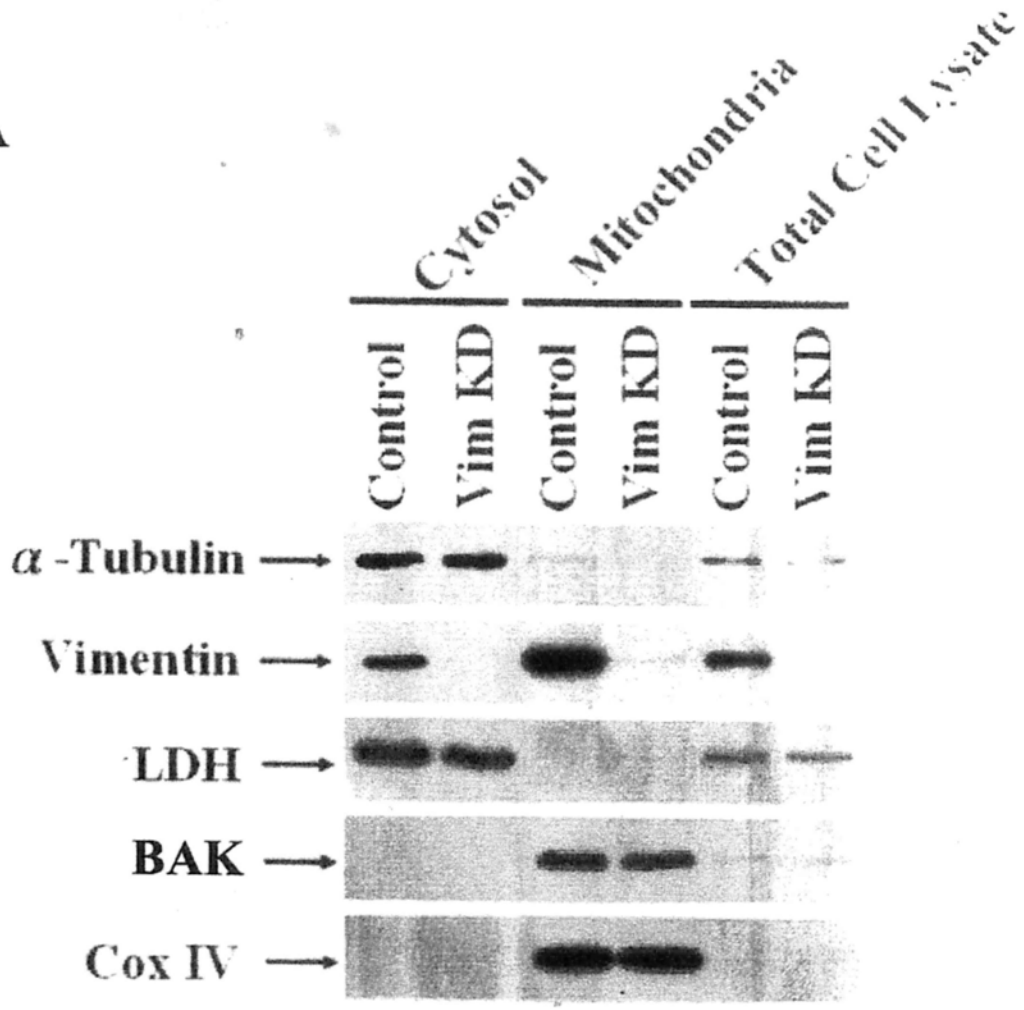
Cytosol
Mitochondria
Total Cell Lysate
Control
Vim KD
Control
Vim KD
Control
Vim KD
α-Tubulin
Vimentin
LDH
BAK
Cox IV

B

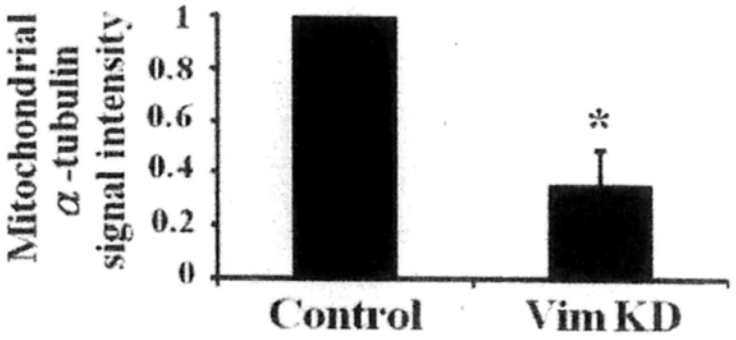
Mitochondrial α-tubulin signal intensity
1
0.8
0.6
0.4
0.2
0
*
Control
Vim KD

Figure 5.7 Reduction of mitochondrial microtubules in vimentin-knockdown cells. Subcellular fractionation of vimentin-knockdown COS-7 cells. **(A)** Western blot analysis of microtubules (α-tubulin) and vimentin in the cytosolic (Cytosol) and mitochondrial-enriched (Mitochondria) fractions, and total cell lysate of COS-7 cells transfected with non-specific siRNA (Control) or siRNA specific to vimentin (Vim KD). BAK and Cox IV served as the mitochondrial outer- and inner-membrane markers respectively. LDH served as a cytosolic marker. **(B)** Mean±S.D. of the relative signal intensity of the mitochondrial α-tubulin signal (mitochondrial α-tubulin signal/total α-tubulin signal) in the control and the vimentin knockdown cells from three independent measurements. Mean $\pm$ s.d., n=3, $*P<0.002$.

microtubules mediate the mitochondrial morphology, organization and function by interacting with mitochondrial-associated vimentin.

5.4 Conclusion

Vimentin is one of the intermediate filaments that functions in structural support, signal transduction and organelle positioning of a cell. In the present study, we report the contribution of vimentin in mitochondrial morphology and organization. Using subcellular fractionation, immunoprecipitation and fluorescence microscopy analyses, we found that vimentin was associated with mitochondria. Knockdown of vimentin resulted in mitochondrial fragmentation, swelling and disorganization. We further demonstrated that the vimentin cytoskeleton co-localized and interacted with mitochondria to a greater extent than other cytoskeletal components known to support mitochondria. Our results also suggest that vimentin could participate in the mitochondrial association of microtubules. As mitochondrial morphologies determine mitochondrial function, our findings revealed a potentially important relationship between the vimentin-based intermediate filaments and the regulation of mitochondrial morphology, organization and function. Further investigation into the molecular mechanism of this process is certainly required.

Chapter 6

Perspectives

Chapter 6

Perspectives

Our research demonstrates reversal of apoptosis in mammalian cells. In this moment, the regulatory mechanisms, the roles and the consequences of reversal of apoptosis remain unknown. To further study reversal of apoptosis, it is important to develop a biosensor that allows us to continue to tract the cells after they reversed apoptosis, and identify the regulatory mechanisms that reverse apoptosis.

6.1 Development of a biosensor to track reversal of apoptosis

Visualizing the recovery of dying cells can provide evidence for the reversibility of apoptosis. The first insight came from a flow-cytometic study in B cell lymphoma. Cells that stained positively for Annexin V, an early indicator of apoptosis, might not die but continue to proliferate (Hammill et al., 1999), suggesting that cells can survive after initiation of apoptosis. Time course studies of the engulfment and clearance of dying cells in *Caenorhabditis elegans* further show that apoptotic cells, according to morphological criteria, in mutants defective in phagocytic activity and pro-apoptotic pathways could regain normal morphology. This suggests that blocking phagocytosis and apoptosis could promote survival of the dying cells (Hoeppner et

al., 2001; Reddien et al., 2001). My Ph.D. study demonstrated, by living cell imaging, reversal of the dying process following removal of apoptotic inducers (Tang et al., 2009). However, all these current methods are limited. What is needed is a method that allows continuous identification and monitoring of cells that have undergone reversal of apoptosis in living animals.

To identify and tract cells after reversal of apoptosis, one of the most critical tasks is to develop a biosensor, which allows to track the fate of the cells after they reversed apoptosis. This sensor is composed of 2 elements, a caspase-activatable Cre recombinase, and an existing *loxP* technique, the *Cre-lox* site-specific recombination system (Sauer 1987; Sauer and Henderson 1988). Cre recombinase is a site-specific DNA recombinase which catalyses the recombination of DNA between specific sites in a DNA molecule known as *loxP* sequences, thereby splicing the DNA between the sequences. I propose to construct a Cre protein that is tethered to the plasma membrane via a caspase-cleavable linker peptide and a transmembrane domain. Upon caspase activation, the peptide is cleaved and Cre protein is released and translocates to nucleus. This triggers a Cre dependent genetic recombination event, which excises the stop cassette separating a promoter and green fluorescent protein (GFP) open reading frame, resulting in permanent expression of green fluorescent

protein (GFP). This provides an important tool for generation of transgenic mouse expressing caspase-inducible Cre protein. This in vivo biosensor will allow us to track the cells that experience caspase-activation, a hallmark of apoptosis, and therefore, will allow us identify the cells that reverse apoptosis, as well as the progeny from cells that reverse apoptosis.

6.2 Study of the molecular mechanisms regulating reversal of apoptosis

Elucidating the mechanisms of reversal of apoptosis enhances our understanding on the functional role of this process. This also allows us to regulate reversal of apoptosis for potential therapeutic purpose.

To further study the regulation on reversal of apoptosis on a genomic scale, we performed time-course RNA microarray to determine the transcriptional profiles of the liver cells undergoing reversal of ethanol-induced apoptosis. We observed enhanced gene expression of multiple pro-survival signals, including anti-apoptotic family member of BCL-2, X-linked inhibitor of apoptosis protein (XIAP), the murine double minute (MDM2), activating transcription factor 3 (ATF3) and heat shock proteins (HSPs), following reversal of apoptosis (Figure 6.1). Our preliminarily and ongoing research reveals their contributing role in reversing apoptosis is revealed

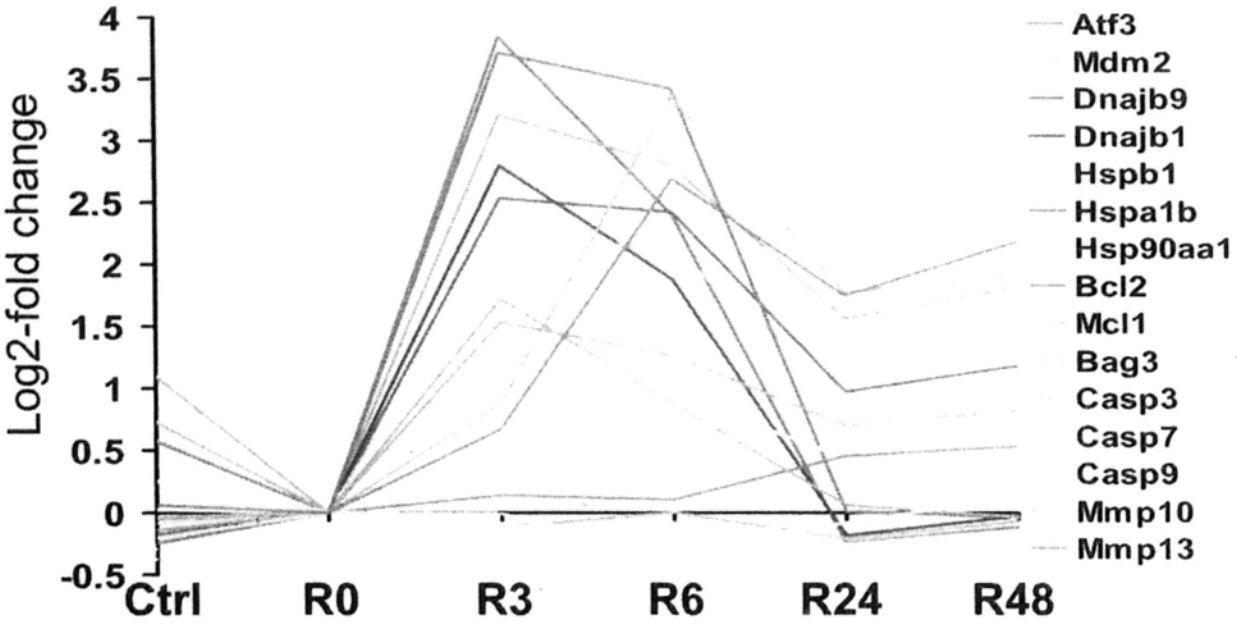

Figure 6.1 A time course microarray study of gene expression in the reversal of ethanol-induced apoptosis in primary mouse liver cells. Log2-fold change of gene expression comparison between ethanol-induced apoptotic cells (R0) to the untreated cells (Ctrl), and the induced cells that were then washed and further cultured in fresh medium for 3 hours (R3), 6 hours (R6), 24 hours (R24) and 48 hours (R48). Three biological replicates' log2 signal values were averaged (Geometric Mean) for each time point to create this figure and to verify statistical significance.

their corresponding specific inhibitor might suppress reversal of apoptosis (Figure 6.2). These results reveal critical pathways in regulating reversal of apoptosis by suppressing the activated apoptotic machineries, and expressing new transcripts to repairing the cells (Figure 6.3).

The gene expression profile during the reversal of apoptosis will be investigated in different cell lines from different origin and species in different apoptotic inductions. This will provide us insights into the mechanisms of reversal of apoptosis, and also the way to promote or suppress the reverse of apoptosis by targeting the genes which mediate this process. The functional role of the identified genes will be characterized by RNAi technology to investigate whether the knockdown of the gene could enhance or inhibit the reversal of apoptosis. Large scale RNAi screening (Boutros et al., 2004) could be also perform to test our identified candidate genes in our current or other different cell models including at RNAi screening center at Harvard (http://www.flyrnai.org/DRSC-ASO.html). The selected positive genes will be tested in animal models such as in flies and then in mouse.

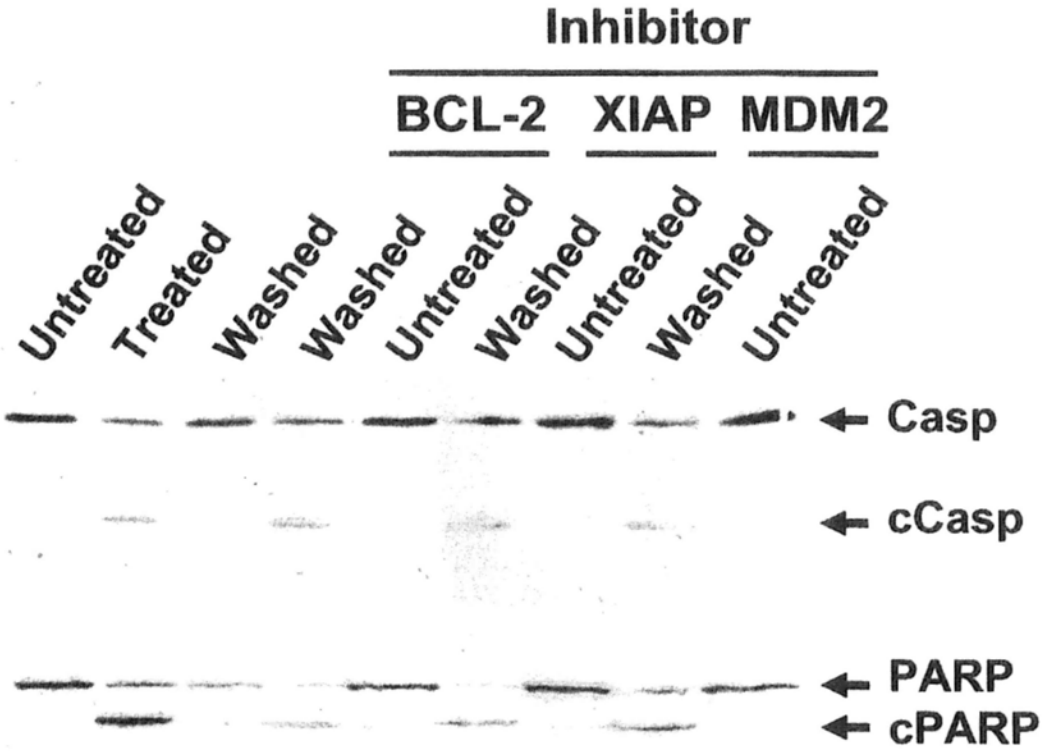

Figure 6.2 Suppression of reversal of ethanol-induced apoptosis in primary mouse liver cells. Western blot analysis on the total cell lysate of the healthy (untreated) liver cells, the cells were exposed to 4.5% ethanol for 5 hours (treated), the induced cells were washed to remove apoptotic inducers and further cultured for 24 hours (Washed), for the protein level of caspase-3 (Casp-3) and PARP. c, cleaved form. Specific inhibitors targeting BCL-2 (ABT 263, 3 μ M), XIAP (Embelin, 20 μ M) and MDM2 (MDM2 inhibitor, 20 μ M) were applied to the medium of the cells immediately after removal of the ethanol induction for 24 hours.

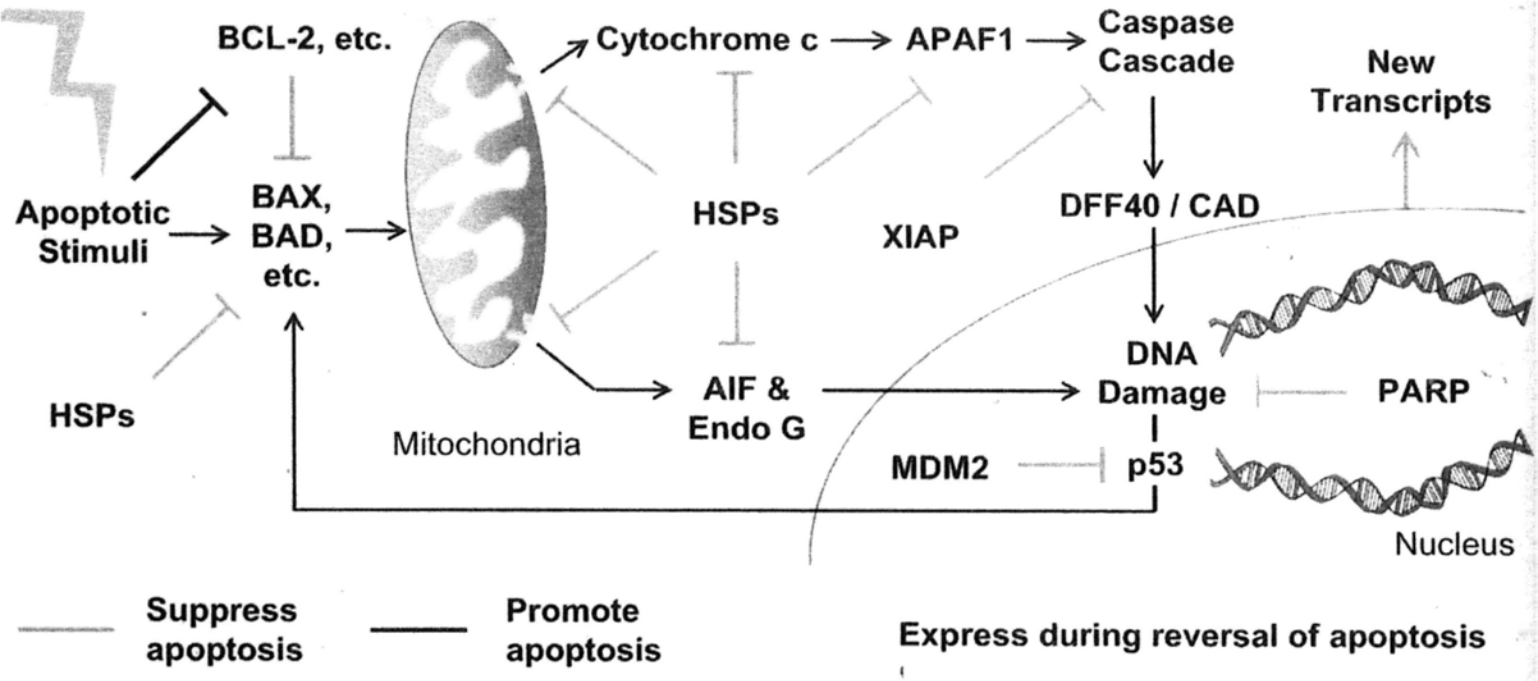

Figure 6.3 Model of reversal of apoptosis. Expression of multiple pro-survival proteins and new transcripts during reversal of apoptosis promotes cell survival by suppressing the activated apoptotic pathways and by repairing the cells.

References

Albeck, J. G., Burke, J. M., Aldridge, B. B., Zhang, M., Lauffenburger, D. A. & Sorger, P. K. Quantitative analysis of pathways controlling extrinsic apoptosis in single cells. *Mol. Cell* **30,** 11-25 (2008).

Alnemri, E. S., Livingston, D. J., Nicholson, D. W., Salvesen, G., Thornberry, N. A., Wong, W. W. & Yuan, J. Human ICE/CED-3 protease nomenclature. *Cell* **87,** 171 (1996).

Alirol, E. & Martinou, J. C. Mitochondria and cancer: is there a morphological connection? *Oncogene* **25,** 4706–4715 (2006).

Anesti, V. & Scorrano, L. The relationship between mitochondrial shape and function and the cytoskeleton. *Biochim. Biophys. Acta* **1757,** 692–699 (2006).

Andersen, M. H., Becker, J. C. & Straten, P. Regulators of apoptosis: suitable targets for immune therapy of cancer. *Nat. Rev. Drug Discov.* **4,** 399-409 (2005).

Arimura, E., Kotoh, K., Nakamuta, M., Morizono, S., Enjoji, M. & Nawata, H. Local recurrence is an important prognostic factor of hepatocellular carcinoma. *World J. Gastroenterol.* **11,** 5601-5606 (2005).

Baehrecke, E. H. How death shapes life during development. *Nat. Rev. Mol. Cell Biol.* **3,** 779-787 (2002).

Berenson, L. & Levine, M. In Basic Business Statistics: Concepts and Applications (7th edn), p. 793, (Prentice-Hall, Upper Saddle River, 1999).

Bertrand, R., Solary, E., O'Connor, P., Kohn, K. W. & Pommier, Y. Induction of a common pathway of apoptosis by staurosporine. *Exp. Cell Res.* **211,** 314-321 (1994).

Bloom, A. D. Induced chromosomal aberrations: biological and clinical significance. *J. Pediatr.* **81,** 1-8 (1972).

Boffetta, P. & Hashibe, M. Alcohol and cancer. *Lancet Oncol.* **7,** 149-156 (2006).

Boutros, M., Kiger, A. A., Armknecht, S., Kerr, K., Hild, M., Koch, B., Haas, S. A., Paro, R., Perrimon, N. & Heidelberg Fly Array Consortium. Heidelberg Fly Array Consortium. Genome-wide RNAi analysis of growth and viability in *Drosophila* cells. *Science* **303,** 832-835 (2004).

Bremer, E., ten Cate, B., Samplonius, D. F., de Leij, L. F. & Helfrich, W. CD7-restricted activation of Fas-mediated apoptosis: a novel therapeutic approach for acute T-cell leukemia.CD7-restricted activation of Fas-mediated apoptosis: a novel therapeutic approach for acute T-cell leukemia. *Blood* **107,** 2863-2870 (2006).

Brown, J. M. & Attardi, L. D. The role of apoptosis in cancer development and treatment response. *Nat. Rev. Cancer* **5,** 231-237 (2005).

Canny, J. F. A computational approach to edge detection. IEEE Trans. *Pattern Anal. Mach. Intell.* **8**, 679–698 (1986).

Carmona-Gutierrez, D., Eisenberg, T., Büttner, S., Meisinger, C., Kroemer, G. & Madeo, F. Apoptosis in yeast: triggers, pathways, subroutines. *Cell Death Differ*. **17,** 763-773 (2010).

Caviston, J. P. & Holzbaur, E. L. F. Microtubule motors at the intersection of trafficking and transport. *Trends Cell Biol.* **16,** 530–537 (2006).

Chabner, B. A. & Roberts, T. G. Jr. Timeline: Chemotherapy and the war on cancer. Timeline: Chemotherapy and the war on cancer. *Nat. Rev. Cancer* **5,** 65-72 (2005).

Chan, D. C. Mitochondria: dynamic organelles in disease, aging, and development. *Cell* **125,** 1241-1252 (2006).

Charke, E. J. & Allan, V. Intermediate filaments: vimentin move in. *Curr. Biol.* **12,** R596–R598 (2002).

Chen, H., Detmer, S. A., Ewald, A. J., Griffin, E. E., Fraser, S. E. & Chan, D. C. Mitofusins Mfn1 and Mfn2 coordinately regulate mitochondrial fusion and are essential for embryonic development. *J. Cell Biol.* **160,** 189–200 (2003).

Chen, H., Chomyn, A. & Chan, D. C. Disruption of fusion results in mitochondrial

heterogeneity and dysfunction. *J. Biol. Chem.* **280,** 26185–21692 (2005).

Chipuk, J. E., Moldoveanu, T., Llambi, F., Parsons, M. J. & Green, D. R. The BCL-2 Family Reunion. *Mol. Cell* **37,** 299-310 (2010).

Cifone, M. A. & Fidler, I. J. Correlation of patterns of anchorage-independent growth with in vivo behavior of cells from a murine fibrosarcoma. *Proc. Natl. Acad. Sci. U.S.A.* **77,** 1039–1043 (1980).

Clarke, D. M., Robilotto, A. T., VanBuskirk, R. G., Baust, J. G., Gage, A. A. & Baust, J. M. Targeted induction of apoptosis via TRAIL and cryoablation: a novel strategy for the treatment of prostate cancer. *Prostate Cancer Prostatic Dis.* **10,** 175-184 (2007).

D'Amours, D, Sallmann, F. R., Dixit, V. M. & Poirier, G. G. Gain-of-function of poly (ADP-ribose) polymerase-1 upon cleavage by apoptotic proteases: implications for apoptosis. *J. Cell Sci.* **114,** 3771-3778 (2001).

Davaris, P., Fytiza, R., Androulakakis, P. & Papacharalampous, N. Carcinogenesis associated with dimethyl sulfoxide. *Urol. Int.* **48,** 120 (1992).

Davis, A. J. & Tannock, J. F. Repopulation of tumour cells between cycles of chemotherapy: a neglected factor. *Lancet Oncol.* **1,** 86-93 (2000).

Dean, M., Fojo, T. & Bates, S. Tumour stem cells and drug resistance. *Nat. Rev. Cancer* **5,** 275-284 (2005).

Dörken, B. & Daniel, P. T. Combined p53/Bax mutation results in extremely poor prognosis in gastric carcinoma with low microsatellite instability. *Cell Death Differ.* **10,** 461-467 (2003).

Du, C., Fang, M., Li, Y., Li, L. & Wang, X. Smac, a mitochondrial protein that promotes cytochrome c-dependent caspase activation by eliminating IAP inhibition. *Cell* **102,** 33-42 (2000).

Dutcher, S. K. The tubulin fraternity: a to h. *Curr. Opin. Cell Biol.* **13,** 49–54 (2001).

Eguchi, K. Apoptosis in autoimmune diseases. *Intern. Med.* **40,** 275-284 (2001).

Eisenberg, T., Büttner, S., Kroemer, G. & Madeo, F. The mitochondrial pathway in yeast apoptosis. *Apoptosis* **12,** 1011-1023 (2007).

Enari, M., Sakahira, H., Yokoyama, H., Okawa, K., Iwamatsu, A. & Nagata, S. A.caspase-activated DNase that degrades DNA during apoptosis, and its inhibitor ICAD. *Nature* **391,** 43-50 (1998).

Fan, Y. & Bergmann, A. Apoptosis-induced compensatory proliferation. The Cell is dead. Long live the Cell. *Trends Cell Biol.* **18,** 467-473 (2008).

Fenech, M. Cytokinesis-block micronucleus cytome assay. *Nat. Protoc.* **2,** 1084-1104 (2007).

Friedlander, R. M. Apoptosis and caspases in neurodegenerative diseases. *N. Engl. J. Med.* **348,** 1365-1375 (2003).

Gao, Y. & Sztul, E. A novel interaction of the Golgi complex with the vimentin intermediate filament cytoskeleton. *J. Cell Biol.* **152,** 877–894 (2001).

German, J. Cytological Evidence for Crossing-over in Vitro in Human Lymphoid Cells. *Science* **144,** 298-301 (1964).

Gourlay, C. W., Du, W. & Ayscough, K. R. Apoptosis in yeast-mechanisms and benefits to a unicellular organism. *Mol. Microbiol.* **62,** 1515-1521 (2006).

Green, D. R. & Kroemer, G. The pathophysiology of mitochondrial cell death. *Science* **305,** 626-629 (2004).

Gross, S. P., Vershinin, M. & Shubeita, G. T. Cargo transport: two motors are sometimes better than one. *Curr. Biol.* **17,** R478–R486 (2007).

Hammill, A. K., Uhr, J. W. & Scheuermann, R. H. Annexin V staining due to loss of membrane asymmetry can be reversible and precede commitment to apoptotic death. *Exp. Cell Res.* **251,** 16-21 (1999).

Hartig, R., Shoeman, R. L., Janetzko, A., Tolstonog, G. & Traub, P. DNA-mediated transport of the intermediate filament protein vimentin into the nucleus of cultured cells. *J. Cell Sci.* **111,** 3573–3584 (1998).

Hengartner, M. O. & Horvitz, H. R.C. elegans cell survival gene ced-9 encodes a functional homolog of the mammalian proto-oncogene bcl-2. *Cell* **76,** 665-76 (1994).

Heggeness, M. H., Simon, M. & Singer, S. J. Association of mitochondria with microtubules in cultured cells. *Proc. Nat. Acad. Sci. U.S.A.* **75,** 3863–3866 (1978).

Helfand, B. T., Mikami, A., Vallee, R. B. & Goldman, R. D. A requirement for cytoplasmic dynein and dynactin in intermediate filament network assembly and organization. *J. Cell Biol.* **157,** 795–806 (2002).

Hentschel, S. J. & Lang, F. F. Current surgical management of glioblastoma. *Cancer J.* **9,** 113-125 (2003).

Hirokawa, N. Cross-linker system between neurofilaments, microtubules, and membranous organelles in frog axons revealed by the quick-freeze, deep-etching method. *J. Cell Biol.* **94,** 129–142 (1982).

Hoeppner, D. J., Hengartner, M. O. & Schnabel, R. Engulfment genes cooperate with ced-3 to promote cell death in Caenorhabditis elegans. *Nature* **412,** 202-206 (2001).

Hotchkiss, R. S., Strasserm, A., McDunn, J. E. & Swanson, P. E. Cell death. *N. Engl. J. Med.* **361,** 1570-1583 (2009).

Jaiswal, J. K., Mattoussi, H., Mauro, J. M. & Simon, S. M. Long-term multiple color imaging of live cells using quantum dot bioconjugates. *Nat. Biotechnol.* **21;** 47-51 (2003).

Jacobson, M. D., Weil, M. & Raff, M. C. Programmed cell death in animal development. *Cell* **88,** 347-354 (1997).

Jagasia, R., Grote, P., Westermann, B. & Conradt, B. DRP-1-mediated mitochondrial fragmentation during EGL-1-induced cell death in C. elegans. *Nature* **433,** 754–760 (2005).

Johnstone, R. W., Ruefli, A. A. & Lowe, S. W. Apoptosis: a link between cancer genetics and chemotherapy. *Cell* **108,** 153-164 (2002).

Jordan, M. A., Wendell, K., Gardiner, S., Derry, W. B., Copp, H. & Wilson, L. Mitotic block induced in HeLa cells by low concentrations of paclitaxel (Taxol) results in abnormal mitotic exit and apoptotic cell death. *Cancer Res.* **56,** 816–825 (1996).

Kamura, T, Alteration of metastatic potential of ovarian cancer in clinical course. *Nippon Sanka Fujinka Gakkai Zasshi* **48,** 607-617 (1996).

Kedzior, J., Masaoka, M., Kurono, C., Spodnik, J. H., Hallmann, A., Majczak, A., Niemczyk, E., Trzonkowski, P., Mysliwski, A., Soji, T. & Wakabayashi, T. Changes in physicochemical properties of microtubules lead to the formation of a single spherical structure of mitochondrial assembly enveloping nuclear chromatins. *J. Electron Microsc.* **53,** 659–670 (2004).

Kerr, J. F., Wyllie, A. H. & Currie, A, R. Apoptosis: a basic biological phenomenon with wide-ranging implications in tissue kinetics. *Br. J. Cancer.* **26,** 239-257 (1972).

Kim, J. J. & Tannock, I. F. Repopulation of cancer cells during therapy: an important cause of treatment failure. *Nat. Rev. Cancer* **5,** 516-525 (2005).

Kook, S., Shim, S. R., Kim, J. I., Ahnn, J. H., Jung, Y. K., Paik, S. G. & Song, W. K. Degradation of focal adhesion proteins during nocodazole-induced apoptosis in rat-1 cells. *Cell Biochem. Funct.* **18,** 1–7 (2000).

Kroemer, G. & Martin, S. J. Caspase-independent cell death. *Nat. Med.* **11,** 725-730 (2005).

Kuida, K., Zheng, T. S., Na, S., Kuan, C., Yang, D., Karasuyama, H., Rakic, P. & Flavell, R. A. Decreased apoptosis in the brain and premature lethality in CPP32-deficient mice. *Nature* **384,** 368-372 (1996).

Lam, E. Controlled cell death, plant survival and development. *Nat. Rev. Mol. Cell Biol.* **5,** 305-315 (2004).

Lazebnik, Y. A., Kaufmann, S. H., Desnoyers, S., Poirier, G. G. & Earnshaw, W. C. Cleavage of poly(ADP-ribose) polymerase by a proteinase with properties like ICE. *Nature* **371,** 346-347 (1994).

Letai, A. G. Diagnosing and exploiting cancer's addiction to blocks in apoptosis. *Nat. Rev. Cancer* **8,** 121–132 (2008).

Li, H., Zhu, H., Xu, C. J. & Yuan, J. Cleavage of BID by caspase 8 mediates the mitochondrial damage in the Fas pathway of apoptosis. *Cell* **94,** 491-501 (1998).

Li, P., Nijhawan, D., Budihardjo, I., Srinivasula, S. M., Ahmad, M., Alnemri, E. S. & Wang, X. Cytochrome c and dATP-dependent formation of Apaf-1/caspase-9 complex initiates an apoptotic protease cascade. *Cell* **91,** 479-489 (1997).

Li, L. Y., Luo, X. & Wang, X. Endonuclease G is an apoptotic DNase when released from mitochondria. *Nature* **412,** 95-99 (2001).

Li, Q. X., Yu, D. H., Liu, G., Ke, N., McKelvy, J. & Wong-Staal, F. (2008) Selective anticancer strategies via intervention of the death pathways relevant to cell transformation. *Cell Death Differ.* **15,** 1197-1210

Li, Z., Okamoto, K., Hayashi, Y. & Sheng, M. The importance of dendritic mitochondria in the morphogenesis and plasticity of spines and synapses. *Cell* **119,** 873–887 (2004).

Liao, G. & Gundersen, G. G. Kinesin is a candidate for cross-bridging microtubules and intermediate filaments. Selective binding of kinesin to detyrosinated tubulin and vimentin. *J. Biol. Chem.* **273,** 9797–9803 (1998).

Lockshin, R. A. & Williams, C. M. Programmed cell death. II. Endocrine potentiation of the breakdown of the intersegmental muscles of silkmoths. *J. Insect Physiol.* **10,** 643-649 (1964).

Luo, X., Budihardjo, I., Zou, H., Slaughter, C. & Wang, X. Bid, a Bcl2 interacting protein, mediates cytochrome c release from mitochondria in response to activation of cell surface death receptors. *Cell* **94,** 481-490 (1998).

Lüthi, A. U. & Martin, S. J. The CASBAH: a searchable database of caspase substrates. *Cell Death Differ.* **14,** 641-650 (2007).

MacLeod, R. A., Kaufmann, M. & Drexler, H. G. Cytogenetic harvesting of commonly used tumor cell lines. *Nat. Protoc.* **2,** 372-382 (2007).

Madeo, F., Herker, E., Maldener, C., Wissing, S., Lächelt, S., Herlan, M., Fehr, M., Lauber, K., Sigrist, S. J., Wesselborg, S. & Fröhlich, K. U. A caspase-related protease regulates apoptosis in yeast. *Mol. Cell* **9,** 911-917 (2002).

Marine, J. C. & Lozano, G. Mdm2-mediated ubiquitylation: p53 and beyond. *Cell Death Differ.* **17,** 93-102 (2010).

Martin, F. A., Perez-Garijo, A. & Morata, G. Apoptosis in Drosophila: compensatory proliferation and undead cells. *Int. J. Dev. Biol.* **53,** 1341-1347 (2009).

McKillop, I. H. & Schrum, L. W. Alcohol and liver cancer. *Alcohol* **35,** 195-203 (2005).

Milner, D. J., Mavroidis, M., Weisleder, N. & Capetanaki, Y. Desmin cytoskeleton linked to muscle mitochondrial distribution and respiratory function. *J. Cell Biol.* **150,** 1283–1298 (2000).

Minchinton, A. I & Tannock I. F. Drug penetration in solid tumours. *Nat. Rev. Cancer* **6,** 583-592 (2006).

Miramar, M. D., Costantini, P., Ravagnan, L., Saraiva, L. M., Haouzi, D., Brothers, G., Penninger, J. M., Peleato, M. L., Kroemer, G. & Susin, S. A. NADH oxidase activity of mitochondrial apoptosis-inducing factor. *J. Biol. Chem.* **276,** 16391-16398 (2001).

Mori, S., Chang, J. T., Andrechek, E. R., Matsumura, N., Baba, T., Yao, G., Kim, J. W., Gatza, M., Murphy, S. & Nevins, J. R. Anchorage-independent cell growth signature identifies tumors with metastatic potential. *Oncogene* **28,** 2796-2805 (2009).

Mrózek, A., Petrowsky, H., Sturm, I., Kraus, J., Hermann, S., Hauptmann, S., Lorenz, M., Dörken, B. & Daniel, P. T. Combined p53/Bax mutation results in extremely poor prognosis in gastric carcinoma with low microsatellite instability. *Cell Death Differ.* **10,** 461-467 (2003).

Nagata, S., Nagase, H., Kawane, K., Mukae, N. & Fukuyama, H. Degradation of chromosomal DNA during apoptosis. *Cell Death Differ.* **10,** 108-116 (2003).

Nguyen, D. X., Bos, P. D. & Massagué, J. Metastasis: from dissemination to organ-specific colonization. *Nat. Rev. Cancer* **9,** 274-284 (2009).

Norton, L. & Simon, R. Tumour size, sensitivity to therapy, and design of treatment schedules. *Cancer Treat. Rep.* **61,** 1307-1317 (1977).

Odaka, C., Sanders, M. L. & Crews, P. Jasplakinolide induces apoptosis in various transformed cell lines by a caspase-3-like protease-dependent pathway. *Clin. Diagn. Lab. Immunol.* **7,** 947–952 (2000).

Olive, P. L. & Banath, J. P. The comet assay: a method to measure DNA damage in individual cells. *Nat. Protoc.* **1,** 23-29 (2006).

Orlando, A., Leandro, G., Olivo, M., Andriulli, A. & Cottone, M. Radiofrequency thermal ablation vs. percutaneous ethanol injection for small hepatocellular carcinoma in cirrhosis: meta-analysis of randomized controlled trials. *Am. J. Gastroenterol.* **104,** 514-524 (2009).

Orrenius, S., Zhivotovsky, B. & Nicotera, P. Regulation of cell death: the calcium-apoptosis link. *Nat. Rev. Mol. Cell Biol.* **4,** 552-565 (2003).

Phillips, B. J. & Jenkinson, P. Is ethanol genotoxic? A review of the published data. *Mutagenesis* **16,** 91-101 (2001).

Reddien, P. W., Cameron, S. & Horvitz, H. R. Phagocytosis promotes programmed cell death in C. elegans. *Nature* **412,** 198-202 (2001).

Reed, J. CCytochrome c: can't live with it-can't live without it. *Cell* **91,** 559–562 (1997).

Ricci, J. E., Muñoz-Pinedo, C., Fitzgerald, P., Bailly-Maitre, B., Perkins, G. A., Yadava, N., Scheffler, I. E., Ellisman, M. H. & Green, D. R. Disruption of mitochondrial function during apoptosis is mediated by caspase cleavage of the p75 subunit of complex I of the electron transport chain. *Cell* **117,** 773-786 (2004).

Riedl, S. J., Renatus, M., Schwarzenbacher, R., Zhou, Q., Sun, C., Fesik, S. W., Liddington, R. C. & Salvesen, G. S. Structural basis for the inhibition of caspase-3 by XIAP. *Cell* **104,** 791-800 (2001).

Riedl, S. J. & Shi, Y. Molecular mechanisms of caspase regulation during apoptosis. *Nat. Rev. Mol. Cell Biol.* **5,** 897-907 (2004).

Ríos, A., Galindo, P. J., Torres, J., Roca, M. J., Robles, R., Luján, J. A. & Parrilla, P. Factors causing early relapse after lung metastasis surgery. *Eur. J. Cancer Care (Engl).* **16,** 26-32 (2007).

Rouleau, M., Patel, A., Hendzel, M. J., Kaufmann, S. H. & Poirier, G. G. PARP inhibition: PARP1 and beyond. *Nat. Rev. Cancer* **10,** 293-301 (2010).

Rubin, H. Cell-cell contact interactions conditionally determine suppression and selection of the neoplastic phenotype. *Proc. Natl. Acad. Sci. U.S.A.* **105,** 6215-6221 (2008).

Sakahira, H., Enari, M. & Nagata, S. Cleavage of CAD inhibitor in CAD activation and DNA degradation during apoptosis. *Nature* **391,** 96-99 (1998).

Sander, J., Burkle, G. & Burkle, V. [Induction of lungtumors and tumors of the urinary bladder in rats by di-n-butyl nitrosamine in dimethyl sulfoxide]. *Z. Krebsforsch. Klin. Onkol. Cancer Res. Clin. Oncol.* **82,** 83-89 (1974).

Santos, N. C., Figueira-Coelho, J., Martins-Silva, J. & Saldanha, C. Multidisciplinary utilization of dimethyl sulfoxide: pharmacological, cellular, and molecular aspects. *Biochem. Pharmacol.* **65,** 1035-1041 (2003).

Sauer, B. Functional expression of the cre-lox site-specific recombination system in the yeast Saccharomyces cerevisiae. *Mol. Cell Biol.* **7,** 2087-2096 (1987).

Sauer, B. & Henderson, N. Site-specific DNA recombination in mammalian cells by the Cre recombinase of bacteriophage P1. *Proc. Natl. Acad. Sci. U.S.A.* **85,** 5166-5170 (1988).

Sawicki, S. G. & Godman, G. C. On the recovery of transcription after inhibition by actinomycin D. *J. Cell Biol.* **55,** 299-309 (1972).

Sherwood, S. W., Sheridan, J. P. & Schimke, R. T. (1994) Induction of apoptosis by the anti-tubulin drug colcemid: relationship of mitotic checkpoint control to the induction of apoptosis in HeLa s3 cells. *Exp. Cell Res.* **215,** 373–379

Sheridan, C. & Martin, S. J. Commitment in apoptosis: slightly dead but mostly alive. *Trends Cell Biol.* **18,** 353-357 (2008).

Spector, D. L., Goldman, R. D. and Leinwand, L. A. Cells: a Laboratory Manual, pp. 41.1–41.7, (Cold Spring Harbor Laboratory Press, Cold Spring Harbor, 1997).

Steeq, P. S. Tumor metastasis: mechanistic insights and clinical challenges. *Nat. Med.* **12,** 895-904 (2006).

Stephens, T. C. & Peacock, J. H. Tumour volume response, initial cell kill and cellular repopulation in B16 melanoma treated with cyclophosphamide and 1-(2-chloroethyl)-3-cyclohexyl-1-nitrosourea. *Br. J. Cancer* **36,** 313–321 (1977).

Stowers, R. S., Megeath, L. J., Górska-Andrzejak, J., Meinertzhagen, I. A. & Schwarz, T. L. Axonal transport of mitochondria to synapses depends on milton, a novel Drosophila protein. *Neuron* **36,** 1063–1077 (2002).

Stratton, M. R., Campbell, P. J. & Futreal, P. A. The cancer genome. *Nature* **458,** 719-724 (2009).

Stupp, R., Hegi, M. E., van den Bent, M. J., Mason, W. P., Weller, M., Mirimanoff, R. O. & Cairncross, J. G. European Organisation for Research and Treatment of Cancer Brain Tumor and Radiotherapy Groups; National Cancer Institute of Canada Clinical Trials Group. Changing paradigms--an update on the multidisciplinary management of malignant glioma. *Oncologist* **11,** 165-80 (2006).

Styers, M. L., Salazar, G., Love, R., Peden, A. A., Kowalczyk, A. P. & Faundez, V. The endo-lysosomal sorting machinery interacts with the intermediate filament cytoskeleton. *Mol. Biol. Cell* **15,** 5369–5382 (2004).

Silva, M. T., do Vale, A. & dos Santos, N. M. Secondary necrosis in multicellular animals: an outcome of apoptosis with pathogenic implications. *Apoptosis* **13,** 463-482 (2008).

Summerhayes, I. C., Wong, D. & Chen, L. B. Effect of microtubules and

intermediate filaments on mitochondrial distribution. *J. Cell Sci.* **6,** 87–105 (1983).

Susin, S. A., Lorenzo, H. K., Zamzami, N., Marzo, I., Snow, B. E., Brothers, G. M., Mangion, J., Jacotot, E., Costantini, P., Loeffler, M., Larochette, N., Goodlett, D. R., Aebersold, R., Siderovski, D. P., Penninger, J. M. & Kroemer, G. Molecular characterization of mitochondrial apoptosis-inducing factor. *Nature* **397,** 441-446 (1999).

Svitkina, T. M., Verkhovsky, A. B. & Borisy, G. G. Plectin sidearms mediate interaction of intermediate filaments with microtubules and other components of the cytoskeleton. *J. Cell Biol.* **135,** 991–1007 (1996).

Tang, H. L., Lung, H. L., Wu, K. C., Le, A. H., Tang, H. M. & Fung, M. C. Vimentin supports mitochondrial morphology and organization. *Biochem J.* **410,** 141-146 (2008).

Tang, H. L., Yuen, K. L., Tang, H. M. & Fung, M. C. Reversibility of apoptosis in cancer cells. *Br. J. Cancer.* **100,** 118–122 (2009).

Taylor, R. C., Cullen, S. P. & Martin, S. J. Apoptosis: controlled demolition at the cellular level. *Nat. Rev. Mol. Cell Biol.* **9,** 231-241 (2008).

Toivola, D. M., Tao, G. Z., Habtezion, A., Liao, J. & Omary, M. B. Cellular integrity plus: organelle-related and protein-targeting functions of intermediate filaments. *Trends Cell Biol.* **15,** 608–617 (2005).

van Loo, G., Schotte, P., van Gurp, M., Demol, H., Hoorelbeke, B., Gevaert, K., Rodriguez, I., Ruiz-Carrillo, A., Vandekerckhove, J., Declercq, W., Beyaert, R. & Vandenabeele, P. Endonuclease G: a mitochondrial protein released in apoptosis and involved in caspase-independent DNA degradation. *Cell Death Differ.* **8,** 1136-1142 (2001).

Vaux, D. L., Weissman, I. L. & Kim, S. K. Prevention of programmed cell death in Caenorhabditis elegans by human bcl-2. *Science* **258,** 1955-1957 (1992).

Vazquez, A., Bond, E. E., Levine, A. J. & Bond, G. L. The genetics of the p53 pathway, apoptosis and cancer therapy. *Nat Rev Drug Discov.* **7,** 979-987 (2008).

Verhagen, A. M., Ekert, P. G., Pakusch, M., Silke, J., Connolly, L. M., Reid, G. E., Moritz, R. L., Simpson, R. J. & Vaux, D. L. Identification of DIABLO, a mammalian protein that promotes apoptosis by binding to and antagonizing IAP proteins. *Cell* **102,** 43-53 (2000).

Villavicencio, A. T., Burneikiene, S., Romanelli, P., Fariselli, L., McNeely, L., Lipani, J. D., Chang, S. D., Nelson, E. L., McIntyre, M., Broggi, G. & Adler, J. R. Jr. Survival following stereotactic radiosurgery for newly diagnosed and recurrent glioblastoma multiforme: a multicenter experience. *Neurosurg. Rev.* **32,** 417-424 (2009).

Voeltz, G. K. & Prinz, W. A. Sheets, ribbons and tubules? How organelles get their shape. *Nat. Rev. Mol. Cell Biol.* **8,** 258–264 (2007).

Wang X. The expanding role of mitochondria in apoptosis. *Genes Dev.* **15,** 2922-2933 (2001).

Waterhouse, N. J., Goldstein, J. C., von Ahsen, O., Schuler, M., Newmeyer, D. D. & Green, D. R. Cytochrome c maintains mitochondrial transmembrane potential and ATP generation after outer mitochondrial membrane permeabilization during the apoptotic process. *J. Cell Biol.* **153,** 319-328 (2001).

Widlak, P. & Garrard, W. T. Discovery, regulation, and action of the major apoptotic nucleases DFF40/CAD and endonuclease G. *J. Cell Biochem.* **94,** 1078-1187 (2005).

Wu, L. & Tannock, I. F. Repopulation in murine breast tumours during and after sequential treatments with cyclophosphamide and 5-fluorouracil. *Cancer Res.* **63,** 2134–2138 (2003).

Xu, D., Woodfield, S. E., Lee, T. V., Fan, Y., Antonio, C. & Bergmann, A. Genetic control of programmed cell death (apoptosis) in *Drosophila*. *Fly (Austin)* **3,** 78-90 (2009).

Yaffe, M. P. The machinery of mitochondrial inheritance and behavior. *Science* **283,** 1493–1497 (1999).

Yoon, M., Moir, R. D., Prahlad, V. & Goldman, R. D. Motile properties of vimentin

intermediate filament networks in living cells. *J. Cell Biol.* **143,** 147–157 (1998).

Youle, R. J. & Karbowski, M. Mitochondrial fission in apoptosis. *Nat. Rev. Mol. Cell Biol.* **6,** 657–663 (2005).

Young, C., Klocke, B. J., Tenkova, T., Choi, J., Labruyere, J., Qin, Y. Q., Holtzman, D. M., Roth, K. A. & Olney, J. W. Ethanol-induced neuronal apoptosis in vivo requires BAX in the developing mouse brain. *Cell Death Differ.* **10,** 1148–1155 (2003).

Zeiner, G. M., Cleary, M. D., Fouts, A. E., Meiring, C. D., Mocarski, E. S. & Boothroyd, J. C. RNA analysis by biosynthetic tagging using 4-thiouracil and uracil phosphoribosyltransferase. *Methods Mol. Biol.* **419,** 135-146 (2008).

Zilberfarb, V., Pietri-Rouxel, F., Jockers, R., Krief, S., Delouis, C., Issad, T. & Strosberg, A. D. Human immortalized brown adipocytes express functional b3-adrenoceptor coupled to lipolysis. *J. Cell Sci.* **110,** 801–807 (1997).

Zurlo, J. & Arterburn, L. M. Characterization of a primary hepatocyte culture system for toxicological studies. *In Vitro Cell Dev. Biol. Anim.* **32,** 211-220 (1996).

List of Publications

Tang, H. L., Yuen, K. L., Tang, H. M. & Fung, M. C. Reversibility of apoptosis in cancer cells. *Br. J. Cancer.* **100,** 118–122 (2009).

Tang, H. L., Lung, H. L., Wu, K. C., Le, A. H., Tang, H. M. & Fung, M. C. Vimentin supports mitochondrial morphology and organization. *Biochem J.* **410,** 141-146 (2008).